Dear Authors,

Thank you for your responses to your referees and for your revised manuscript.

After reviewing these, I am generally satisfied that your manuscript is now suitable for publication.

However, there are two points in your response to Referee 2 in which you mention performing additional work to address comments: "We expect these experiments to come to equilibrium state within a month and may be able to comment on them then"; and then, later, "Also, we are currently running a new experiment [that] could possibly be integrated within the manuscript in a few sentences".

For obvious reasons, the version of your manuscript that accompanies these responses does not currently address these points. As such, I am returning your manuscript to you for further revision that clarifies and finalises these points. Assuming that the additional work alluded to is complete (or will complete shortly), please revise your manuscript appropriately.

If you have any questions, please do not hesitate to get in contact.

With best regards,

Andrew Yool.

Dear Editor,

We have included new data based on the suggestions of reviewers 2 and 3 regarding the treatment of biological carbon fractionation and incorporated these results within the manuscript. Specifically, within the carbon isotope section. A new figure (4) and table (3) are introduced.

We have not included experiments suggested by reviewer 2 where remineralisation is made somewhat independent of oxygen, such that organic matter is remineralised even when oxygen is not sufficient. This suggestion was meant as a possible solution to reducing vertically expansive oxygen minimum zones, but it will require a greater effort of model development to incorporate the nitrogen cycle.

We have also taken the opportunity to clean up the manuscript by making minor edits in certain places outside of the carbon isotope section. We made a special effort is to make the description of the carbon isotope equations easier to understand and also the discussion of model-data comparison of carbon isotopes. Figures 2 and 4 (now figure 5) have been updated.

Finally, it should be noted that the lead author is now located at the Department of Earth, Ocean and Ecological Sciences, University of Liverpool, Liverpool, UK at pearse.buchanan@liverpool.ac.uk.

Thank you,

Pearse Buchanan, Richard Matear, Zanna Chase, Steven Phipps and Nathan Bindoff.

Response to Reviewer 1

Reviewer 1 provided some very generous comments of our work and we would like to thank them for those comments. The reviewer also had one primary suggestion that we agree would improve the manuscript.

Their concern about not including CESM simulations of carbon and nitrogen isotopes is valid. We have contacted the lead authors of two publications that contain model output of the nitrogen and carbon isotopes in this model.

We have subsequently heard back from Simon Yang, the author of a study using N isotopes (Yang & Gruber, 2016, Global Biogeochemical Cycle), and Alexandra Jahn, the author of a study using C isotopes (Jahn et al., 2015, Geoscientific Model Development), and have included these results in the paper.

Response to Reviewer 2 (Christopher Somes)

Christopher Somes had some specific questions and comments before publication of the manuscript could be recommended. These relate to (1) our treatment of biological fractionation in the carbon isotope routine, (2) some issues with our interpretation/discussion of results.

Page 7, lines 9-13: Biological carbon fractionation.

There should be more discussion justifying why you only account for a species effect and not aqueous CO_2 concentration (Popp et al., 1989; Rau et al., 1989) and/or phytoplankton growth rate (Laws et al., 1995). There are of course large uncertainties, but there seems to be some general relationship with aqueous CO_2 so I am surprised that this in not included in a model designed for palaeoceanography.

We have implemented this functionality and have quantified the effect of a "variable" fractionation factor (Laws 1995 relationship) versus fixed at 21 per mille.

The effect is significant in terms of absolute values of carbon isotopes, but does not have a significant effect on other measures of model skill.

Please see the altered discussion of carbon isotope model-data assessment.

Page 8: N_2 fixation fractionation.

Since N_2 fixers have a lower del15N value than the atmospheric N_2, this implies some fractionation right? Does the del15N value go into diazotrophs biomass and then remineralize or go directly into NO_3?

Yes N_2 fixers do actually fractionate when fixing N_2 to NH_4 that is then incorporated into biomass and I suppose our wording here is misleading. We have corrected the sentence to illustrate that while N_2 fixers do fractionate during their conversion of N_2 gas (with a del15N of +0.7 per mil (Klots & Benson, 1963)) to NH_4 that is incorporated into biomass (typically with a value of -1 per mille), we implicitly account for these transformations by specifying the end product.

Because we simulate NO_3 and $15NO_3$ as tracers, our calculations require solving for an implicit pool of $14NO_3$ during each reaction involving $15NO_3$. The introduction of NO_3 at a fixed del15N$_{NO_3}$ of -1 ‰ due to remineralisation of N_2 fixer biomass provides a simple example with which we can begin to describe our equations. Setting the isotopic value of newly fixed NO_3 to -1 ‰ is simple because it removes any complications associated with fractionation. We note, however, that in reality the nitrogenase enzyme does fractionate during its conversion of aqueous N_2 (+0.7 ‰) to ammonium, and that the biomass that is subsequently produced can vary substantially depending of the type of nitrogenase enzyme used (vanadium versus molybdenum based) (McRose et al., 2019). However, we choose to implicitly account for these transformations and considerably simplify them by setting the del15N of N_2 fixer biomass equal to -1 ‰, which reflects the more common Mo-nitrogenase during N_2 fixation (Sigman and Casciotti, 2001).

A del15N$_{NO_3}$ of -1 ‰ is equivalent to a $15N:14N$ ratio of 0.999 in our approach where 0 ‰ equals a 1:1 ratio of $15N:14N$. If the amount of NO_3 being added is known alongside its $15N:14N$ ratio, in this case

0.999 for N$_2$ fixation, we are able to calculate how much $_{15}$NO$_3$ is added. The derivation is as follows. We begin with two equations that describe the system.

Page 9, lines 5-20: NO$_3$ utilisation.

Please show the model equation used for the calculation of utilisation in the model (i.e. "u" in equation 15) since it is not straightforward exactly how this is calculated.

We have added an additional equation and information in the paragraph to describe what this utilisation factor is and how we calculate it.

Page 10, Table 1: UVic model.

Although the model is based on UVic, the University of Victoria group has not been involved in the C13 and N15 development. Please replace "UVic" with "UVic-MOBI" (Model of Ocean Biogeochemistry and Isotopes) and "University of Victoria" with "Oregon State University/ GEOMAR Kiel".

Corrected.

Page 10, line 22: "Weak undercurrents that are important for reducing nutrient trapping at the Equator".

Strong undercurrents and so-called nutrient trapping occur in the upper kilometre (mostly upper 400 meters), whereas your largest bias is between 1500-3000 meters, so something is missing here. I guess the main problem is that you switch off organic matter remineralisation when oxygen runs out which allows the organic matter to sink and remineralise much too deep? If so, this should be pointed out here.

We have added a sentence that makes the reader aware of our treatment of organic matter remineralisation.

Alternatively, the expansion oxygen minimum zones could be due to our conservative treatment of organic matter remineralisation (appendix A), where remineralisation will not occur when O2 and NO3 are limiting. Excess, unremineralised organic matter therefore falls deeper in the model in the oxygen-deficient zones.

~~Also, we are currently running a new experiment where this conservative remineralisation scheme is turned off to assess the effect. These could possibly be integrated within the manuscript in a few sentences, but we are undertaking new model development with this form of the model in the coming year ready for version 1.1.~~

More extensive model development will be required to address this issue, and is beyond the scope of this study. It does leave new pathways for development in subsequent versions. By acknowledging this treatment of remineralisation, we hope that the limitations of the model are more transparent.

Page 11, lines 3-7: "… far exceed reconstructions of Eide et al., (2017) .. it is possible that the upper ocean values of Eide et al., (2017) underestimate the preindustrial del13C-DIC field".

I think the robustness of the reconstruction deserves a discussion paragraph if you are going to raise this point. Perhaps there is reason to be somewhat sceptical of this reconstruction in the upper ocean. One important aspect I think they have not accounted for is the anthropogenic effect on biological uptake and remineralisation.

My C13 model simulations predict this anthropogenic effect lowers d13C by 0.5 per mil in the Pacific at 700 meters (compare "Modern" versus "Preind" differences at 15 uM NO_3 in Figure 3 of Glock et al., (2018)), which is due to phytoplankton incorporating the lighter anthropogenic CO_2 and remineralising at depth, whereas their reconstruction suggests basically negligible anthropogenic effect at these depths. Note this effect is required for my model's ability to reproduce the range of modern observations there (see Figure S5 in Glock et al., 2018) and becomes even more important as approach the surface.

Do all of the models significantly overestimate these upper ocean values? It would be really interesting if you could also run a hindcast simulation forced by observed decreasing atmospheric del13CO2 and reproduce the modern observations. If so, I think you would have a legitimate argument that errors/uncertanties in the reconstruction may be significantly contributing to the large model-data misfit. I leave this up to you if it is feasible to accomplish, but I believe it is an important issue to discuss if this dataset is going to be the standard for model comparison.
That said, I still believe your decision not to include an aqueous CO2 dependency in your phytoplankton carbon fractionation is also likely contributing to your overestimated del13DIC, since that reduces phytoplankton fractionation in the warm open ocean gyres.

First, we agree that the underestimation of d13C in the upper ocean in the Eide 2017 dataset is likely due to their neglect of biology introducing low d13C DIC via remineralisation.

Second, thank you for the reference to the Glock et al., 2018 paper. It certainly does seem that the 0.5 per mille offset near the surface (15 uM NO_3) between your PI and Modern simulations fits with the offset between the models in this study and Eide reconstruction.

Third, while it is not feasible to run hindcast/historical simulations for this study, we think that the bulk of evidence from the four models shows that the upper ocean Eide reconstruction is likely biased low, owing to the neglect of the biological introduction of low d13C. Replicate figures of Figure 3 (previously figure 2) for each model are now included in the supplement.

The following alterations to this paragraph have been made:

…However, all models performed most poorly in the Atlantic Ocean, with poor correlations, high variability and greater biases.

Returning to the consistent positive bias in the upper ocean, most models (except iCESM-low) predicted upper ocean del13CDIC >= 2.0 ‰ (Supplementary Figures S1, S2, S3 and S4) similar to CSIRO Mk3L-COAL. As each model has a unique representation of the ecosystem and consequently a unique treatment of biological fractionation, the common prediction of high upper ocean del13C suggests that the upper ocean values between 200 and 500 metres of Eide et al. (2017) may be too low. The underestimation of del13CDIC may be due to a neglect of biology introducing anthropogenic, isotopically-depleted carbon to surface and subsurface layers via remineralisation (the biological Suess effect). This would in turn suggest that a higher global mean of 0.73 ‰

generated from a global compilation of foraminiferal del13C (Schmittner et al., 2017) is perhaps a more accurate representation of preindustrial del13C values.

Page 12: Figure 2
Something seems to be wrong with your color bar scale as it does not match the contours, which I assume are correct.
True! We have corrected the figure.
We have also added the same figures but for the different models to the supp material.

Pages 13-15: Denitrification parameterisations.
It is important to be more transparent about the artificial parameterisations to account for known model biases on both water column (i.e. NO3 reduction value) and sedimentary denitrification (i.e. amplification) in the main text. I have no problem including them, but I think it is fair to at least briefly note the effect they have on your simulations (e.g. how much the global rates changes because of them).
It is not really a fair comparison to include models that include these artificial parameterisations (COAL) to models that don't (your chosen version of UVic-MOBI, PISCES). For example, our following paper with UVic-MOBI (Somes et al., 2017) with improved nitrogen cycle dynamics including sedimentary amplification better reproduces global mean del15NO3 similarly to COAL. It is not important which version of UVic-MOBI you decide to include, but these key denitrification parameterisations in COAL should be stated in the main text given its importance for del15N.
I would argue that if water column denitrification cannot react naturally to climate-induced changes to oxygen and remineralisation, it significantly limits the model's ability as a tool for palaeoceanographic research from a nitrogen isotope perspective. This has led our group to implement physical parameterisations to better mimic equatorial undercurrent (Large et al., 2001; Getzlaff & Dietze, 2013), so we do not have to rely on this artificial water column denitrification reduction parameterisation anymore. This topic should be discussed.

The points raised are important and we have included a discussion of them in the text. We have aimed to be more up front about what the limitations of the model are.

An important caveat to the del15NNO3 routines of CSIRO Mk3L-COAL should be noted. CSIRO Mk3L-COAL underwent significant tuning of water column and sedimentary denitrification parameterisations in order to reproduce known values of del15NNO3 during development. One important parameter is the lower threshold of NO3 concentration at which point water column denitrification is shut off (section A2.3). In CSIRO Mk3L-COAL this is set at 30 mmol m3, which is an arbitrary limit that was implemented to prevent water column denitrification from reducing NO3 to zero in the large suboxic zones. Hence, a caveat of the current model is an inability for water column and sedimentary denitrification to realistically adjust as suboxia changes. However, the parameterisation does allow for targeted experiments where the ratio of water column to sedimentary denitrification can be controlled if, for instance, it is unclear how water column and sedimentary denitrification respond to certain conditions. This is currently the case during the Last Glacial Maximum, where expansive suboxic zones in the Pacific (Hoogakker et al., 2018) were counterintuitively associated with lower water column denitrification (Ganeshram et al., 1995). We have, in this version, chosen to keep this parameterisation and note that future developments

will involve an option to more realistically and dynamically simulate responses to variations in suboxia.

Page 14, line 9: del15N in PISCES

Please cite the paper that describes del15N in PISCES: I am unaware of any publication on del15N in PISCES.

There is currently no paper describing del15N in PISCES. The data was given to me by Laruent Bopp, who is currently working on a GMD paper for this purpose. I will include a citation of Bopp et al., (*in prep*) if this is agreeable to the editor/journal.

Pages 17-24: Section 5. Ecosystem effects.

I liked the sensitivity experiments focusing on a few key parameters/processes. However, I think they would benefit from an extra table (or two) that summarizes their key results. There are so many numbers mentioned directly in the text, I found it difficult to "digest" them all in a comparative context.

We have included a summary table of the major biogeochemical effects (table 5).

Page 18: Variable stoichiometry.

Please cite the key studies here and refer to the specific Appendix section that describes this so readers can quickly find it.

Completed. We have also added similar pointers in the other ecosystem experiment sections.

Page 37: Acknowledgements.

Will your published code and model output be accessible to the public.

Yes. The code is already accessible at https://www.tpac.org.au/csiro-mk3l-access-request/. The data is being placed in an online repository for public access on the National Computational Infrastructure in Australia, which will be minted with its own doi.

Response to Reviewer 3

Reviewer 3 provided helpful suggestions and some very encouraging comments regarding the writing and choice of experiments. Although they had no major concerns with the work, they had minor suggestions that have been helpful to improve the manuscript.

Page 4, lines 4-5: Does running with the offline OGCM restrict experiments to steady-state / timeslice experiments? What is the speed when the OGCM is online (relevant for paleo experiments)?

Rewritten. We added the following in parentheses: "(compared to ~10 years per day in fully coupled mode)."

Page 4, lines 25-27: I found the term "phytoplankton functional types" confusing as this usually refers to ecological models that explicit plankton biomass state variables whereas this model parameterises the biological transformations of biogeochemical tracers (e.g. Hulse et al., 2017).

Rewritten. The sentence containing "phytoplankton functional types" has been replaced with a new sentence. This is:

"**Briefly, the ecosystem model simulates the production, remineralisation and stoichiometry (elemental composition) of a general phytoplankton group, diazotrophs (N$_2$ fixers) and calcifiers.**"

Figure 1: PGorg and PDorg have not been defined so were unclear until I had read more of the manuscript.

Rewritten. Number 3 is now: "
Biological uptake of nutrients and production of organic and inorganic matter. Particulate organic carbon (POC) is produced by the general phytoplankton group and N2 fixers (diazotrophs), while particulate inorganic carbon (PIC) as calcium carbonate (CaCO3) is produced by calcifiers. Export of POC by the general (G) phytoplankton group and N2 fixers (D) are herein referred to as CGorg and CDorg (see appendix A1), respectively."

Page 10, lines 1-2: There are other isotope enabled earth system models (e.g. Hulse et al, 2017, Understanding the causes and consequences of past marine carbon cycling variability through models, Earth Science Reviews, 171, pp. 349-382) but I guess these are those with comparable resolution or similar?

We acknowledge that there are other isotope enabled models out there that include box models and Earth System Models of Intermediate Complexity, but we choose to restrict our comparison to other ocean general circulation models in this instance.

We stand by our current sentence as we make no claim to an exhaustive selection.

"We make these model-data comparisons alongside other isotope-enabled ocean general circulation models (Table 1)."

Page 10, lines 5-6: I do not really understand what this sentence: "…because many solutions were cumulatively run for many tens of thousands of years over the full course of development".

Rewritten. To reduce confusion as to what this means, we have altered the text to convey the important information.

"Each experiment was run towards steady-state under pre-industrial atmospheric conditions over many thousands of years. All results presented in this paper therefore reflect tracers that have achieved an equilibrium solution. We present annual averages of the equilibrium state in the following analysis."

Page 10, lines 20-23: Is there oxygen-dependent remineralisation in the model affecting this? If so, this could be stated more explicit here, perhaps linking to the relevant part of the appendices.

Oxygen-dependent remineralisation is included in the model. We chose to conserve oxygen, nitrate and organic matter in the treatment of remineralisation in all situations, with lots of O_2 or no O_2. So, when there is no O_2, denitrification occurs, but some organic matter will go unremineralised and will fall into the grid cell below.

Conservative treatment of organic matter remineralisation in low O_2 zones therefore causes a vertical expansion of the oxygen minimum zones. However, there are many reasons to suspect that the coarse resolution ocean model is not adequately resolving the complex tropical ocean currents, and this is the true cause of the unrealistic expansion of the OMZs. In contrast, there is no reason to suspect that the rates of export production in the tropics are too large and driving too great oxygen demand. Moreover, the choice to conserve organic matter remineralisation is mechanistically important for paleoclimate simulations where different conditions evolve.

However, we acknowledge that this choice to conserve oxygen is causing a vertical expansion of the OMZs.

"Alternatively, the expansion oxygen minimum zones could be due to our conservative treatment of organic matter remineralisation (appendix A), where remineralisation will not occur when O2 and NO3 are limiting. Excess, unremineralised organic matter therefore falls deeper in the model in the oxygen-deficient zones."

Page 11, lines 4-6: It's also possible that the model is missing something. An alternative approach here might be to force the model with anthropogenic CO_2 and explicitly account for the Suess effect?

We argue that this is outside the scope of this paper. However, future work will involve historical and future scenarios that will explicitly account for the Suess effect, and also paleoclimate experiments where atmospheric $\delta^{13}CO_2$ is different.

Page 11, lines 6-7: Please elaborate on the reason why it may be an overestimate in the lower latitudes.

Rewritten.

"It is also equally possible that our fixed biological fractionation of 21 ‰ may be an overestimate in highly productive tropical regions where high growth rates lower the fractionation factor towards 15 ‰ (Laws et al., 1995)."

~~However, given the concerns of both this reviewer and reviewer 2 (Christopher Somes), we have begun new experiments that include variable biological fractionation, where values between 15 and 25 ‰ are dynamically simulated according to growth rate and [CO₂]ₐq. These experiments will take one month to complete, and so it would be possible to integrate their results within the paper if the reviewers / editor think this would be a beneficial or necessary addition.~~

These experiments are complete and have motivated alteration of our discussion of the carbon isotope model-data comparison. The new paragraph now states:

It is also equally possible that a fixed biological fractionation (ε13Cbio) of 21 ‰ may have driven unrealistic enrichment in the simulated field. High growth rates, such as occurs in the tropical regions, are thought to lower the strength of fractionation during carbon fixation (Laws et al., 1995). To explore the possibility of model-data mismatch caused by our choice to fix ε13Cbio at 21 ‰, we implemented biological fractionation that is dependent on phytoplankton growth rate and aqueous CO2 concentration (Eq. 6). We found the implementation of a variable ε13Cbio reduced high values in the upper part of the low latitude ocean, but that this reduction was small (Fig. 4). The overwhelming effect was an increase in del13CDIC throughout the interior, itself caused by weaker fractionation in the tropical ocean. Global mean del13CDIC subsequently increased by 0.25 ‰. Meanwhile, model skill was unaffected (see CSIRO Mk3L-COAL (vary-ε13Cbio) in Fig. 2). Neither fixed nor variable biological fractionation could reproduce the low upper ocean values of the data.

Tables 1&2: I find it difficult to really comprehend the comparisons in this table format. You could alternatively plot the data on Taylor Diagrams (so keeping the table data on correlation on one axis and the mean-normalised RMSE as the straight line distance) alongside Target diagrams to include the mean. See Jolliff et al., (2009) Summary diagrams for coupled hydrodynamic-ecosystem model skill assessment. Journal of Marine Systems. 76 (1-2), pp. 64-82.

We have remade both the nitrogen and carbon isotope figures into Taylor Diagrams to better convey the model skill. See figures 2 and 5.

The original tables have been altered to only convey the global and regional means.

We have also included the CESM in both comparisons.

Page 12, lines 3-4: "…suggests that the upper ocean values between 200 and 500 metres of Eide et al. (2017) are too low." Or alternatively there are structural errors common to all models?

We argue that the values of the Eide reconstruction are almost certainly too low. Observations and models both produce values in excess of 2 per mille in the upper ocean. We have added these figures to the supplementary material.

Section 4.2: Of the manuscript, I struggled with this section the most. Firstly, I was not familiar with the Schmittner paper itself and I had to go read it to find out what I needed. Secondly, I'm not sure what extra I have learned here other than the mismatches in Fig. 3 are related to mismatches between modelled DIC and observed DIC, which is not really surprising. I think the section could be improved if it included a brief description of the Schmittner calibration and a brief discussion about the challenges of relating the measures forma isotopes and the model output if this is an intended use of the model in the future.

Rewritten.

~~"We extended our assessment of modelled del13CDIC by comparing it to a compilation of benthic del13C values taken from the foraminiferal genus Cibicides (Schmittner et al., 2017), a genus on which much of the palaeoceanographic del13C records are based. For this comparison, we adjusted our predicted del13CDIC using the linear dependence on carbonate ion concentration and depth suggested by Schmittner et al. (2017): del13CCib = 0:45 + del13CDIC – 2.2x10^{-3} * CO3 – 6.6x10^{-5} * z This adjustment is necessary because the incorporation of DIC into foraminiferal tests is altered by the concentration of CO3 ions and pressure, such that a one to one comparison between del13CDIC and del13CCib introduces error. By adjusting our three-dimensional del13CDIC output using Eq. (19), we thus attain predicted del13CCib.We also computed measures of statistical fit for a traditional one to one comparison between del13CDIC and del13CCib to assess the benefit of the calibration."~~

This has subsequently been edited.

We extended our assessment of modelled del13CDIC by comparing it to a compilation of benthic del13C measured within the calcite of foraminifera from the genus Cibicides (Schmittner et al., 2017), a genus on which much of the palaeoceanographic del13C records are based. For this comparison, we adjusted our predicted del13CDIC to predicted del13CCib using the linear dependence on carbonate ion concentration and depth suggested by Schmittner et al. (2017): del13CCib = 0:45 + del13CDIC – 2.2x10^{-3} * CO3 – 6.6x10^{-5} * z

This adjustment accounts for slight fractionation during incorporation of DIC into foraminiferal calcite and is found to be partly explained by the concentration of CO3 ions and pressure. A one to one comparison between del13CDIC and del13CCib hence introduces some degree of error since this fractionation is not accounted for. Because we are interested in applying simulated del13CDIC to a palaeoceanographic context, we must first be able to convert our simulated del13CDIC to del13CCib in an effort to make better comparisons, particularly as the distribution of CO3 is subject to change. By adjusting our three-dimensional del13CDIC output using Eq. (21), we attain predicted del13CCib (see inset entitled "Calibration" in Fig. 5). For good measure, we also computed measures of statistical fit for a traditional one to one comparison between del13CDIC and del13CCib to assess the benefit of the calibration.

Page 12, eqn 18: How variable are the depths of the Cibicides d13C observations? When binning the data to the model grid, do you weight the averages by depth. I'm curious about what error could be introduced if say you compared the d13C calculated using eqn 18 with a mid-depth of the model grid-box in the equation that is 100 m in the depth for example, if the regridded observations fell predominantly in the upper part of the depth range.

The correction of modelled $DI^{13}C$ uses a depth dependent term of 6.6×10^{-5}. Thus, at a depth of 1000 meters, the depth term becomes 0.066 per mille. At 3000-4000 metres it only just begins to be significant at 0.2-0.26 per mille. So first we argue that the depth-dependent term is not the significant effect of the calibration throughout the upper ocean, compared with the CO3 term which is more of the order of 0.2 when CO3 is at 100 mmol/m3 and the constant of 0.45. Second, we argue that taking the bottom, top or mid-depth point of the ocean grid box as the depth used in the correction would have negligible effect on the fidelity of our model-data comparison. We say its negligible because using even the tallest boxes of 450 metres would generate a difference of 0.03 per mille in our model-data comparison.

Page 18: It would help to briefly outline the reasons behind the trends in C:P and N:P when using the variable stoichiometry.

Rewritten. We have added the following text after the first sentence of this section:

"Organic matter had more carbon and nitrogen per unit phosphorus in regions with low PO_4, such as the Atlantic Ocean (Fig 8a), which elevated O_2 and NO_3 demand during oxic and suboxic remineralisation, respectively. Lower ratios were produced in eutrophic regions such as the subarctic Pacific, Southern Ocean and tropical zones of upwelling. Overall, global mean C:P increased from the Redfieldian 106:1 to 117:1, causing an increase in carbon export from 7.6 to 8.0 Pg C yr^{-1}."

Page 20, lines 6-15: Is there any significance of these changes to potential paleoapplications?

Yes, but we suggest that this is covered sufficiently in the current version. We neglect to invoke specific examples of changes in nitrogen and carbon isotopes from past climates because simulations under past climate conditions were not performed. We therefore leave it to the reader to think on our results and possibly identify where interesting effects may lie.

Page 21, line 4: "loss of alkalinity", I'm guessing this in the surface ocean not the global ocean inventory?

Yes. Surface alkalinity. Clarified.

Page 22, lines 1-3: The general statement that CaCO3 production doesn't affect the isotopes much is fine but a caveat should be added: you do not have a representation of CaCO3 sediments in the model and so cannot model any subsequent changes in the alkalinity inventory due to burial/dissolution (e.g. Boudreau et al., 2018: The role of calcification in carbonate compensation, Nature Geoscience, 11 (12) pp. 894-900). These changes would be relevant over the timescales you are discussing and may drive further changes.

Agreed. This is a good point.

We have added a sentence that this a major caveat and will be addressed in future developments.

"However, we stress that version 1.0 of CSIRO Mk3L-COAL does not include CaCO3 burial or dissolution from the sediments according the calcite saturation state of overlying water (Boudreau, 2013). The neglect of ocean-sediment CaCO3 cycling means the neglect of an important aspect of the global carbon cycle active on millennial timescales Sigman et al. (2010). Changes in CaCO3 burial and dissolution could have a non-negligible effect on δ^{13}C through altering whole ocean alkalinity, which would eventually alter air-sea gas exchanges of CO2 and therein affect surface δ^{13}C. While we do not address these effects here, we aim to do so in upcoming versions of the model."

Page 29, line 24: are the results of the manuscript run with the static or variable remineralisation scheme?

Rewritten. This has been clarified by adding **(default)** to the end of these sentences in the Appendix.

Page 43, lines 38-39: Should this be the companion paper: Simulations of radiocarbonin a coarse-resolution world ocean model: 1. Steady state prebomb distributions (https://doi.org/10.1029/JC094iC06p08217)?

We interpret the reviewers suggestion as writing another paper describing the implementation of radiocarbon in the ocean model. This could be possible, but we have not attempted to do so as yet.

Ocean carbon and nitrogen isotopes in CSIRO Mk3L-COAL version 1.0: A tool for palaeoceanographic research

Pearse J Buchanan[1,2,3], Richard J Matear[2,3], Zanna Chase[1], Steven J Phipps[1], and Nathan L Bindoff[1,2,3,4]

[1]Institute for Marine and Antarctic Studies, University of Tasmania, Hobart, Tasmania, Australia.
[2]CSIRO Oceans and Atmosphere, CSIRO Marine Laboratories, G.P.O Box 1538, Hobart, Tasmania, Australia.
[3]ARC Centre of Excellence in Climate System Science, Hobart, Tasmania, Australia
[4]Antarctic Climate and Ecosystems Cooperative Research Centre, Hobart, Tasmania, Australia.

Correspondence: Pearse James Buchanan (pearse.buchanan@liverpool.ac.uk). Now at the Department of Earth, Ocean and Ecological Sciences, University of Liverpool, Liverpool, L69 3GP, United Kingdom.

Abstract. The isotopes of carbon (δ^{13}C) and nitrogen (δ^{15}N) are commonly used proxies for understanding the ocean. When used in tandem, they provide powerful insight into physical and biogeochemical processes. Here, we detail the implementation of δ^{13}C and δ^{15}N in the ocean component of an Earth system model. We evaluate our simulated δ^{13}C and δ^{15}N against contemporary measurements, place the model's performance alongside other isotope-enabled models, and document the response of δ^{13}C and δ^{15}N to changes in ecosystem functioning. The model combines the Commonwealth Scientific and Industrial Research Organisation Mark 3L (CSIRO Mk3L) climate system model with the Carbon of the Ocean, Atmosphere and Land (COAL) biogeochemical model. The oceanic component of CSIRO Mk3L-COAL has a resolution of 1.6° latitude × 2.8° longitude and resolves multi-millennial timescales, running at a rate of ∼400 years per day. We show that this coarse resolution, computationally efficient model adequately reproduces water column and coretop δ^{13}C and δ^{15}N measurements, making it a useful tool for palaeoceanographic research. Changes to ecosystem function involve varying phytoplankton stoichiometry, varying CaCO$_3$ production based on calcite saturation state, and varying N$_2$ fixation via iron limitation. We find that large changes in CaCO$_3$ production have little effect on δ^{13}C and δ^{15}N, while changes in N$_2$ fixation and phytoplankton stoichiometry have substantial and complex effects. Interpretations of palaeoceanographic records are therefore open to multiple lines of interpretation where multiple processes imprint on the isotopic signature, such as in the tropics where denitrification, N$_2$ fixation and nutrient utilisation influence δ^{15}N. Hence, there is significant scope for isotope-enabled models to provide more robust interpretations of the proxy records.

1 Introduction

Elements that are involved in reactions of interest, such as exchanges of carbon and nutrients, experience isotopic fractionation. Typically, the heavier isotope will be enriched in the reactant during kinetic fractionation, in more oxidised compounds during equilibrium fractionation, and in the denser form during phase state fractionation (i.e. evaporation). Because fractionation against one isotope relative to the other is minuscule, the isotopic content of a sample is conventionally expressed as a δ value ($\delta^h E$), where the ratio of the heavy to light element in solution (^{h}E:^{l}E) is compared to a standard ratio (^{h}E$_{std}$:^{l}E$_{std}$) in units

of per mille (‰).

$$\delta^h E = \left(\frac{{}^h E : {}^l E}{{}^h E_{std} : {}^l E_{std}} - 1 \right) \cdot 1000 \tag{1}$$

The strength of fractionation against the heavier isotope during a given reaction, ϵ, is also expressed in per mille notation. Fractionation with an ϵ equal to 10 ‰, for example, will involve 990 units of ${}^h E$ for every 1000 units of ${}^l E$ at a hypothetical

5   standard ratio (${}^h E_{std}$:${}^l E_{std}$) of 1:1. At more realistic standard ratios $<<<$ 1:1, say 0.0112372:1 for a δ^{13}C value of 0 ‰, a fractionation at 10 ‰ would involve $\sim$0.0111123 $\left(0.010 \cdot \frac{0.0112372}{1.0112372} \right)$ units of ^{13}C per unit of ^{12}C. Slightly greater preference of one isotope over another in this case involves a preference for the lighter carbon isotope (^{12}C) over the heavier (^{13}C), which enriches the remaining dissolved inorganic carbon (DIC) in ^{13}C and depletes the product. Certain isotopic preferences, or strengths of fractionation, therefore allow certain reactions to be detected in the environment.

10   The measurement of the stable isotopes of carbon (δ^{13}C) and nitrogen (δ^{15}N) have been fundamental for understanding these important elements cycle within the ocean (e.g. Schmittner and Somes, 2016; Menviel et al., 2017; Rafter et al., 2017; Muglia et al., 2018). We will now briefly introduce each isotope in turn.

The distribution of δ^{13}C is dependent on air-sea gas exchange, ocean circulation and organic matter cycling. These contributions make the δ^{13}C signature difficult to interpret, and several modelling studies have attempted to elucidate their roles

15   (Tagliabue and Bopp, 2008; Schmittner et al., 2013). These studies have shown that preferential uptake of ^{12}C over ^{13}C by biology in surface waters enforces strong horizontal and vertical gradients in δ^{13}C of DIC (δ^{13}C$_{DIC}$), greatly enriching surface waters, particularly in subtropical gyres where vertical exchange with deeper waters is restricted (Tagliabue and Bopp, 2008; Schmittner et al., 2013). Meanwhile, air-sea gas exchange and carbon speciation control the δ^{13}C$_{DIC}$ reservoir over longer timescales (Schmittner et al., 2013). Because air-sea and speciation fractionation are temperature-dependent, such that

20   cooler conditions tend to elevate the δ^{13}C$_{DIC}$ of surface waters, they also tend to smooth the gradients produced by biology by working antagonistically to them. Despite this smoothing, biological fractionation drives strong gradients at the surface, which imparts unique δ^{13}C signatures to the water masses that are carried into the interior. These insights have provided clear evidence of reduced ventilation rates in the deep ocean during glacial climates (Tagliabue et al., 2009; Menviel et al., 2017; Muglia et al., 2018).

25   δ^{15}N is determined by biological processes that add or remove fixed forms of nitrogen. It therefore records the relative rates of sources and sinks within the marine nitrogen cycle (Brandes and Devol, 2002). Dinitrogen (N$_2$) fixation is the largest source of fixed nitrogen to the ocean, the bulk of which occurs in warm, sunlit surface waters and introduces nitrogen with a δ^{15}N of approximately -1 ‰ (Sigman et al., 2009). Denitrification is the largest sink of fixed nitrogen and occurs in deoxygenated water columns and sediments. Denitrification fractionates strongly against ^{15}N at $\sim$25 ‰ (Cline and Kaplan, 1975). Fractionation

30   during denitrification is most strongly expressed in the water column where ample nitrate (NO$_3$) is available, making water column denitrification responsible for elevating global mean δ^{15}N above the -1 ‰ of N$_2$ fixers (Brandes and Devol, 2002). Meanwhile, denitrification occurring in the sediments only weakly fractionates against ^{15}N (Sigman et al., 2009), providing only a slight enrichment of δ^{15}N above that introduced by N$_2$ fixation. Variations in δ^{15}N can therefore tell us about global changes in the ratio of sedimentary to water column denitrification, with increases in δ^{15}N associated with increases in the

proportion of denitrification occurring in the water column (Galbraith et al., 2013), but it can also reflect regional changes in N_2 fixation and denitrification (Ganeshram et al., 1995; Ren et al., 2009; Straub et al., 2013).

However, nitrogen isotopes are also subject to the effect of utilisation, which makes the interpretation of $\delta^{15}N$ more complicated. Basically, when nitrogen is abundant the preference for ^{14}N over ^{15}N increases but when nitrogen is limited this preference disappears (Altabet and Francois, 2001). Complete utilisation of nitrogen therefore reduces fractionation to 0 ‰. While this adds complexity, it also imbues $\delta^{15}N$ as a proxy of nutrient utilisation by phytoplankton. As nitrogen supply to phytoplankton is controlled by physical delivery from below, changes in $\delta^{15}N$ can be interpreted as changes in the physical supply (Studer et al., 2018). Phytoplankton fractionate against ^{15}N at ∼5 ‰ (Wada, 1980) when bioavailable nitrogen is abundant. If nitrogen is utilised to completion, which occurs ~~across vast stretches~~ in much of the low to mid latitude ocean~~(Sigman et al., 2009)~~, then no fractionation will occur and the $\delta^{15}N$ of organic matter will reflect the $\delta^{15}N$ of the nitrogen that was supplied (Sigman et al., 2009). However, in the case where nitrogen is not consumed towards completion, which occurs in zones of strong upwelling/mixing near coastlines, the equator and high latitudes, the bioavailable nitrogen pool will be enriched in ^{15}N as phytoplankton preferentially consume ^{14}N. As the remaining bioavailable N is continually enriched in ^{15}N the organic matter that settles into sediments beneath a zone of incomplete nutrient utilisation will bear this enriched $\delta^{15}N$ signal. In combination with modelling (Schmittner and Somes, 2016), the $\delta^{15}N$ record is able to provide evidence for a more efficient utilisation of bioavailable nitrogen during glacial times (Martinez-Garcia et al., 2014; Kemeny et al., 2018) and a less efficient one during the Holocene (Studer et al., 2018).

Complimentary measurements of $\delta^{13}C$ and $\delta^{15}N$ provide powerful, multi-focal insights into oceanographic processes. $\delta^{13}C$ is largely a reflection of how water masses mix away the strong vertical and horizontal gradients enforced by biology, while $\delta^{15}N$ simultaneously reflects changes in the major sources and sinks of the marine nitrogen cycle and how effectively nutrients are consumed at the surface. However, the interpretation of these isotopes is often difficult. They are subject to considerable uncertainty because there are multiple processes that imprint on the measured values. Our goal is to equip version 1.0 of the CSIRO Mk3L-COAL Earth system model with oceanic $\delta^{13}C$ and $\delta^{15}N$ such that this model can be used for interpreting palaeoceanographic records. First, we introduce CSIRO Mk3L-COAL. Second, we detail the equations that govern the implementation of carbon and nitrogen isotopes. Third, we assess our simulated isotopes against contemporary measurements from both the water column and sediments and compare the model performance against other isotope-enabled models. Finally, as a first test of the model, we take the opportunity to document how changes in ecosystem functioning affect $\delta^{13}C$ and $\delta^{15}N$.

2   CSIRO Mk3L-COAL v1.0

The CSIRO Mk3L-COAL couples a computationally efficient climate system model (Phipps et al., 2013) with biogeochemical cycles in the ocean, atmosphere and land. The model is therefore based on the CSIRO Mk3L climate system model, where the "L" denotes that it is a low-resolution version of the CSIRO Mk3 model that contributed towards the Coupled Model Intercomparison Project Phase 3 (Meehl et al., 2007) and the Fourth Assessment Report of the Intergovernmental Panel on Climate Change (Solomon et al., 2007). See Smith (2007) for a complete discussion of the CSIRO family of climate models. The land

biogeochemical component represents carbon, nitrogen and phosphorus cycles in the Community Atmosphere Biosphere Land Exchange (CABLE) (Mao et al., 2011). The ocean component currently represents carbon, alkalinity, oxygen, nitrogen, phosphorus and iron cycles. The atmospheric component conserves carbon and alters its radiative properties according to changes in its carbon content. For this paper we focus on the ocean biogeochemical model (OBGCM).

5   Previous versions of the OBGCM have explored changes in oceanic properties under past (Buchanan et al., 2016), present (Buchanan et al., 2018) and future scenarios (Matear and Lenton, 2014, 2018). These studies demonstrate that the model can reproduce observed features of the global carbon cycle, nutrient cycling and organic matter cycling in the ocean. The OBGCM offers highly efficient simulations of these processes at computational speeds of ∼400 years per day when the ocean general circulation model (OGCM) is run offline (compared to ∼10 years per day in fully coupled mode). The ocean is made up of grid

10   cells of 1.6° in latitude by 2.8° in longitude, with 21 vertical depth levels spaced by 25 metres at the surface and 450 metres in the deep ocean (Table 1). The OGCM timestep is one hour, while the OBGCM timestep is 1 day. The ability of the OBGCM to reproduce large-scale dynamical and biogeochemical properties of the ocean coupled with its fast computational speed makes the OBGCM useful as a tool for palaeoceanographic research.

2.1   Ocean biogeochemical model (OBGCM)

15   The OBGCM is equipped with 13 prognostic tracers (Figure 1). These can be grouped into carbon chemistry fields, oxygen fields, nutrient fields, age tracers and nitrous oxide (N_2O). Carbon chemistry fields include dissolved inorganic carbon (DIC), alkalinity (ALK), $DI^{13}C$ and radiocarbon (^{14}C). Radiocarbon is simulated according to Toggweiler et al. (1989). Oxygen fields include dissolved oxygen (O_2) and abiotic dissolved oxygen (O_2^{abio}), a purely physical tracer from which true oxygen utilisation (TOU) can be calculated (Duteil et al., 2013). Nutrient fields include phosphate (PO_4), dissolved bioavailable iron

20   (Fe), nitrate (NO_3) and $^{15}NO_3$. Although we define the phosphorus and nitrogen tracers as their dominant species, being PO_4 and NO_3, these tracers can also be thought of as total dissolved inorganic phosphorus and nitrogen pools. Remineralisation, for instance, implicitly accounts for the process of nitrification from ammonium (NH_4) to NO_3 (Paulmier et al., 2009) and therefore implicitly includes NH_4 and nitrite (NO_2) within the NO_3 tracer. Age tracer fields include years since subduction from the surface (Age_{gbl}), and years since entering a suboxic zone where O_2 concentrations are less than 10 mmol m^{-3}

25   (Age_{omz}). Finally, N_2O in μmol m^{-3} is produced via nitrification and denitrification according to the temperature-dependent equations of Freing et al. (2012). All air-sea gas exchanges (CO_2, $^{13}CO_2$ O_2 and N_2O) and carbon speciation reactions are computed according to the Ocean Modelling Intercomparison Project phase 6 protocol (Orr et al., 2017).

Because the isotopes of carbon and nitrogen are influenced by biological processes and there is as yet no accepted standard for ecosystem model parameterisation in the community ~~(see Hülse et al., 2017, for a more detailed discussion)~~(see Hülse et al., 2017, for

30   , we provide a thorough description of the ecosystem component of the OBGCM in appendix A. Default parameters for the OBGCM are further provided in appendix B. Briefly, the ecosystem model simulates the production, remineralisation and stoichiometry (elemental composition) of three types of primary producers: a general phytoplankton group, diazotrophs (N_2 fixers) and calcifiers.

Figure 1. A conceptual representation of the ocean biogeochemical model (OBGCM). The bottom panel shows organic matter cycling involving the isotopes of carbon and nitrogen. (1) Carbon chemistry reactions. (2) Air-sea gas exchange. (3) Biological uptake of nutrients and production of organic and inorganic matter. Particulate organic carbon (POC) is produced by the general phytoplankton group and N_2 fixers (diazotrophs), while particulate inorganic carbon (PIC) as calcium carbonate ($CaCO_3$) is produced by calcifiers. Export of POC by the general (G) phytoplankton group and N_2 fixers (D; diazotrophs) are herein referred to as C_{org}^G and C_{org}^D (see appendix A1), respectively. (4) Remineralisation of sinking organic matter under oxic and suboxic conditions. (5) Sedimentary oxic and suboxic remineralisation. (6) Nitrous oxide production and consumption.
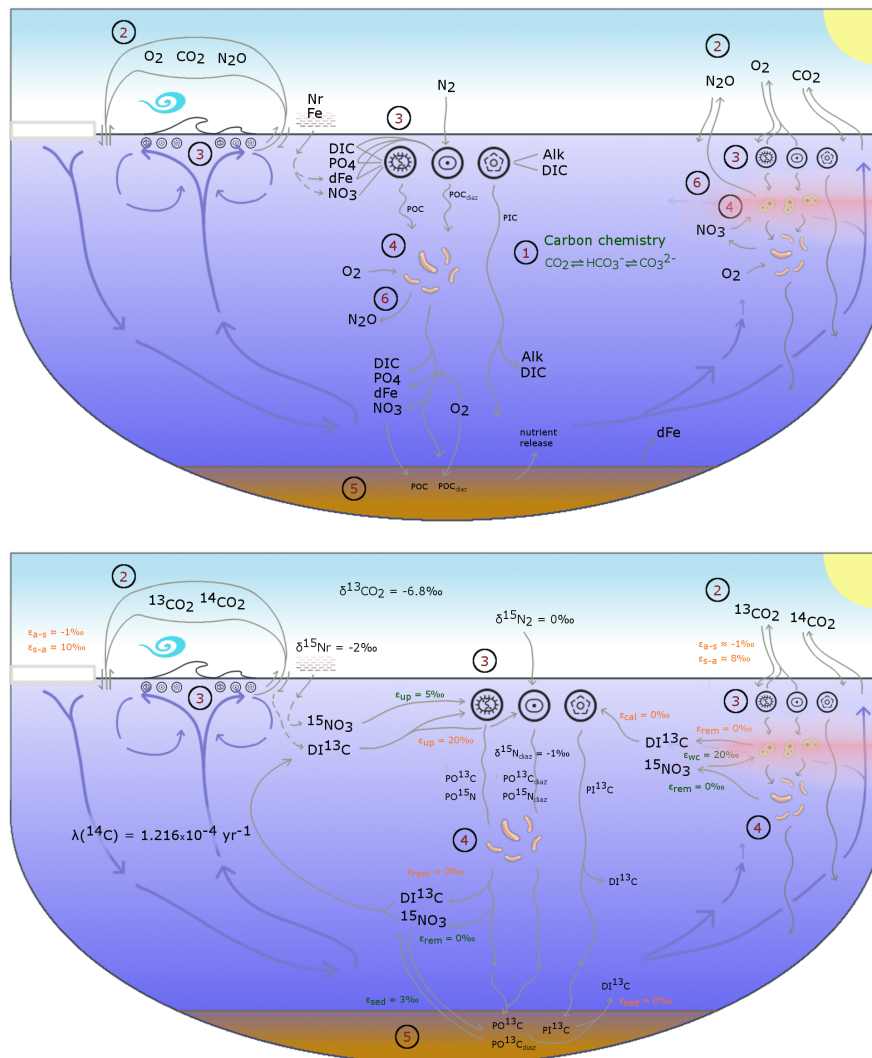
3 Carbon and nitrogen isotope equations

3.1 δ^{13}C

The OBGCM explicitly simulates the fractionation of ^{13}C from the total DIC pool, where for simplicity we make the assumption that the total DIC pool represents the light isotope of carbon and is therefore DI^{12}C. Fractionation occurs during air-sea gas exchange, equilibrium reactions and biological consumption in the euphotic zone.

The **air-sea gas exchange** of ^{13}CO$_2$ is calculated as the exchange of CO$_2$ with additional fractionation factors applied to the sea-air and air-sea components (Zhang et al., 1995; Orr et al., 2017). The flux of ^{13}CO$_2$ across the air-sea interface, $F(^{13}CO_2)$, therefore takes the form of CO$_2$ with additional terms that convert to units of ^{13}C in both environments. Without any isotopic fractionation, the equation requires the gas piston velocity of carbon dioxide in m s^{-1} (k_{CO_2}), the concentration of aqueous CO$_2$ in both mediums at the air-sea interface in mmol m^{-3} (CO$_2^{air}$ and CO$_2^{sea}$), and the ratios of ^{13}C:^{12}C in both mediums (R_{atm} and R_{sea}):

$$F(^{13}CO_2) = k_{CO_2} \cdot \left(CO_2^{air} \cdot R_{atm} - CO_2^{sea} \cdot R_{DIC} \right) \tag{2}$$

where,

$$R_{DIC} = \frac{DI^{13}C}{DI^{13}C + DI^{12}C}$$

$$R_{atm} = \frac{^{13}CO_2}{^{13}CO_2 + ^{12}CO_2} = 0.011164381$$

A transfer of ^{13}C into the ocean is therefore positive ~~,~~ and an outgassing is negative. The R_{atm} is set to a preindustrial atmospheric δ^{13}C of -6.48 ‰ (Friedli et al., 1986).

The fractionation of carbon isotopes during air-sea exchange involves three components. These are (ϵ_k^C) a kinetic fractionation that occurs during transfer of gaseous CO$_2$ into or out of the ocean, ($\epsilon_{aq \leftarrow g}^C$) a fractionation that occurs as gaseous CO$_2$ becomes aqueous CO$_2$ (is dissolved in solution), and ($\epsilon_{DIC \leftarrow g}^C$) an equilibrium isotopic fractionation as carbon speciates into dissolved inorganic carbon (DIC) constituents (H$_2$CO$_2 \Leftrightarrow$ HCO$_3^- \Leftrightarrow$ CO$_3^{2-}$). The kinetic fractionation during transfer, ϵ_k^C, is constant at 0.99912, thus ~~imparting a~~ reducing the δ^{13}C ~~signature of -0.88 ‰ to~~ of carbon entering the ocean by 0.88 ‰. Conversely, carbon outgassing increases the δ^{13}C of the ocean. The fractionation during dissolution ($\epsilon_{aq \leftarrow g}^C$) and speciation ($\epsilon_{DIC \leftarrow g}^C$) are both dependent on temperature. Fractionation during speciation is also dependent on the fraction of CO$_3^{2-}$ relative to total DIC ($f_{CO_3^{2-}}$). These fractionation factors are ~~calculated~~ parameterised as:

$$\epsilon_{aq \leftarrow g}^C = \frac{0.0049 \cdot T - 1.31}{1000} + 1 \tag{3}$$

$$\epsilon_{DIC \leftarrow g}^C = \frac{0.0144 \cdot T \cdot f_{CO_3^{2-}} - 0.107 \cdot T + 10.53}{1000} + 1 \tag{4}$$

Dissolution of CO$_2$ into ~~the ocean~~ seawater ($\epsilon_{aq \leftarrow g}^C$) therefore ~~imparts a~~ preferences the lighter isotope and lowers δ^{13}C ~~signature of between -1.32 and -1.14~~ by between 1.32 and 1.14 ‰, while the speciation of gaseous CO$_2$ into DIC ~~imparts a~~ instead preferences the heavier isotope and raises δ^{13}C ~~signature of between approximately +10 and +6.5 ‰, preferencing the heavier isotope,~~ by between 10.7 and 6.8 ‰ for temperatures between -2 and 35 °C.

These fractionation factors are applied to the gaseous exchange of CO_2 (Eq. (2)) to calculate carbon isotopic fractionation.

$$F(^{13}CO_2) = k \cdot \epsilon_k^C \cdot \epsilon_{aq\leftarrow g}^C \cdot \left(CO_2^{air} \cdot R_{atm} - \frac{CO_2^{sea} \cdot R_{DIC}}{\epsilon_{DIC\leftarrow g}^C} \right) \tag{5}$$

Because fractionation to aqueous CO_2 from DIC ($\epsilon_{aq\leftarrow DIC}^C$) is equal to $\frac{\epsilon_{aq\leftarrow g}^C}{\epsilon_{DIC\leftarrow g}^C}$, ~~we find that the fractionation associated with an outgassing of carbon to the atmosphere is greater than the fractionation during ingassing. Overall, outgassing imparts a $\delta^{13}C$ signature of approximately -12 to -8~~ a strong preference to hold the heavy isotope in solution exists ($\epsilon_{aq\leftarrow DIC}^C$ = -11.9 to -7.9 ‰ ~~to the carbon remaining in solution~~ between -2 and 35 °C). Aqueous carbon that is transferred to the atmosphere is hence depleted in ^{13}C. It is therefore the equilibrium fractionation associated with carbon speciation that is largely responsible for bolstering the oceanic $\delta^{13}C$ signature above the atmospheric signature, as it tends to shift ^{13}C towards the oxidised species (CO_3^{2-}), ~~particularly~~ a tendency that strengthens under cooler conditions.

~~The~~ In the default version of CSIRO Mk3L-COAL v1.0, the fractionation of carbon during **biological uptake** ($\epsilon_{bio}^{13}C$) is set at 21 ‰ for general phytoplankton, 12 ‰ for diazotrophs (e.g. Carpenter et al., 1997) and at 2 ‰ for the formation of calcite (Ortiz et al., 1996). However, a variable fractionation rate for the general phytoplankton group may be activated and depends on the aqueous CO_2 concentration ($CO_2(aq)$ in mmol m^{-3}) and the growth rate (μ in day^{-1}, as a function of temperature and limiting resources) following Tagliabue and Bopp (2008):

$$\epsilon_{bio}^{13}C = \left(0.371 - \frac{\mu}{CO_2(aq)} \right)/0.015 \tag{6}$$

An upper bound of 25 ‰ exists within Eq. (6) when $\frac{\mu}{CO_2(aq)}$ approaches zero, but a lower bound does not. We chose to limit $\epsilon_{bio}^{13}C$ to a minimum of 15 ‰ given the reported variations of $\epsilon_{bio}^{13}C$ from culture studies (e.g. Laws et al., 1995).

$$\epsilon_{bio}^{13}C = \max\left(15, \epsilon_{bio}^{13}C \right) \tag{7}$$

Biological fractionation of ^{13}C is then applied to the uptake and release of organic carbon.

$$\Delta DI^{13}C = R_{DIC} \cdot C_{org} \cdot \epsilon_{bio}^{13}C \left(1 - \frac{\epsilon_{bio}^{13}C}{1000} \right) \tag{8}$$

Because biological fractionation is strong for the general phytoplankton group, which dominates export production throughout most of the ocean, this imparts a negative $\delta^{13}C$ signature to the deep ocean. Subsequent remineralisation releases DIC with no fractionation. Finally, the concentration of DI^{13}C is converted into a $\delta^{13}C$ via:

$$\delta^{13}C = \left(\frac{DI^{13}C}{DIC} \cdot \frac{1}{0.0112372} - 1 \right) \cdot 1000 \tag{9}$$

where 0.0112372 is the Pee Dee Belemnite standard (Craig, 1957).

3.2 $\delta^{15}N$

The OBGCM explicitly simulates the fractionation of ^{15}N from the pool of bioavailable nitrogen. For simplicity we treat this bioavailable pool as nitrate (NO_3), where total NO_3 is the sum of $^{15}NO_3$ and $^{14}NO_3$. We therefore chose to ignore fractionation

during reactions involving ammonium, nitrite and dissolved organic nitrogen, which can vary in their isotopic composition independent of NO_3 but represent a small fraction of the bioavailable pool of nitrogen.

The isotopic signatures of N_2 fixation and atmospheric deposition, and the fractionation during water column denitrification (ϵ_{wc}^{15N}) and sedimentary denitrification (ϵ_{sed}^{15N}) determine the global $\delta^{15}N$ of NO_3 (Brandes and Devol, 2002). Biological assimilation (ϵ_{bio}^{15N}) and remineralisation are internal exchanges of the oceanic nitrogen cycle and affect the distribution of $\delta^{15}NO_3$. N_2 fixation and atmospheric deposition introduce $^{15}NO_3$ to the ocean with $\delta^{15}N$ values of -1 ‰ and -2 ‰, respectively, while biological assimilation, water column denitrification and sedimentary denitrification fractionate against $^{15}NO_3$ at 5 ‰, 20 ‰ and 3 ‰, respectively ~~(Sigman et al., 2009)~~(Sigman et al., 2009, Fig. 1).

The accepted standard ^{15}N:^{14}N ratio used to measure variations in nature is the average atmospheric ^{15}N:^{14}N ratio of 0.0036765. To minimise numerical errors caused by the OGCM, we set the atmospheric standard to 1. This scales up the $^{15}NO_3$ such that a $\delta^{15}N$ value of 0 ‰ was equivalent to an ^{15}N:^{14}N ratio of 1:1.

Because we simulate NO_3 and $^{15}NO_3$ as tracers, our calculations require solving for an implicit pool of $^{14}NO_3$ during each reaction involving $^{15}NO_3$. The introduction of NO_3 at a fixed $\delta^{15}N_{NO_3}$ of -1 ‰ due to remineralisation of N_2 fixer biomass provides a simple example with which we can begin to describe our equations. Setting the isotopic value of newly fixed NO_3 to -1 ‰ is simple because it removes any complications associated with fractionation. We note, however, that in reality the nitrogenase enzyme does fractionate during its conversion of aqueous N_2 (+0.7 ‰) to ammonium and the biomass that is subsequently produced can vary substantially depending of the type of nitrogenase enzyme used (vanadium versus molybdenum based) (McRose et al., 2019). However, we choose to implicitly account for these transformations and considerably simplify them by setting the $\delta^{15}N$ of N_2 fixer biomass equal to -1 ‰, which reflects the biomass of N_2 fixers associated with the more common Mo-nitrogenase(Sigman et al., 2009).

A $\delta^{15}N_{NO_3}$ of -1 ‰ is equivalent to a ^{15}N:^{14}N ratio of 0.999 in our approach where 0 ‰ equals a 1:1 ratio of ^{15}N:^{14}N. If the amount of NO_3 being added is known alongside its ^{15}N:^{14}N ratio, in this case 0.999 for N_2 fixation, we are able to calculate how much $^{15}NO_3$ is added. ~~The derivation is as follows.~~ We begin with two equations that describe the system.

$$NO_3 = ^{15}NO_3 + ^{14}NO_3 \tag{10}$$

$$\delta^{15}N_{NO_3} = \left(\frac{^{15}NO_3/^{14}NO_3}{^{15}N_{std}/^{14}N_{std}} - 1 \right) \cdot 1000 \tag{11}$$

Ultimately, we need to solve for the change in $^{15}NO_3$ associated with an introduction of NO_3 by ~~N_2 fixation~~**N_2 fixation**. Our knowns are the change in NO_3, the $\delta^{15}N$ of that NO_3, and the $^{15}N_{std}/^{14}N_{std}$. Our two unknowns are $^{15}NO_3$ and $^{14}NO_3$. We must solve for $^{14}NO_3$ implicitly by describing it according to $^{15}NO_3$ by rearranging Eq. (11).

$$^{14}NO_3 = ^{15}NO_3 / \left(\left(\frac{\delta^{15}N_{NO_3}}{1000} + 1 \right) \cdot ^{15}N_{std}/^{14}N_{std} \right) \tag{12}$$

This allows us to replace the $^{14}NO_3$ term in Eq. (10), such that

$$NO_3 = ^{15}NO_3 + ^{15}NO_3 / \left(\left(\frac{\delta^{15}N_{NO_3}}{1000} + 1 \right) \cdot ^{15}N_{std}/^{14}N_{std} \right) \tag{13}$$

In our example of N$_2$ fixation we know the δ^{15}N of the newly added NO$_3$ as being -1 ‰. We also know $^{15}N_{std}/^{14}N_{std}$ as equal to 1:1, or 1. Our equation is simplified.

$$NO_3 = ^{15}NO_3 + ^{15}NO_3/0.999 \tag{14}$$

We can now solve for ^{15}NO$_3$ by rearranging the equation.

$$^{15}NO_3 = \frac{0.999 \cdot NO_3}{1 + 0.999}. \tag{15}$$

The same calculation is applied to NO$_3$ addition via ~~atmospheric deposition~~ **atmospheric deposition** except at a constant fraction of 0.998 (δ^{15}N = -2 ‰), and can be applied to any addition or subtraction of ^{15}NO$_3$ relative to NO$_3$ where the isotopic signature is known.

Fractionating against ^{15}NO$_3$ during ~~biological assimilation~~ **biological assimilation** (ϵ_{bio}^{15N}), ~~water column denitrification~~ **water column denitrification** (ϵ_{wc}^{15N}) and ~~sedimentary denitrification~~ **sedimentary denitrification** (ϵ_{sed}^{15N}) involves more considerations because we must account for the preference of ^{14}NO$_3$ over ^{15}NO$_3$. We begin with an ϵ of 5 ‰ for biological assimilation. This is equivalent to an ^{15}NO$_3$:^{14}NO$_3$ ratio of 0.995 when our atmospheric standard is equal to 1:1 using the following equation.

$$\epsilon = \left(\frac{^{15}N/^{14}N}{^{15}N_{std}/^{14}N_{std}} - 1 \right) \cdot 1000 \tag{16}$$

Note that a positive ϵ value returns an ^{15}NO$_3$:^{14}NO$_3$ ratio < 1, while a negative δ^{15}N in the previous example with N$_2$ fixation also returned an ^{15}NO$_3$:^{14}NO$_3$ ratio < 1. This works because the reactions are in opposite directions. N$_2$ fixation adds NO$_3$, while assimilation removes NO$_3$. This means that 0.995 units of ^{15}NO$_3$ are assimilated per unit of ^{14}NO$_3$. As we have seen, a more useful way to quantify this is per unit of NO$_3$ assimilated into organic matter. Using Eq. (15), we find that $\sim$0.4987 units of ^{15}NO$_3$ and $\sim$0.5013 units of ^{14}NO$_3$ are assimilated per unit (1.0) of NO$_3$ when ϵ equals 5 ‰. Biological assimilation therefore leaves slightly more ^{15}N in the unused NO$_3$ pool relative to ^{14}N, which increases the δ^{15}N of NO$_3$ while creating more ^{15}N-deplete organic matter (δ^{15}N$_{org}$).

However, we must also account for the effect that NO$_3$ availability has on fractionation. The preference of ^{14}NO$_3$ over ^{15}NO$_3$ strongly depends on the availability of NO$_3$, such that when NO$_3$ is abundant the preference for the lighter isotope will be strongest. ~~However, the~~ This preference (fractionation) becomes weaker as NO$_3$ is depleted because cells will absorb any NO$_3$ that is available irrespective of its isotopic composition (Mariotti et al., 1981). Thus, as NO$_3$ is utilised, u, towards 100 % of its availability ($u = 1$), the fractionation against ^{15}NO$_3$ decreases to an ϵ of 0 ‰. This means that when u is equal to 1, no fractionation occurs and equal parts ^{15}N and ^{14}N (0.5:0.5 per unit NO$_3$) are assimilated. ~~We use~~ As we are interested in long timescales, we chose the accumulated product equations (Altabet and Francois, 2001) to approximate this process, where:

$$u = \min \left(0.999, \max \left(0.001, \frac{N_{org}}{NO_3} \right) \right) \tag{17}$$

$$\epsilon_u = \epsilon \cdot \frac{1-u}{u} \cdot \ln(1-u) \tag{18}$$

For numerical reasons, we limited the domain of u to (0.001,0.999) rather than (0,1), such that ~~for an ϵ of 5 ‰,~~ the utilisation-affected ϵ_u has a range of -4.997 to 0.035 ‰ for an ϵ of 5 ‰. ϵ_u is then converted into ratio units by dividing by 1000,

and added to the ambient ^{15}N:^{14}N of NO$_3$ in the reactant pool to determine the ^{15}N:^{14}N of the product. In this case, it is the ^{15}N:^{14}N of newly created organic matter, but could also be unused NO$_3$ effluxed from denitrifying cells in the case for denitrification.

$$^{15}N_{org}:^{14}N_{org} = {}^{15}NO_3:^{14}NO_3 + \epsilon_u \tag{19}$$

We then solve for how much ^{15}NO$_3$ is assimilated into organic matter using Eq. (15) because we now know the change in NO$_3$
5 (~~DeltaNO$_3$~~ $\underline{\Delta NO_3}$) and the ^{15}N:^{14}N of the product, which is ^{15}N$_{org}$/^{14}N$_{org}$ in our example of biological assimilation.

$$\Delta^{15}NO_3 = \frac{^{15}N_{org}/^{14}N_{org} \cdot \Delta NO_3}{1 + {}^{15}N_{org}/^{14}N_{org}} \tag{20}$$

Here, the change in ^{15}NO$_3$ is equivalent to that assimilated into organic matter. Following assimilation into organic matter, the release of ^{15}NO$_3$ through the water column during remineralisation occurs with no fractionation, such that the same δ^{15}N signature is released throughout the water column.

We apply these calculations to each reaction in the nitrogen cycle that involves fractionation (assimilation, water column
10 denitrification and sedimentary denitrification). They could be applied to any form of fractionation process with knowledge of ϵ, the isotopic ratio of the reactant, the amount of reactant that is used, and the total amount of reactant available.

4   Model performance

CSIRO Mk3L-COAL adequately reproduces the large-scale thermohaline properties and circulation of the ocean under pre-industrial conditions in numerous prior studies (Phipps et al., 2013; Matear and Lenton, 2014; Buchanan et al., 2016, 2018).
15 Rather than reproduce these studies, we concentrate here on how the biogeochemical model performs relative to measurements of δ^{13}C and δ^{15}N in the water column (Eide et al., 2017, δ^{15}N$_{NO_3}$ data courtesy of The Sigman Lab at Princeton University) and in the sediments (Tesdal et al., 2013; Schmittner et al., 2017). We make these model-data comparisons alongside other isotope-enabled ocean general circulation models (Table 1).

All analyses of model performance were undertaken using the default parameterisation of the biogeochemical model, which
20 is summarised in the tables of appendix B. Each experiment was run towards steady-state under ~~pre-industrial atmospheric conditions~~ $\underline{preindustrial\ atmospheric\ conditions\ over\ many\ thousands\ of\ years}$. All results presented in this paper therefore reflect tracers that have achieved an equilibrium solution. We present annual averages of the equilibrium state in the following analysis.

4.1 δ^{13}C of dissolved inorganic carbon (δ^{13}C$_{DIC}$)

25 The recent reconstruction of ~~pre-industrial~~ $\underline{preindustrial}$ δ^{13}C$_{DIC}$ by Eide et al. (2017) provides a large dataset for comparison. We chose this dataset over the compilation of point location water column data of Schmittner et al. (2017) because it offers a gridded product where short-term and small-scale variability are smoothed, making for more appropriate comparison with model output.

Table 1. Models assessed against isotope data. The University of Victoria - Model of Ocean Bigeochemistry and Isotopes (UVic-MOBI) fields taken from Schmittner and Somes (2016). Pelagic Interactions Scheme for Carbon and Ecosystem Studies (PISCES) fields provided by Laurent Bopp (Bopp et al., *in prep for Geoscientific Model Development*). LOch–Vecode-Ecbilt-CLio-agIsm Model (LOVECLIM) fields taken from Menviel et al. (2017). The isotope-enabled Community Earth System Model (iCESM) fields for δ^{13}C (low resolution) provided by Alexandra Jahn (Jahn et al., 2015) and those for δ^{15}N (high resolution) provided by Simon Yang (Yang and Gruber, 2016). PISCES and CESM model resolutions have a range of longitude/latitude spacings to reflect regions of finer resolution, including the equator and polar regions.

Model	Group	Lon $\times$ Lat	Vertical levels
CSIRO Mk3L-COAL	Commonwealth Scientific and Industrial Research Organisation	$2.8125° \times \sim 1.6°$	21
UVic-MOBI	Oregon State University / GEOMAR Kiel	$3.6° \times 1.8°$	19
PISCES	Nucleus for European Modelling of the Ocean	$1° \times \sim 0.05\text{-}0.95°$	75
LOVECLIM	Université catholique de Louvain	$3° \times 3°$	20
iCESM-low	National Center for Atmospheric Research	$\leq 3.4° \times \sim 3.6°$	60
iCESM-high	National Center for Atmospheric Research	$\leq 1.1° \times \leq 0.6°$	60

Predicted values of δ^{13}C$_{DIC}$ from CSIRO Mk3L-COAL broadly replicated the ~~pre-industrial~~ preindustrial distribution. The predicted global mean of 0.41 ‰ reflected that of the reconstructed mean of 0.42 ‰ (Table 2). ~~This mean is lower than the 0.64 ‰ of Schmittner et al. (2017) because Eide et al. (2017) excluded the Arctic and upper 200 metres in their reconstruction, which we adhere to in our comparison. If the Arctic and upper ocean were included the mean was 0.51 ‰.~~ Spatial agreement was acceptable with a global correlation of 0.80 (G marker in Fig. 2). Regionally, the Southern Ocean performed well with the lowest RMS error of 0.42 ‰, while a greater degree of disagreement in the values of δ^{13}C$_{DIC}$ existed in the middle and lower latitudes of each major basin, particularly in the Atlantic where model-data agreement (correlation, RMS error and normalised standard deviation) was poorest. Subsurface δ^{13}C$_{DIC}$ was too low in the tropics of the major basins by ~ 0.2 ‰, and too high in the North Pacific and North Atlantic by 0.4 to 0.6 ‰ (Fig. 3).

~~While the simulated δ^{13}C$_{DIC}$ field was generally consistent with observations, several key inconsistencies existed and were~~ These inconsistencies were likely related to physical ~~limitations of the OGCM~~and biological limitations of CSIRO Mk3L-COAL. δ^{13}C$_{DIC}$ in subsurface tropical waters was too low because restricted horizontal mixing and high carbon export drove very negative δ^{13}C$_{DIC}$ values. The very negative δ^{13}C values were associated with very large oxygen minimum zones and were thus a product of poorly represented, fine-scale equatorial dynamics. Coarse resolution OGCMs are known to have weak equatorial undercurrents that lead to oxygen minimum zones that are too large (Matear and Holloway, 1995; Oschlies, 2000) and CSIRO Mk3L-COAL is no exception. Alternatively, the large oxygen minimum zones could be due to our conservative treatment of organic matter remineralisation (appendix A), where remineralisation is prevented when O$_2$ and NO$_3$ are unavailable. ~~Excess, unremineralised organic~~ Organic matter therefore falls deeper into the interior through oxygen-deficient zones, leading to ~~a vertical expansionof O$_2$ depleted water.~~

~~Too positive~~ their vertically expansion. Almost certainly, however, it was the poorly represented dynamics within the Pacific basin that were responsible for high $\delta^{13}C_{DIC}$ in the subsurface North Pacific~~reflects the inability of the OGCM to resolve the transport of tropical subsurface waters northward, which would mix negative~~, which contains low O_2, low $\delta^{13}C_{DIC}$ ~~across the subsurface North Pacific basin. Too positive $\delta^{13}C_{DIC}$ in the North Atlantic reflects too much transport of high $\delta^{13}C_{DIC}$~~

5 ~~surface waters into the interior by North Atlantic Deep Water. Our predicted $\delta^{13}C_{DIC}$ in the upper 500 metres, in fact, appears to far exceed the reconstruction of Eide et al. (2017) and was the source of the consistent positive bias~~water due to northward transport from the tropics.

Another inconsistency was a positive bias in the upper 200-500 metres, with values exceeding 2 ‰in many areas of the lower latitudes. However, values as high as 2 ‰ have been measured in the upper 500 metres of the Indo-Pacific (Schmittner

10 et al., 2017). Given the difficulties associated with accounting for the Suess Effect (invasion of isotopically light fossil fuel CO_2) it is possible that the upper ocean values of Eide et al. (2017) underestimate the preindustrial $\delta^{13}C_{DIC}$ surface field.

It is also equally possible that ~~our~~ a fixed biological fractionation (ϵ_{bio}^{13C}) of 21 ‰ may ~~be an overestimate in highly productive tropical regions where high growth rateslower the fractionation factor towards roughly 15~~ have driven unrealistic enrichment in the simulated field. High growth rates, such as occurs in the tropical regions, are thought to lower the strength of fractionation

15 during carbon fixation (Laws et al., 1995). To explore the possibility of model-data mismatch caused by our choice to fix ϵ_{bio}^{13C} at 21 ‰ ~~(Laws et al., 1995). Weaker biological fractionation in the tropics would also tend to elevate the anomalously low~~, we implemented biological fractionation that is dependent on phytoplankton growth rate and aqueous CO_2 concentration (Eq. 6). We found the implementation of a variable ϵ_{bio}^{13} reduced high values in the upper part of the low latitude ocean, but that this reduction was small (Fig. 4). The overwhelming effect was an increase in $\delta^{13}C_{DIC}$ ~~within oxygen minimum~~

20 ~~zones.~~ throughout the interior, itself caused by weaker fractionation in the tropical ocean. Global mean $\delta^{13}C_{DIC}$ subsequently increased by 0.25 ‰. Meanwhile, model skill was unaffected (see CSIRO Mk3L-COAL (vary-ϵ_{bio}^{13C}) in Fig. 2). Neither fixed nor variable biological fractionation could reproduce the low upper ocean values of the data.

Table 2. Comparison of global and region mean $\delta^{13}C_{DIC}$ between observations (Eide et al., 2017) and model simulations. Means are annual averages and do not include the Arctic nor the upper 200 metres of the water column. All data was regridded onto the CSIRO Mk3L-COAL gridspace.

	Global	Southern Ocean	Atlantic	Pacific	Indian
Eide et al. (2017)	**0.44 ‰**	**0.61 ‰**	**0.97 ‰**	**0.11 ‰**	**0.39 ‰**
CSIRO Mk3L-COAL	0.41 ‰	0.61 ‰	0.87 ‰	0.17 ‰	0.21 ‰
CSIRO Mk3L-COAL (vary-ϵ_{bio}^{13C})	0.67 ‰	0.81 ‰	1.04 ‰	0.47 ‰	0.53 ‰
LOVECLIM	0.44 ‰	0.57 ‰	0.74 ‰	0.23 ‰	0.45 ‰
UVic-MOBI	0.65 ‰	0.74 ‰	1.15 ‰	0.37 ‰	0.66 ‰
PISCES	0.40 ‰	0.57 ‰	0.89 ‰	0.09 ‰	0.44 ‰
iCESM-low	0.37 ‰	0.61 ‰	0.84 ‰	0.01 ‰	0.45 ‰

12

~~We can~~

It is helpful to place our predicted $\delta^{13}C_{DIC}$ alongside those of other global ocean models (Fig. 2; Table 2), both for skill assessment and to further understand the cause of the positive bias in the upper ocean. We take annually averaged, ~~pre-industrial~~ preindustrial $\delta^{13}C_{DIC}$ distributions from the UVic-MOBI, PISCES, LOVECLIM and iCESM-low biogeochemical models,

5   most of which have been used in significant palaeoceanographic modelling studies (Menviel et al., 2017; Tagliabue et al., 2009; Schmittner and Somes, 2016). Predicted $\delta^{13}C_{DIC}$ performs adequately in CSIRO Mk3L-COAL relative to these state-of-the-art models. LOVECLIM showed good fit in terms of global and regional means (Table 2), but had lower correlations (Fig. 2), suggesting that its values were accurate but its distribution biased. UVic-MOBI had high correlations, but it consistently overestimated the preindustrial field by ∼0.2 ‰. Interestingly, the bias of UVic-MOBI, which treats biological fractionation as

10   a function of growth rate and aqueous CO_2, is similar to CSIRO Mk3L-COAL when this form of fractionation was activated (vary-ϵ_{bio}^{13C}). PISCES and iCESM-low were the best performing models, equally demonstrating high correlations, low biases, accurate regional and global means and the lowest RMS errors. This is perhaps not surprising considering the significantly finer vertical resolutions of these OGCMs and their more complex horizontal grid structure that enables an improved representation of ocean dynamics (Table 1). However, all models performed most poorly in the Atlantic Ocean, with poor correlations, high

15   variability and greater biases~~, and~~.

Returning to the consistent positive bias in the upper ocean, most models (except iCESM-low) predicted upper ocean $\delta^{13}C_{DIC} \geq 2.0$ ‰ (Supplementary Figures S1, S2, S3 and S4) similar to CSIRO Mk3L-COAL. As each model has a unique representation of the marine ecosystem and consequently a unique treatment of biological fractionation, the common prediction of high upper ocean $\delta^{13}C$ once more suggests that the upper ocean values between 200 and 500 metres of ~~(Eide et al., 2017)~~

20   Eide et al. (2017) may be too low. The underestimation of $\delta^{13}C_{DIC}$ may be due to a neglect of biology introducing anthropogenic, isotopically-depleted carbon to surface and subsurface layers ~~in the Eide et al. (2017) reconstruction.~~ via remineralisation (the biological Suess effect). This would in turn suggest that a higher global mean of 0.73 ‰ generated from a global compilation of foraminiferal $\delta^{13}C$ (Schmittner et al., 2017) is perhaps a more accurate representation of preindustrial $\delta^{13}C$ values.

25   Overall, CSIRO Mk3L-COAL performed acceptably in terms of its mean values and correlations, but had consistently greater RMS errors in major basins outside of the Southern Ocean. This indicates that CSIRO Mk3L-COAL exaggerated regional minima and maxima ~~, as discussed in the previous paragraph~~ as discussed. Despite the regional biases of CSIRO Mk3L-COAL, the comparison demonstrates that all models have strengths and weaknesses. Given its low resolution and computational efficiency, CSIRO Mk3L-COAL performs adequately among other biogeochemical models in its simulation of $\delta^{13}C_{DIC}$.

30   ## 4.2 $\delta^{13}C$ of *Cibicides* foraminifera ($\delta^{13}C_{Cib}$)

We extended our assessment of modelled $\delta^{13}C_{DIC}$ by comparing it to a compilation of benthic $\delta^{13}C$ measured within the calcite of foraminifera from the genus *Cibicides* (Schmittner et al., 2017), a genus on which much of the palaeoceanographic $\delta^{13}C$ records are based. For this comparison, we adjusted our predicted $\delta^{13}C_{DIC}$ to predicted $\delta^{13}C_{Cib}$ using the linear dependence

Figure 2. Global and regional fits between data (Eide et al., 2017) and simulated $\delta^{13}C$ of dissolved inorganic carbon displayed as Taylor Diagrams (Taylor, 2001). Shading of the markers represent normalised bias. G = Global; S = Southern Ocean (90°S - 40°S); A = Atlantic (40°S - 70°N); P = Pacific (40°S - 70°N); I = Indian (40°S - 70°N). Measures of fit do not include the Arctic nor the upper 200 metres of the water column. All data was regridded onto the CSIRO Mk3L-COAL gridspace before comparison.
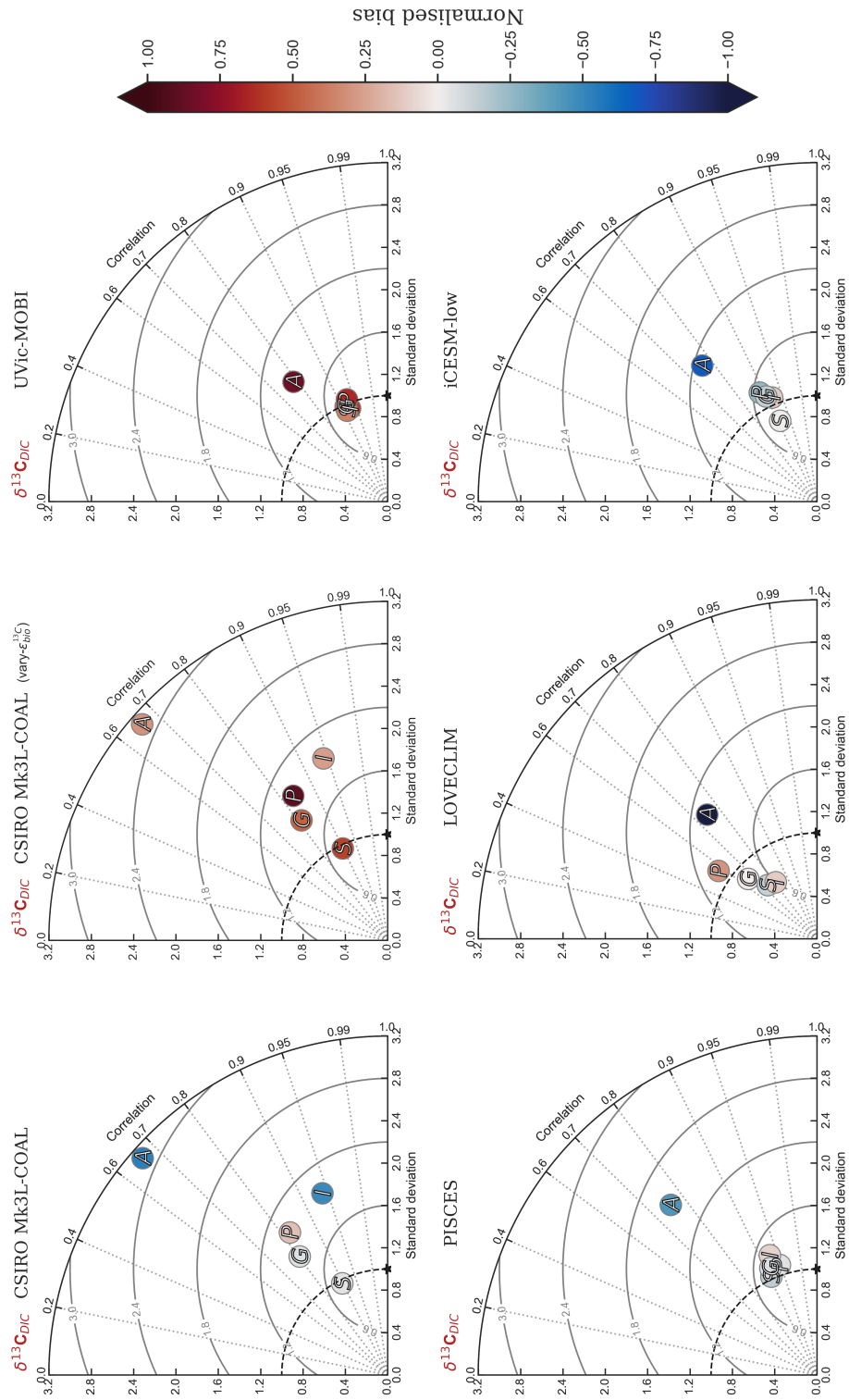
Figure 3. Zonal mean observed (top) and modelled (bottom) δ^{13}C of DIC produced by CSIRO Mk3L-COAL for each major basin. The red dashed line marks the upper 175 metres and is used for comparison between observed and modelled distributions. Replicate figures for the other models are available in the supplement.
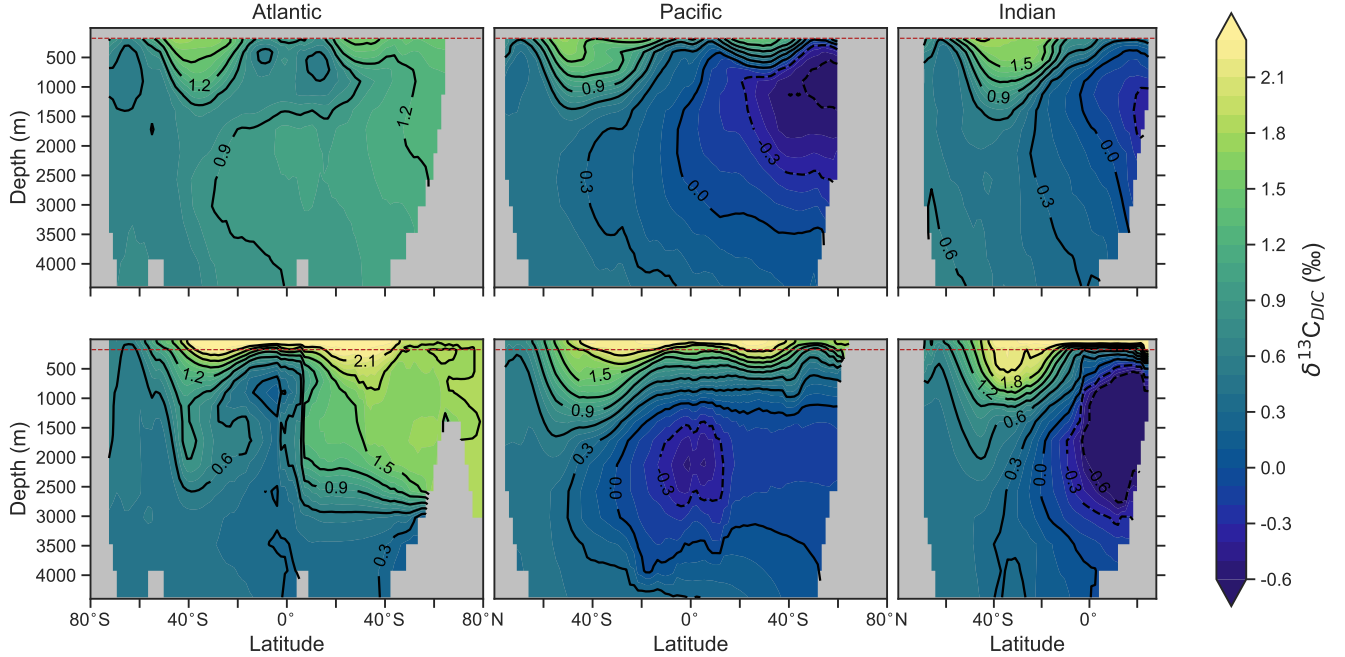
on carbonate ion concentration and depth suggested by Schmittner et al. (2017):

$$\delta^{13}C_{Cib} = 0.45 + \delta^{13}C_{DIC} - 2.2 \times 10^{-3} \cdot CO_3 - 6.6 \times 10^{-5} \cdot z \tag{21}$$

This adjustment ~~is necessary because the~~ accounts for slight fractionation during incorporation of DIC into foraminiferal calcite ~~is altered~~ and is found to be partly explained by the concentration of CO_3^{2-} ions and pressure~~, such that a~~. A one to one comparison between $\delta^{13}C_{DIC}$ and $\delta^{13}C_{Cib}$ ~~introduces unnecessary error .~~ hence introduces some degree of error since this fractionation is not accounted for. Because we are interested in applying simulated $\delta^{13}C_{DIC}$ to a palaeoceanographic context, we must first be able to convert our simulated $\delta^{13}C_{DIC}$ to $\delta^{13}C_{Cib}$ in an effort to make better comparisons, particularly as the distribution of CO_3^{2-} is subject to change. By adjusting our three-dimensional $\delta^{13}C_{DIC}$ output using Eq. (21), we ~~thus~~ attain predicted $\delta^{13}C_{Cib}$ ~~.~~ ~~We~~ (see inset entitled "Calibration" in Fig. 5). For good measure, we also computed measures of statistical fit for a traditional one to one comparison between $\delta^{13}C_{DIC}$ and $\delta^{13}C_{Cib}$ to assess the benefit of the calibration.

Measured $\delta^{13}C_{Cib}$ ~~from Schmittner et al. (2017) was~~ data from Schmittner et al. (2017) were binned into model grid boxes and averaged for the comparison. Those measurements that fell within the OGCM's land mask were excluded. Transfer and

Figure 4. The introduction of variable carbon fractionation by phytoplankton (top) and the consequent change in $\delta^{13}C_{DIC}$ represented as a zonal mean (bottom) relative to a case where ϵ_{bio}^{13C} is fixed at 21 ‰.

Variable biological carbon fractionation (ϵ_{bio}^{13C})

Variable minus static fractionation during biological assimilation
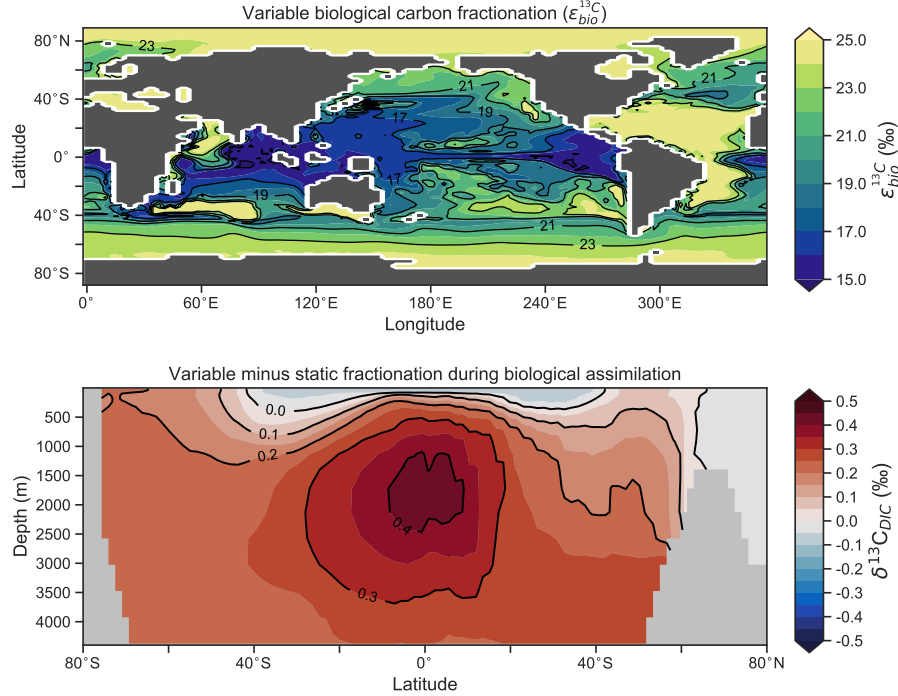
averaging onto the coarse resolution OGCM grid reduced the number of points for comparison from 1,763 to 690, lowered the mean of measured $\delta^{13}C_{Cib}$ from 0.76 ‰ to 0.52 ‰ and reduced the absolute range from -0.9→2.1 to -0.7→2.1.

Adjusted $\delta^{13}C_{Cib}$ using Eq. (21) showed good fit to measured $\delta^{13}C_{Cib}$ given the sparsity of data, with a global correlation of 0.64, a mean of 0.57 ‰ and an RMS error of 0.63 ‰ (Table 3). If a one to one relationship between $\delta^{13}C_{DIC}$ and $\delta^{13}C_{Cib}$

5 was used, the global correlation was ~~significantly worse at 0.03, despite little change in the global mean~~ ~~from 0.52 to 0.59~~ ~~‰ nor the RMS error from 0.63 to 0.67 ‰~~not affected and only slightly worse skill was detected in mean, RMS error and standard deviation. Accounting for the regional influence of carbonate ion concentration and depth ~~were therefore important~~ ~~for correcting the spatial patterns of modelled $\delta^{13}C_{Cib}$~~was therefore beneficial, likely because very negative and positive values were slightly adjusted towards the mid-range (inset in Fig. 5), but this was not necessary for an adequate comparison.

10 This conclusion was also reached by Schmittner et al. (2017). Likewise, implementing variable fractionation by phytoplankton (ϵ_{bio}^{13C}) had little effect except to increase values and slightly improve measures of skill (Table 3). Of the 690 data points used in the comparison, ~~392~~ 419 fell within the error around what could be considered a good fit (Shaded red area in Fig. 5). The error was taken as 0.29 ‰, and represents the standard deviation associated with the relationship between $\delta^{13}C_{DIC}$ with $\delta^{13}C_{Cib}$ measurements (Schmittner et al., 2017).

15 ~~Even so, some~~

16

Table 3. Statistical comparison of coretop $\delta^{13}C_{Cib}$ with predicted values produced by the CSIRO Mk3L-COAL ocean model.

	Global (N=690)			
	Average	SD	RSME	r^2
Observations	0.52 ‰	0.50 ‰	0.00 ‰	1.0
Raw comparison	0.44 ‰	0.82 ‰	0.67 ‰	0.64
Calibration	0.49 ‰	0.76 ‰	0.63 ‰	0.64
Calibration (vary-ϵ_{bio}^{13C})	0.73 ‰	0.60 ‰	0.61 ‰	0.65

Some notable over and underestimation occurred in the adjusted $\delta^{13}C_{Cib}$ output that more or less mirrored those inconsistencies previously discussed for $\delta^{13}C_{DIC}$. Values as low as -1.9 ‰, well below measured $\delta^{13}C_{Cib}$ minima of -0.7 ‰, existed in the equatorial subsurface Pacific and Indian Oceans (i.e. where the oxygen minimum zones existed). This can be seen in figure 5, where some values in the equatorial band are well below the shaded region of good fit. Meanwhile, very high values

5   of $\delta^{13}C_{Cib}$ were predicted in Arctic surface waters. The exaggeration of these local minima and maxima reflect those found in the modelled $\delta^{13}C_{DIC}$ distribution. Despite these local inconsistencies, CSIRO Mk3L-COAL shows good potential for direct comparisons to palaeoceanographic data sets of foraminiferal $\delta^{13}C$ ~~following calibrationusing carbonate ion concentration and depth~~with or without calibration.

4.3 $\delta^{15}N$ of nitrate ($\delta^{15}N_{NO_3}$)

10   We produced univariate measures of fit by comparing measurements of $\delta^{15}N_{NO_3}$ with equivalent values from CSIRO Mk3L-COAL at the nearest point (Fig. 6; Table 4). Measured $\delta^{15}N_{NO_3}$ were collected over a 30 year period using a variety of collection and measurement methods with a distinct bias towards the Atlantic Ocean. To try and remove some temporal and spatial bias, we binned and averaged measurements into equivalent model grids.

Table 4. Comparison of global and region mean $\delta^{15}N_{NO_3}$ between observations and model simulations. Model means are annual averages. All data was regridded onto the CSIRO Mk3L-COAL gridspace. The $\delta^{15}N$ data (5,330 measurements courtesy of The Sigman Lab, Princeton University) was binned into corresponding grid boxes and averaged for direct comparison, which reduced the data to 2,532 points. More than one data point of $\delta^{15}N$ may therefore contribute to each simulated value.

	Global	Southern Ocean	Atlantic	Pacific	Indian
data	**5.4 ‰**	**5.3 ‰**	**4.8 ‰**	**6.8 ‰**	**6.7 ‰**
CSIRO Mk3L-COAL	5.5 ‰	5.4 ‰	4.7 ‰	7.8 ‰	5.2 ‰
UVic-MOBI	6.6 ‰	5.5 ‰	6.2 ‰	7.6 ‰	7.4 ‰
PISCES	4.3 ‰	4.6 ‰	3.7 ‰	5.6 ‰	5.1 ‰
iCESM-high	6.2 ‰	5.3 ‰	5.2 ‰	8.6 ‰	6.2 ‰

**Figure 5.** Measured versus modelled $\delta^{13}C_{Cib}$ (N = 690) of CSIRO Mk3L-COAL coloured by latitude. Red shading about the 1:1 line is an estimate of the variability implicit in the relationship between $\delta^{13}C_{Cib}$ and $\delta^{13}C_{DIC}$ of Schmittner et al. (2017). The inset at the bottom right shows the effect of the calibration of Eq. (21).
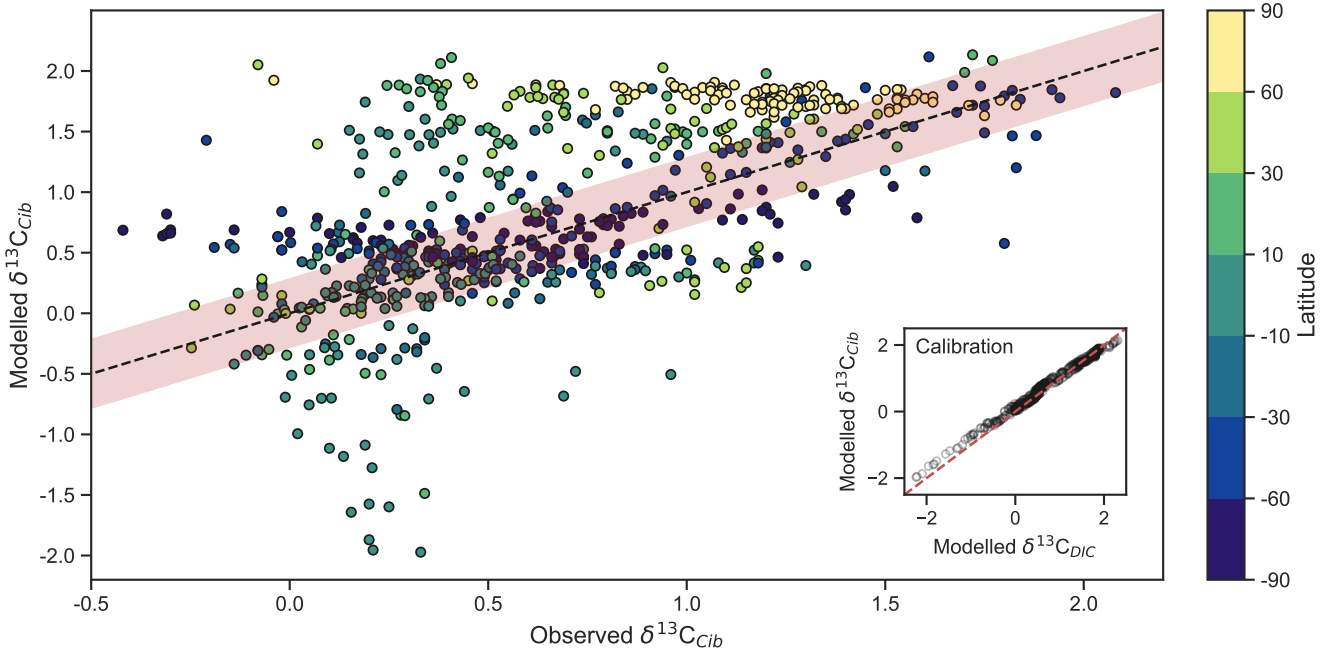

CSIRO Mk3L-COAL adequately reproduced the global patterns of $\delta^{15}N_{NO_3}$. We found excellent agreement in the volume-weighted means of $\delta^{15}N_{NO_3}$ (Table 4). Tight agreement in the means was a consequence of reproducing similar values where the majority of observed data existed. Most $\delta^{15}N_{NO_3}$ measurements have been taken from the upper 1,000 meters in the North Atlantic where values cluster at just under 5 ‰ (see lefthand panels in Fig. 7). Closer inspection of the Atlantic using depth and zonally averaged sections (Figs. 8 and 9) revealed that the model adequately reproduced the low $\delta^{15}N$ signature of ~4 ‰ caused by N$_2$ fixation occurring in the tropical Atlantic (Marconi et al., 2017). A basin-wide rate of Atlantic N$_2$ fixation equal to ~33 Tg N yr^{-1} lowered Atlantic values below 5 ‰ and was fundamental for reproducing the observations. Outside the Atlantic where data is more sparse, the model successfully reproduced the meridional gradients across the Antarctic, Subantarctic and Subtropical zones, the subsurface $\delta^{15}N_{NO_3}$ maxima in the tropics of all major basins, and the tongues of high and low values in surface waters of the Pacific consistent with changes in nitrate utilisation (Figs. 8 and 9).

Some important regional inconsistencies between the simulated and measured values did exist (refer to Figs. 8 and 9) and degraded the correlation. Much like the high values of $\delta^{13}C_{DIC}$ that were transported too deeply into the North Atlantic interior, a low $\delta^{15}N_{NO_3}$ signature was transported too far into the deep North Atlantic. CSIRO Mk3L-COAL therefore unde-

Figure 6. Global and regional fits between observations and simulated $\delta^{15}N_{NO_3}$ displayed as Taylor Diagrams (Taylor, 2001). Shading of the markers represent normalised bias. G = Global; S = Southern Ocean (90°S - 40°S); A = Atlantic (40°S - 70°N); P = Pacific (40°S - 70°N); I = Indian (40°S - 70°N). The $\delta^{15}N$ data (5,330 measurements courtesy of The Sigman Lab, Princeton University) was binned into corresponding grid boxes and averaged for direct comparison, which reduced the data to 2,532 points. More than one data point of $\delta^{15}N$ may therefore contribute to each simulated value.
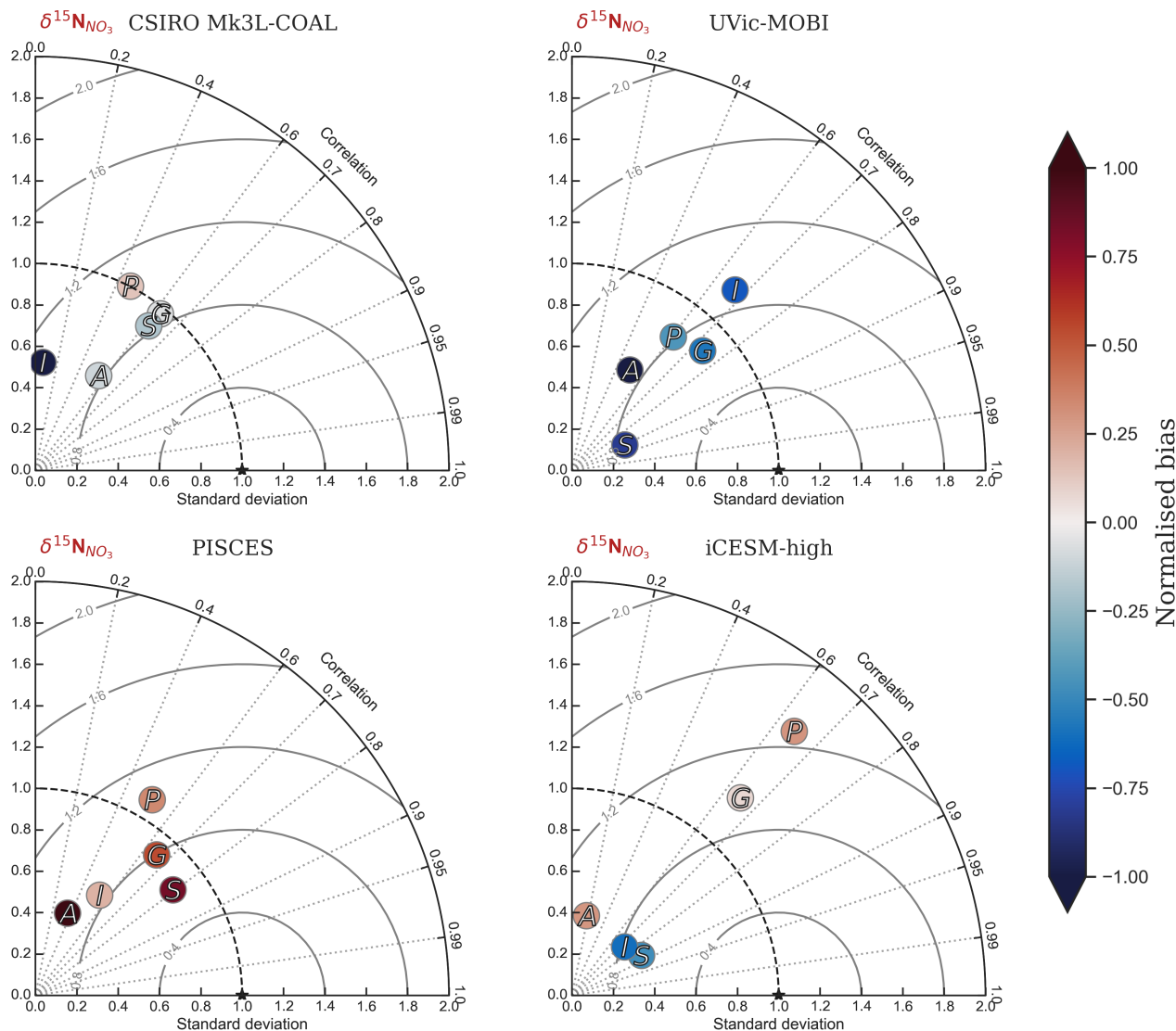
Figure 7. Observed (left) and modelled (right) δ^{15}N of NO_3 data (N = 5,004) plotted against depth (a and b), latitude (c and d) and longitude (e and f). Colour shading represents the density of data, such that the darker a mass of data points is the more data is represented there.
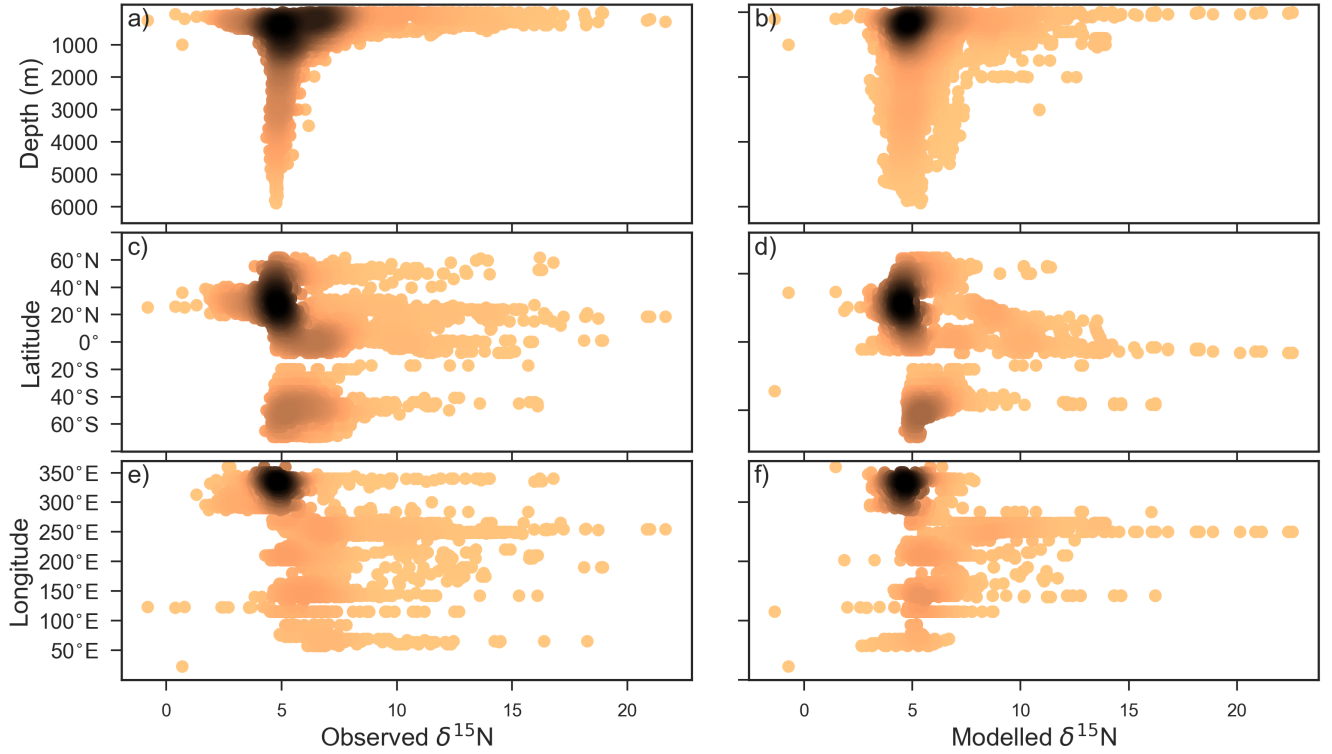
restimated deep $\delta^{15}N_{NO_3}$ before mixing through to the South Atlantic restored values towards the measurements. Subsurface values in the North Pacific were also underestimated, which can be attributed to the inability of the coarse resolution OGCM to transport low O_2, high $\delta^{15}N_{NO_3}$ water northwards from the Eastern Tropical Pacific. Simulated values in the Indian Ocean, specifically near to the Arabian Sea, significantly underestimated the data because the suboxic zone was misrepresented in the
5   Bay of Bengal. Misrepresentation of the North Indian seas was responsible for very poor model-data fit in the Indian Ocean (Fig. 6). Meanwhile, the deep (> 1,500 metres) Eastern Tropical Pacific tended to overestimate the data, owing to a large, deep, unimodal suboxic zone. These physically-driven inconsistencies in the oxygen field are common to other coarse resolution models (Oschlies et al., 2008; Schmittner et al., 2008), and like the $\delta^{13}C$ distribution, were the main cause of the misfit between simulated and observed $\delta^{15}N_{NO_3}$. The correlations reflected these regional under and overestimations, particularly in
10   the Indian Ocean.

Finally, we placed CSIRO Mk3L-COAL in the context of other isotope-enabled global models: UVic-MOBI, PISCES and iCESM-high (Table 1). This comparison demonstrated that the modelled distribution of $\delta^{15}N_{NO_3}$ was adequately placed among

Figure 8. Depth averaged sections of modelled (colour contours) and observed (overlaid markers) $\delta^{15}N_{NO_3}$.
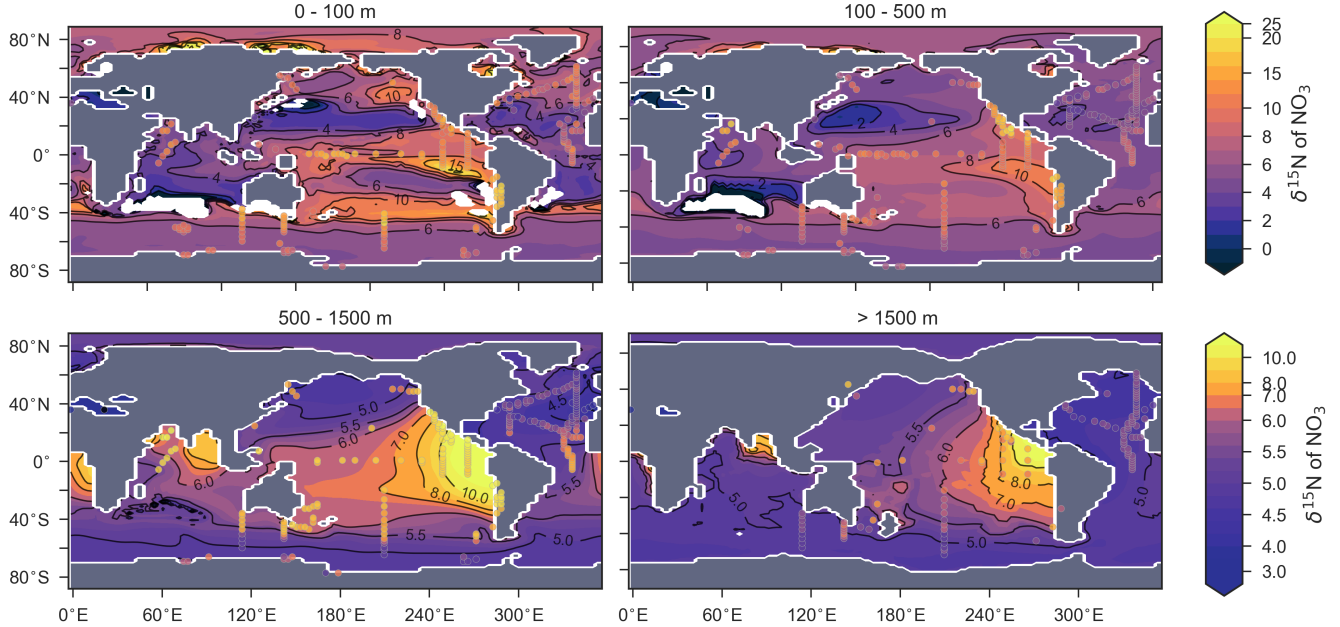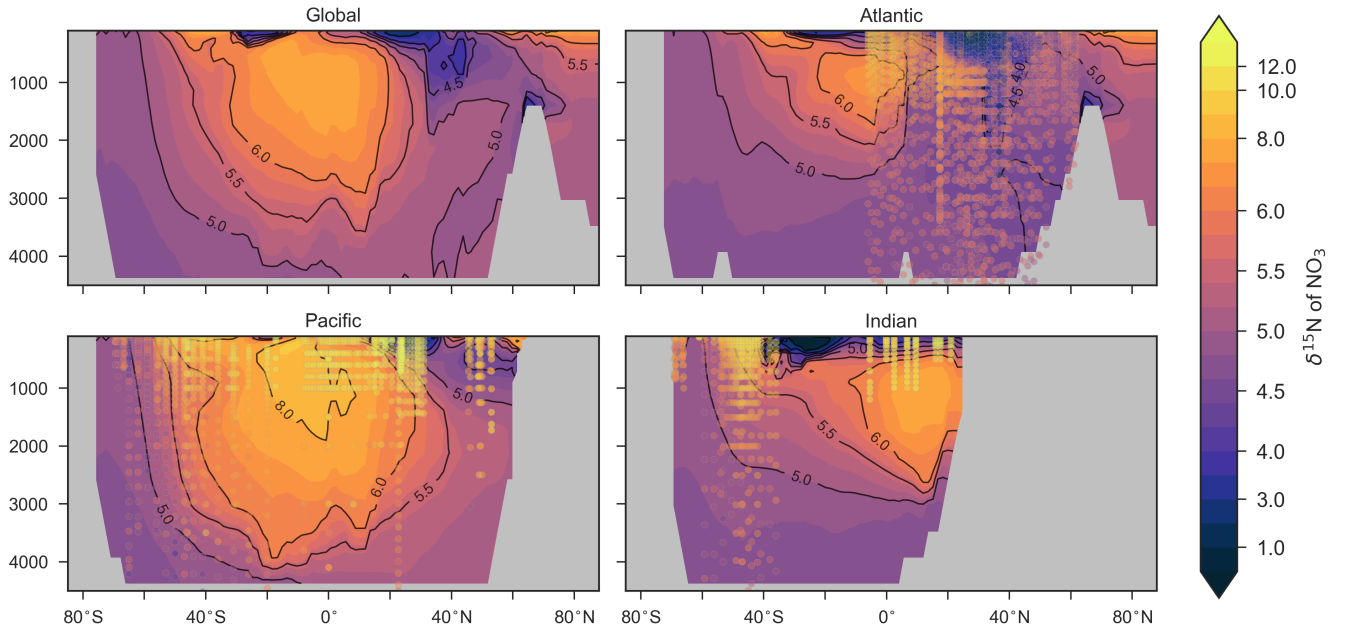

the current generation of models. The global and regional means were more accurately reproduced by CSIRO Mk3L-COAL than for UVic-MOBI, PISCES and iCESM-high (Table 4; also see shading in Figure 6). Atlantic $\delta^{15}N_{NO_3}$ was best reproduced by CSIRO Mk3L-COAL. Meanwhile, ~~the~~ correlations tended to be slightly lower <u>for CSIRO Mk3L-COAL</u> than UVic-MOBI and iCESM-high, and consistently lower than PISCES (Figure 6). UVic-MOBI underestimated the data, but produced high cor-

5 relations in the Southern Ocean and globally. Regionally, PISCES was best correlated to the measurements of $\delta^{15}N_{NO_3}$ of the three models, although it had a consistent positive bias. iCESM-high was acceptably correlated to the data in the global sense, but was highest in RMS errors, particularly in the Pacific. CSIRO Mk3L-COAL therefore showed an acceptable measure of fit to the noisy and sparse $\delta^{15}N_{NO_3}$ data and reproduced most regional patterns, albeit with misrepresentation in the Indian Ocean and some exaggerations of local minima/maxima as discussed. Future model-data comparisons with CSIRO Mk3L-COAL ~~in~~

10 ~~both a model and palaeoceanographic setting~~ should therefore take these limitations into account. Overall, however, we find that CSIRO Mk3L-COAL broadly reproduced the $\delta^{15}N_{NO_3}$ data. Annual rates of N$_2$ fixation, water column denitrification and sedimentary denitrification at roughly 122, 52 and 78 Tg N yr^{-1}, respectively, produced this agreement.

An important caveat to the $\delta^{15}N_{NO_3}$ routines of CSIRO Mk3L-COAL should be noted. CSIRO Mk3L-COAL underwent significant tuning of water column and sedimentary denitrification parameterisations in order to reproduce known values of

15 $\delta^{15}N_{NO_3}$ during development. One important parameter is the lower threshold of NO$_3$ concentration at which point water column denitrification is shut off (section A2.3). In CSIRO Mk3L-COAL this is set at 30 mmol m^{-3}, which is an arbitrary

21

Figure 9. Zonally averaged sections of modelled (colour contours) and observed (overlaid markers) $\delta^{15}\text{N}_{NO_3}$. The global zonal average encompasses all basins.

limit that was implemented to prevent water column denitrification from reducing NO_3 to zero in the large suboxic zones. Hence, a caveat of the current model is an inability for water column and sedimentary denitrification to realistically adjust as suboxia changes. However, the parameterisation does allow for targeted experiments where the ratio of water column to sedimentary denitrification can be controlled if, for instance, it is unclear how water column and sedimentary denitrification respond to certain conditions. This is currently the case during the Last Glacial Maximum, where expansive suboxic zones in the Pacific (Hoogakker et al., 2018) were counter-intuitively associated with ~~lower~~ reduced rates of water column denitrification (Ganeshram et al., 1995). We have, in this version, chosen to keep this parameterisation and note that future developments will ~~involve an option to more realistically and dynamically simulate~~ focus on dynamic responses to variations in suboxia.

4.4 $\delta^{15}\text{N}$ of organic matter ($\delta^{15}\text{N}_{org}$)

CSIRO Mk3L-COAL tracks the $\delta^{15}\text{N}$ signature of organic matter ($\delta^{15}\text{N}_{org}$) that is deposited in ~~sediments of the model~~the sediments. We compared the simulated $\delta^{15}\text{N}_{org}$ to the coretop compilation of Tesdal et al. (2013) with 2,176 records of $\delta^{15}\text{N}_{org}$. These records were binned and averaged onto the CSIRO Mk3L-COAL ocean grid, such that the 2,176 records became 592. When comparing sediment coretop measurements of $\delta^{15}\text{N}$ to that of the model, it is necessary to consider how $\delta^{15}\text{N}_{org}$ is altered by early burial. As records in the compilation of Tesdal et al. (2013) are from bulk nitrogen, we can assume

22

that the "diagenetic offset" as described by Robinson et al. (2012) is active. The diagenetic offset involves an increase in the δ^{15}N of sedimentary nitrogen of between 0.5 and 4.1 ‰ relative to that of ~~sinking~~ particulate organic matter ~~sinking towards the sediments within the water column~~ and appears to be ~~have a relationship with pressure (Robinson et al., 2012)~~related to pressure (Robinson et al., 2012), although the reasoning behind this relationship remains to be defined.

5 In light of the diagenetic offset, we make three comparisons with the compilation of Tesdal et al. (2013). A raw comparison is made, alongside an attempt to account for the diagenetic offset using two depth-dependent corrections (Table 5 and Fig. 10):

$$\delta^{15}N_{org}^{cor:1} = \begin{cases} \delta^{15}N_{org}, & \text{if } z(km) < 1km \\ \delta^{15}N_{org} + \left(1 \cdot z(km) + 1\right), & \text{if } z(km) \geq 1km \end{cases} \tag{22}$$

$$\delta^{15}N_{org}^{cor:2} = \delta^{15}N_{org} + 0.9 \cdot z(km) \tag{23}$$

The first correction ($\delta^{15}\text{N}_{org}^{cor:1}$) is taken from Robinson et al. (2012), while the second ($\delta^{15}\text{N}_{org}^{cor:2}$) originates from how Schmittner and Somes (2016) treated sedimentary nitrogen isotope data in their study of the ~~last glacial maximum~~Last Glacial Maximum. Both are based on the observation that the diagenetic offset increases with pressure, in this case represented by

10 depth (z) in kilometres (km).

Following binning and averaging onto the model grid, the raw comparison immediately showed a consistent underestimation of the coretop data, with a predicted mean of 2.7 ‰ well below the observed mean of 4.7 ‰. Our correlation was 0.27, which indicates a limited ability to replicate regional patterns. This underestimation and low correlation is easily seen when predicted values are compared directly to the coretop data in Fig. 10. ~~However, like~~ Like the nitrogen isotope model of Somes et al.

15 (2010), we find that the offset between simulated and observed coretop bulk $\delta^{15}\text{N}_{org}$ is roughly equivalent to the observed average diagenetic offset of $\sim 2.3 \pm 1.8$ ‰. This indicates that diagenetic alteration of $\delta^{15}\text{N}_{org}$ is active during early burial in the coretop data.

Including a diagenetic offset therefore improved agreement between our predicted $\delta^{15}\text{N}_{org}$ and the coretop data considerably (Table 5 and Fig. 10). Both corrections accounted for the enrichment of δ^{15}N in deeper regions and the minor diagenetic

20 alteration in areas of high sedimentation that typically occur in shallower sediments. The average $\delta^{15}\text{N}_{org}$ increased to 4.5 ‰ for $\delta^{15}\text{N}_{org}^{cor:1}$ and 5.2 ‰ for $\delta^{15}\text{N}_{org}^{cor:2}$. Correlations increased from 0.27 to 0.47 and 0.53, respectively. The improvement was clearly observed in the Southern Ocean, where both the magnitude and spatial ~~patterns~~pattern of $\delta^{15}\text{N}_{org}$ were well replicated by the model. Changes in the Southern Ocean over glacial-interglacial cycles reflect shifts in the global marine nitrogen cycle and nutrient utilisation (Martinez-Garcia et al., 2014; Studer et al., 2018), and the ability of CSIRO Mk3L-COAL to account

25 for these patterns in the coretop data is encouraging for future study. We suggest that future palaeoceanographic model-data comparisons of $\delta^{15}\text{N}_{org}$ use the depth-correction of Schmittner and Somes (2016) as it provided the best correlations and ~~maintained~~ reproduced Southern Ocean $\delta^{15}\text{N}_{org}$ at 0.5 ‰ ~~higher~~greater than the global mean (see Table 5).

Figure 10. Direct comparison of observed versus modelled $\delta^{15}N_{org}$ incident on the sediments. Left-side panels show spatial distribution of simulated $\delta^{15}N_{org}$ overlain by coretop data from the compilation of Tesdal et al. (2013). Right-side panels compare all coretop data against simulated $\delta^{15}N_{org}$. Top panels depicts raw output of the model, while the middle and bottom panels depict the predicted values of the model following two depth-dependent offsets (Eqs. (22) and (23)) that account for diagenetic alteration.
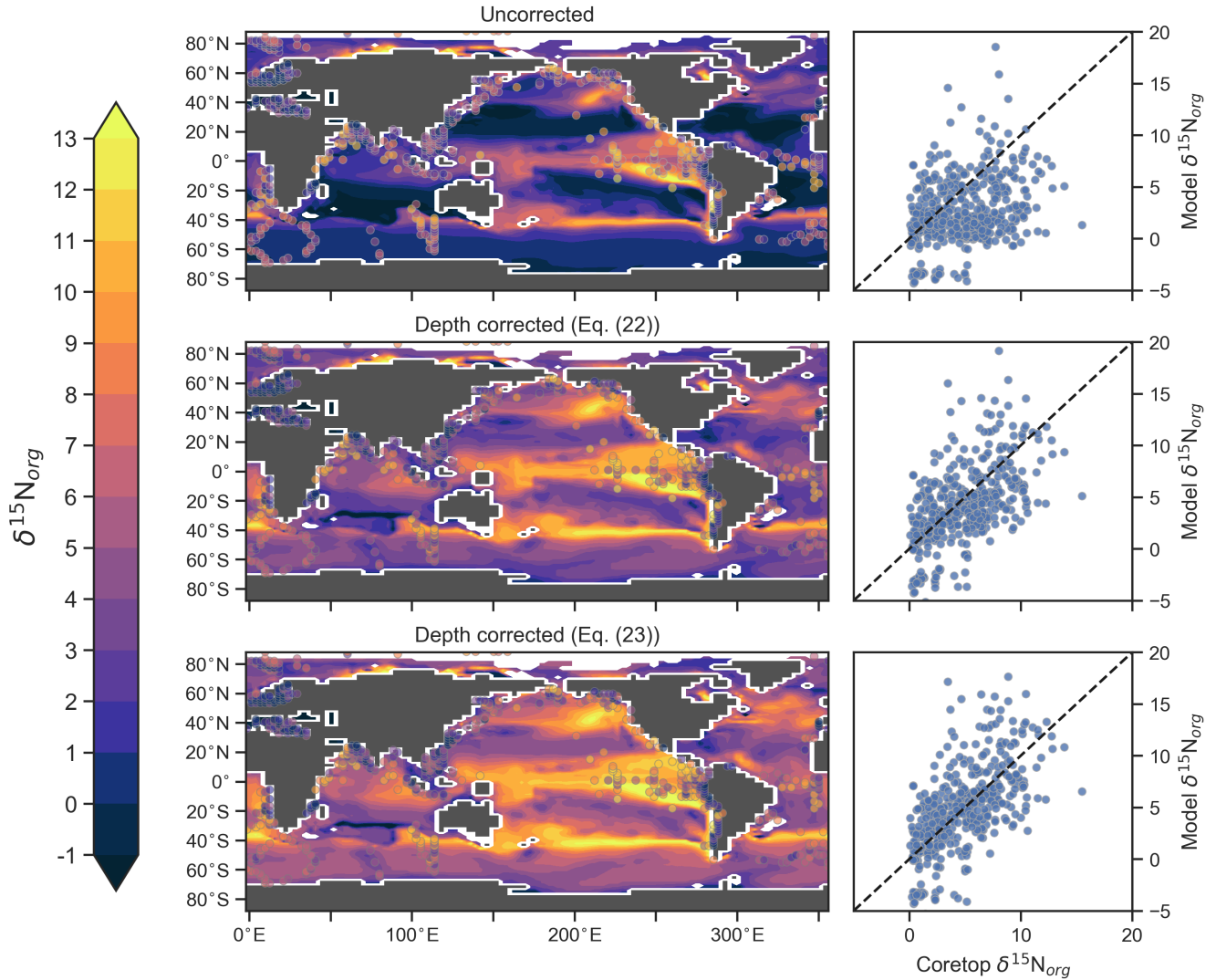
Table 5. Statistical comparison of coretop $\delta^{15}N_{org}$ with predicted values of the CSIRO Mk3L-COAL ocean model. The ~~offset to the predicted values is informed by the 1.0‰ km^{-1} + 1.0‰ relationship presented by Robinson et al. (2012) that accounts for alterations to the~~ corrected vales ($\delta^{15}N_{org}^{cor:1}$ and $\delta^{15}N_{org}^{cor:2}$) account for alteration during early diageneis following burial.

	Global (N=592)			Southern Ocean (N=81)		
	Average	SD	r^2	Average	SD	r^2
Observations	4.7‰	3.1‰	1.0	5.2‰	1.7‰	1.0
Raw comparison	2.7‰	3.2‰	0.27	1.1‰	1.6‰	0.13
$\delta^{15}N_{org}^{cor:1}$	4.5‰	3.8‰	0.47	4.3‰	1.8‰	0.45
$\delta^{15}N_{org}^{cor:2}$	5.2‰	4.2‰	0.53	5.7‰	1.9‰	0.47

5 Ecosystem effects

As a first test of the isotope-enabled ocean model, we undertook simple ecosystem experiments to assess the effect on $\delta^{13}C$ and $\delta^{15}N$. For reference, the assessment of model performance described above used model output with variable stoichiometry activated, a fixed 8% rain ratio of $CaCO_3$ to organic carbon, and a strong iron limitation of N_2 fixers that enforced a low degree

5　of spatial coupling between N_2 fixers and denitrification zones. A summary of the biogeochemical effects of the different experiments is provided in Table 6.

5.1 Variable versus Redfieldian stoichiometry

Enabling variable stoichiometry (see appendix A3) of the general phytoplankton group (P_{org}^G) over a Redfieldian ratio (C:N:P:O_2^{rem}:NO_3^{rem} = 106:16:1:-138:-94.4) altered the rate and distribution of organic matter export. Organic matter had more carbon and nitrogen

10　per unit phosphorus in regions with low PO_4, such as the Atlantic Ocean (Fig. 11a), which elevated O_2 and NO_3 demand during oxic and suboxic remineralisation (denitrification), respectively. Lower ratios were produced in eutrophic regions such as the subarctic Pacific, Southern Ocean and tropical zones of upwelling. Overall, global mean C:P increased from the Redfieldian 106:1 to 117:1 and caused an increase in carbon export from 7.6 to 8.0 Pg C yr^{-1}. Approximately 0.1 Pg C yr^{-1}, or 25 % of the increase, was attributed purely to organic carbon export from N_2 fixation, which increased from 107 to 122 Tg N

15　yr^{-1} as higher N:P ratios in the tropics broadened their competitive niche. The total contribution of N_2 fixation to the increase in carbon export was likely greater than 25 %, as NO_3 also became more available to NO_3-limited ecosystems in the lower latitudes (Moore et al., 2013). The increase in carbon export under variable stoichiometry as compared to a Redfieldian ocean was therefore felt largely in the lower latitudes between 40°S and 40°N (Fig. 11b). Export production decreased poleward of 40°, particularly in the Southern Ocean, because C:P ratios were lower than the 106:1 Redfield ratio (Fig. 11a).

20　　Distributions of both isotopes were affected by the change in carbon export and the marine nitrogen cycle. Global mean $\delta^{13}C_{DIC}$ increased from 0.52 to 0.54 ‰, and $\delta^{15}N_{NO_3}$ increased from 5.1 to 5.6 ‰. These are not great changes on the global scale and they had little influence on model-data measures of fit. However, the spatial distribution of these isotopes was

Figure 11. Simulated difference in the C:P ratio of exported organic matter due to variable stoichiometry as compared to Redfield stoichiometry (top) and the resulting change in carbon export out of the euphotic zone (bottom).
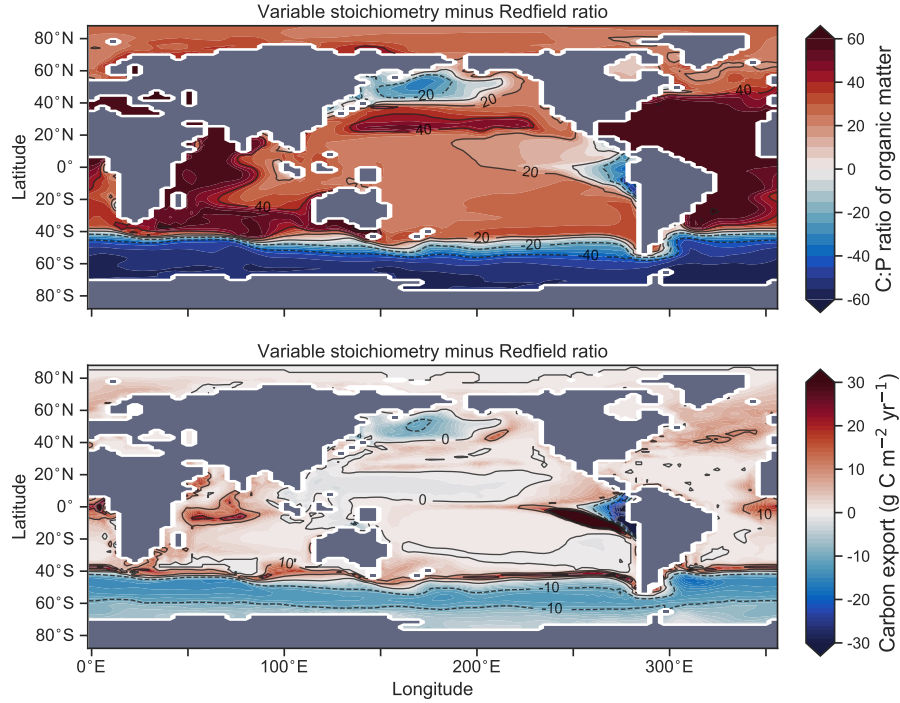
significantly altered. Intermediate waters leaving the Southern Ocean were depleted in $\delta^{13}C_{DIC}$ by up to 0.1 ‰ and $\delta^{15}N_{NO_3}$ by up to 1 ‰, while the deep ocean, particularly the Pacific, was enriched in both isotope to a similar degree (Fig. 12). Depletion of both isotope in waters subducted between 40°S and 60°S reflected the local loss in export production as a result of lower C:P and N:P ratios, such that biological fractionation was unable to enrich DIC and NO_3 in the heavier isotope to the same degree as surface waters travelled north. Enrichment of $\delta^{13}C$ in the deep ocean was the result of reduced carbon export in the Antarctic zone due to low C:P ratios, while enrichment of $\delta^{15}N$ in the deep ocean was the result of increased tropical production that increased water column denitrification ($\epsilon_{wc}^{15N} = 20$ ‰). Lower C:P and N:P ratios in both the Antarctic and Subantarctic zones therefore elicited divergent isotope effects in deep and intermediate waters leaving the Southern Ocean.

Meanwhile, each isotope showed a different response in the suboxic zones of the tropics where variable stoichiometry increased the volume of suboxia ($O_2 < 10$ mmol m^{-3}) by 0.5 %. The increase in water column denitrification caused by the expansion of suboxia increased $\delta^{15}N_{NO_3}$, while the local increase in carbon export that drove the increase in water column denitrification reduced $\delta^{13}C_{DIC}$ in the same waters (Fig. 12). Overall, the increase in low latitude carbon export caused an expansion of water column suboxia and elicited diverging behaviours in the isotopes, whereby $\delta^{15}N_{NO_3}$ increased and $\delta^{13}C_{DIC}$ decreased.

Figure 12. Differences in $\delta^{13}C_{DIC}$ (top) and $\delta^{15}N_{NO_3}$ (bottom) as a result of variable stoichiometry as compared to Redfield stoichiometry. Values are zonal means.
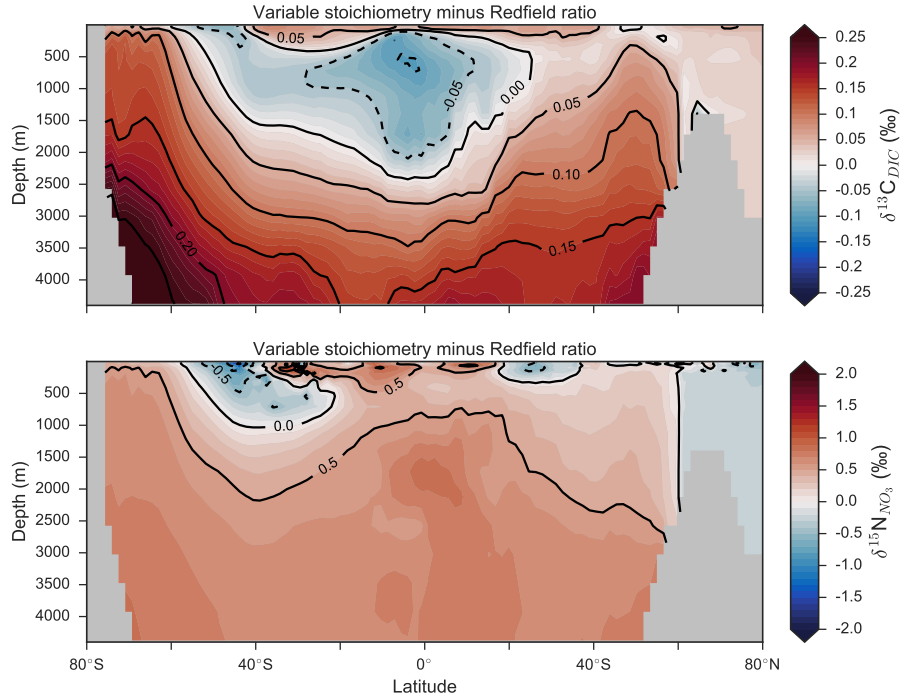
5.2 Calcifier dependence on calcite saturation state

The rate of calcification of planktonic foraminifera and coccolithophores is dependent on the calcite saturation state (Zondervan et al., 2001). In previous experiments, the production of $CaCO_3$ was fixed at a rate of 8 % per unit of organic carbon produced in accordance with the modelling study of Yamanaka and Tajika (1996) and produced 0.54 Pg $CaCO_3$ yr^{-1}. Now we investigate how spatial variations in the $CaCO_3$:C_{org} ratio (R_{CaCO_3} in Eq. (A17)) affected $\delta^{13}C_{DIC}$ and $\delta^{13}C_{Cib}$ (see appendix A1.3). We applied three different values of η to Eq. (A18) to alter the quantity of $CaCO_3$ produced per unit of organic carbon (C_{org}^G) given the calcite saturation state (Ω_{ca}). The η coefficients were 0.53, 0.81 and 1.09. These numbers are equivalent to those in the experiments of Zhang and Cao (2016).

Mean R_{CaCO_3} was 4.5, 6.6 and 9.5 % and annual $CaCO_3$ production was 0.32, 0.47 and 0.68 Pg $CaCO_3$ yr^{-1} in the three experiments. Although different in total $CaCO_3$ production, the three experiments shared the same spatial patterns. Low latitude waters were high in R_{CaCO_3}, particularly the oligotrophic subtropical gyres, while high latitudes were low, particularly the Antarctic zone where ~~strong vertical mixing~~ mixing of old waters into the surface depressed the calcite saturation state (Fig. 13). These regional patterns in R_{CaCO_3} therefore had the largest effect in areas of high export production. Productive, high latitude areas like the Southern Ocean, subpolar Pacific and North Atlantic waters all produced less $CaCO_3$ when compared to an

Table 6. Summary of the biogeochemical effects of the different treatments of the ecosystem in CSIRO Mk3L-COAL. C_{org} is the total organic carbon exported from the euphotic zone composed of both general and diazotrophic phytoplankton groups ($C_{org}^{G} + C_{org}^{D}$; see appendix A1), while C_{CaCO_3} is the total export of $CaCO_3$ out of the euphotic zone. The sum of C_{org} and C_{CaCO_3} equal the global rate of carbon export referred to in the text. Sed:WC refers to the sedimentary to water column denitrification ratio. Note that the global mean $\delta^{13}C_{DIC}$ is higher than reported in Table 2 because it includes the upper 200 metres and the Arctic.

	C_{org}	C_{CaCO_3}	N_2 fix	Sed:WC	O_2	Suboxia	DIC	$\delta^{13}C_{DIC}$	$\delta^{15}N_{NO_3}$
	Pg C yr^{-1}		Tg N yr^{-1}	ratio	mmol m^{-3}	% ocean	Pg C	‰	
Variable versus Redfieldian stoichiometry (section 5.1)									
Redfield	7.08	0.52	107	1.5	187	1.5	33908	0.47	5.1
Variable	7.42	0.54	122	1.5	193	2.1	33870	0.51	5.6
Calcifier dependence on calcite saturation state (section 5.2)									
Fixed (8% of C_{org}^{G})	7.42	0.54	122	1.5	193	2.1	33870	0.51	5.6
Variable ($\eta = 0.53$)	7.41	0.32	122	1.5	193	2.1	34010	0.52	5.6
Variable ($\eta = 0.81$)	7.41	0.47	122	1.5	193	2.1	33916	0.50	5.6
Variable ($\eta = 1.09$)	7.42	0.68	122	1.5	193	2.1	33783	0.48	5.6
Strength of coupling between N_2 fixation and denitrification(section 5.3)									
Weak	7.42	0.54	122	1.5	193	2.1	33870	0.51	5.6
Moderate	7.72	0.48	144	1.9	188	2.5	34079	0.45	5.2
Strong	7.	0.46	154	2.1	187	2.7	34182	0.42	5.0

enforced 8 % rain ratio, while $CaCO_3$ production between 40°S and 40°N relative to a fixed R_{CaCO_3} of 8 % was dependent on η. The highest η coefficient of 1.09 achieved greater export of $CaCO_3$ in the mid to lower latitude regions of high export production (Fig. 13). The consequence of increasing $CaCO_3$ production in the mid-lower latitudes was a loss of upper ocean alkalinity, subsequent outgassing of CO_2 and losses in the DIC inventory. Losses in global DIC were 95 and 130 Pg C as

5   R_{CaCO_3} increased from $4.6 \rightarrow 6.6 \rightarrow 9.5$ % (Table 6), equivalent to $\frac{1}{5}^{th}$ of the glacial increase in oceanic carbon (Ciais et al., 2011).

Despite the significant changes associated with the implementation of Ω_{ca}-dependent $CaCO_3$ production, effects were negligible on both $\delta^{13}C_{DIC}$ and $\delta^{13}C_{Cib}$. Global mean $\delta^{13}C_{DIC}$ was 0.51 ‰, when R_{CaCO_3} was fixed at 8 %, and this changed to 0.52, 0.50 and 0.48 ‰ under η coefficients of 0.53, 0.81 and 1.09 (Table 6). Likewise, global mean $\delta^{13}C_{Cib}$ was 0.59 ‰, when

10   R_{CaCO_3} was fixed at 8 %, and this changed to 0.60, 0.58 and 0.55 ‰. Minimal change in $\delta^{13}C_{Cib}$ indicated minimal change in the CO_3^{2-} concentration (see Eq. (21)), which varied by ≤ 2 mmol m^{-3} between experiments. Visual inspection of the change in $\delta^{13}C_{DIC}$ and $\delta^{13}C_{Cib}$ distributions showed an enrichment of these isotopes in the upper ocean north of 40°S. Subsequent increases in η, which increased low latitude $CaCO_3$ production, magnified the enrichment. Enrichment of $\delta^{13}C_{DIC}$ and $\delta^{13}C_{Cib}$ was caused by outgassing of CO_2 as surface alkalinity decreased in response to greater $CaCO_3$ production (Fig. 14). The

Figure 13. Global distribution of CaCO$_3$ export as a percentage of organic carbon (C$_{org}$) export (top), and the change in the CaCO$_3$ production field as a result of making CaCO$_3$ production dependent on calcite saturation state ($\eta = 1.09$) compared to when it was a fixed 8 % of C$_{org}$ (bottom). Areas where export production does not occur due to severely nutrient limited conditions are masked out.
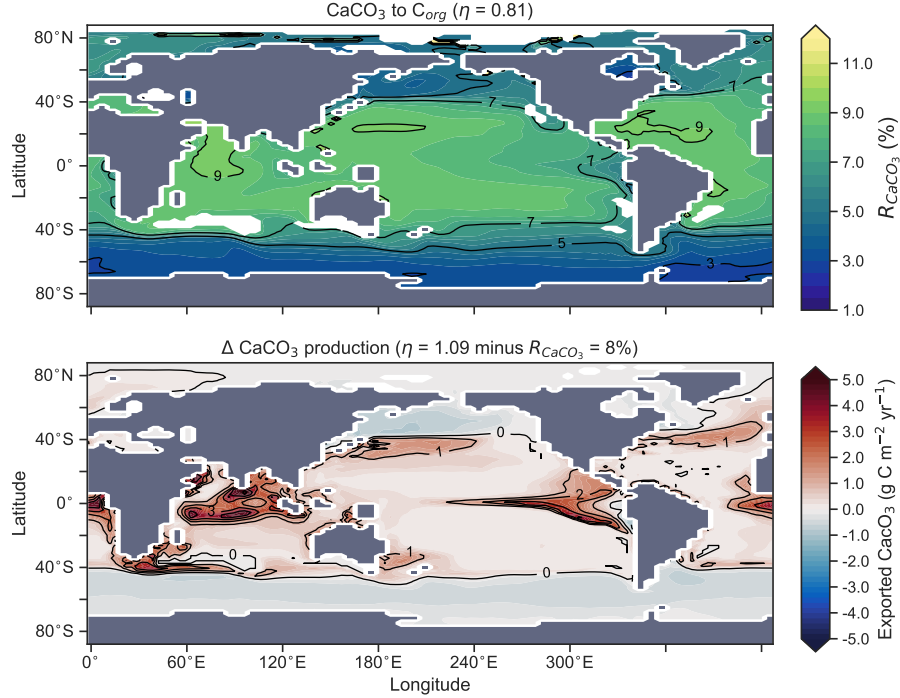
change, however, was at most 0.1 ‰, which lies well within one standard deviation of variability known in the proxy data (Schmittner et al., 2017). We therefore find little scope for recognising even large variations in global CaCO$_3$ production (0.32 to 0.68 Pg CaCO$_3$ yr^{-1}) in the signature of carbon isotopes despite considerable effects on the oceanic inventory of DIC.

However, we stress that version 1.0 of CSIRO Mk3L-COAL does not include CaCO$_3$ burial or dissolution from the sediments according the calcite saturation state of overlying water (Boudreau, 2013). To neglect ~~of~~ ocean-sediment CaCO$_3$ cycling is to neglect of an important aspect of the global carbon cycle active on millennial timescales (Sigman et al., 2010). Changes in CaCO$_3$ burial and dissolution could have a non-negligible effect on δ^{13}C through altering whole ocean alkalinity and thereby air-sea gas exchange of CO$_2$, which would in turn affect surface δ^{13}C as we have seen. While we do not address these effects here, we aim to do so in upcoming versions of the model equipped with carbon compensation dynamics.

5.3 Strength of coupling between N$_2$ fixation and denitrification

The degree to which N$_2$ fixers are spatially coupled to the tropical denitrification zones is controlled by altering the degree to which N$_2$ fixers are limited by iron (K^D_{Fe}) in Eq. (A12) (see appendix A1.2). Decreasing K^D_{Fe} ensures that N$_2$ fixation becomes less dependent on iron supply, and as such is released from regions of high aeolian deposition, such as the North Atlantic, to

Figure 14. Changes in the distribution of carbon isotopes ($\delta^{13}C_{DIC}$ and $\delta^{13}C_{Cib}$; top) and carbon chemistry (dissolved inorganic carbon and alkalinity; bottom) as a result of increasing $CaCO_3$ production in surface waters between 40°S and 40°N.
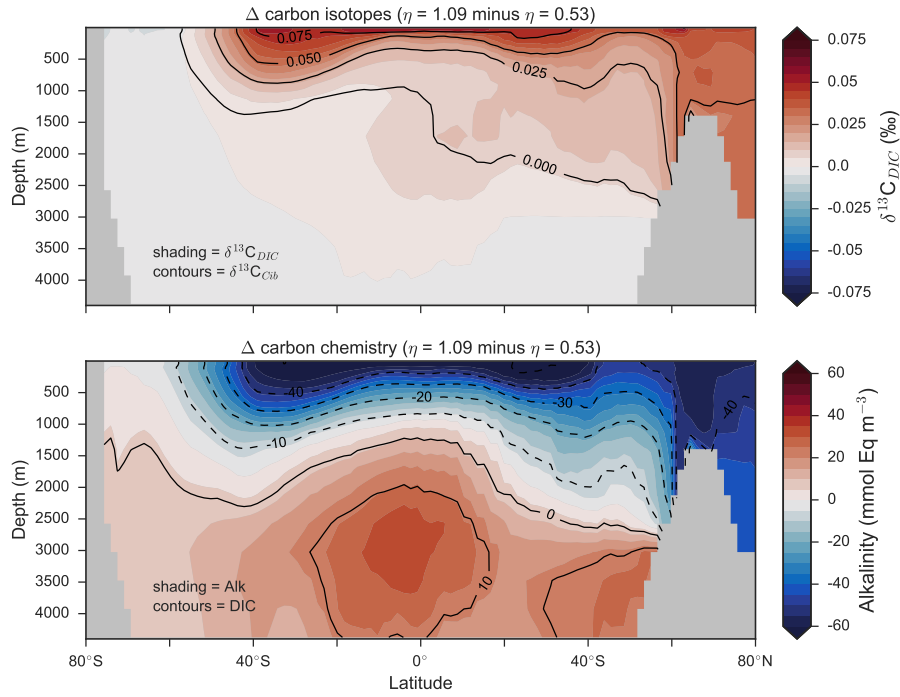
inhabit areas of low NO_3:PO_4 ratios. Areas of low NO_3:PO_4 exist in the tropics proximal to water column denitrification zones. Releasing N_2 fixers from Fe limitation therefore increases the spatial coupling between N_2 fixation and water column denitrification and increases the global rate of N_2 fixation.

We steadily decreased iron limitation (K_{Fe}^D) to increase the strength of spatial coupling between N_2 fixers and the tropical denitrification zones (Fig. 15). As N_2 fixers coupled more strongly to regions of low NO_3:PO_4, the rate of N_2 fixation increased from 122 to 144 to 154 Tg N yr^{-1} (Table 6). An expansion of ~~the suboxic zones~~ suboxia from 2.1 to 2.5 to 2.7 % of global ocean volume in the tropics accompanied the increase in N_2 fixation, as did a decrease in global mean $\delta^{13}C_{DIC}$ of 0.06 and 0.1 ‰, since greater rates of N_2 fixation stimulated tropical export production. Due to the expansion of the already large suboxic zones, which occurred in both horizontal and vertical directions, the amount of organic carbon that reached ~~the sediments~~ tropical sediments (20°S to 20°N) increased from 0.35 to 0.46 to 0.51 Pg C yr^{-1} ~~between 20°S and 20°N~~.

The overarching consequence for $\delta^{15}N_{NO_3}$ due to an expansion of the suboxic zones was an increase in the sedimentary to water column denitrification ratio from 1.5 to 1.9 to 2.2, which decreased mean $\delta^{15}N_{NO_3}$ from 5.6 to 5.2 to 5.0 ‰ (Table 6). The increase in N_2 fixation ($\delta^{15}N_{org}$ = -1 ‰) and sedimentary denitrification (ϵ_{sed}^{15N} = 3 ‰) in the tropics was felt globally for $\delta^{15}N_{NO_3}$ (Fig. 16). Lower $\delta^{15}N_{NO_3}$ by 0.5 and 0.9 ‰ permeated water columns in the Southern Ocean and tropics, respectively. Meanwhile, $\delta^{15}N_{NO_3}$ was up to 10 ‰ lower in surface waters of the tropical and subtropical Pacific, which is

where the greatest increase in N$_2$ fixation and sedimentary denitrification occurred. The dramatic reduction in surface δ^{15}N$_{NO_3}$ was ~~transferred~~ subsequently conveyed to the sediments as δ^{15}N$_{org}$ ~~within $\pm$ 1 to 2~~ 1-2 ‰.

These simple experiments demonstrate that the insights garnered from sedimentary records of δ^{15}N are open to multiple lines of interpretation. An expansion of the suboxic zones, normally associated with an increase in δ^{15}N$_{NO_3}$ (Galbraith et al., 2013), could instead cause a decrease in δ^{15}N$_{NO_3}$ if more organic matter reached the sediments to stimulate sedimentary denitrification. There is good evidence that the suboxic zones might have undergone a vertical expansion (Hoogakker et al., 2018) and that more organic matter reached the tropical sediments under glacial conditions (Cartapanis et al., 2016). The glacial decrease in bulk δ^{15}N$_{org}$ recorded in the eastern tropical Pacific (Ganeshram et al., 1995; Liu et al., 2008) therefore does not necessarily mean a decrease in suboxia. Rather, our experiments show that lower δ^{15}N$_{org}$ might also be caused by an increase in local N$_2$ fixation and sedimentary denitrification. ~~In fact, the decrease in δ^{15}N$_{org}$ seen throughout the tropical Pacific as N$_2$ fixation coupled more strongly to the denitrification zones was associated with greater consumption of surface PO$_4$, which decreased from a mean of 0.18 to 0.09 to 0.06 mmol m^{-3} between 40°S and 40°N.~~ The decrease in δ^{15}N$_{NO_3}$ associated with more sedimentary denitrification and local N$_2$ fixation ~~demonstrated~~ demonstrates the complexity of interpreting sedimentary δ^{15}N$_{org}$ records in the lower latitudes.
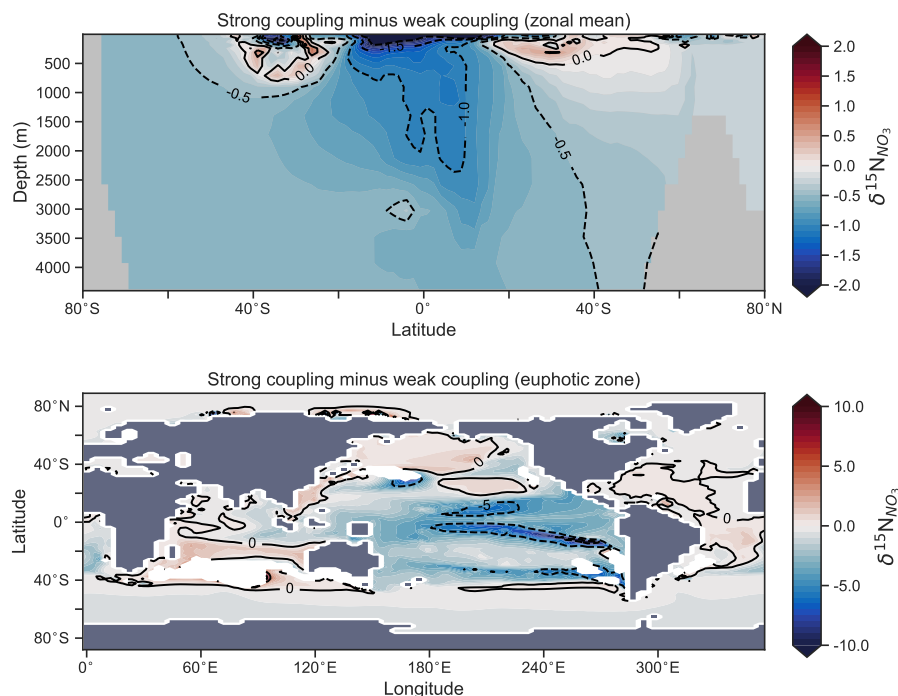
6 Conclusions

The stable isotopes of carbon (δ^{13}C) and nitrogen (δ^{15}N) are proxies that have been fundamental for understanding the ocean. We have included both isotopes into the ocean component of an Earth System Model, CSIRO Mk3L-COAL, to enable future studies with the capability for direct model-proxy data comparisons. We detailed how these isotopes are simulated, how to conduct model-data comparisons ~~to~~ using both water column and sedimentary data, and some basic assessment of changes caused by altered ecosystem functioning. We made three overall findings. First, CSIRO Mk3L-COAL performs well alongside a number of isotope-enabled global ocean GCMs. Second, ~~palaeoceanographic comparisons between modelled and measured isotopes must involve some simple corrections if they are to be useful. With regard to δ^{13}C, the correction must account for~~ alteration of δ^{13}C during formation of foraminiferal calcite ~~, which is dependent on carbonate ion and pressure. With regard to δ^{15}N, the correction must account for the~~ does not jeopardise simple one to one comparisons with simulated δ^{13}C of DIC, while diagenetic alteration of bulk organic δ^{15}N ~~that occurs in bulk sediment, which appears to be related to pressure~~ during early burial must be accounted for in model-data comparisons. Third, ~~we showed changes in marine ecosystem functioning~~ changes in how marine ecosystems function can have significant and complex effects on δ^{13}C and δ^{15}N. Our idealised experiments hence showed that the interpretation of palaeoceanographic records may suffer from multiple lines of interpretation, particularly records from the lower latitudes where multiple processes imprint on the isotopic signatures laid down in sediments. Future work will involve palaeoceanographic simulations of CSIRO Mk3L-COAL that seek to understand how the oceanic carbon and nitrogen cycles respond to and influence important climate transitions.

Figure 15. Changes in the distribution of marine N_2 fixation caused by altering how limiting iron is to the growth of N_2 fixers via the coefficient K^D_{Fe} in Eq. (A12). Iron limitation is sequentially relaxed from top to bottom.
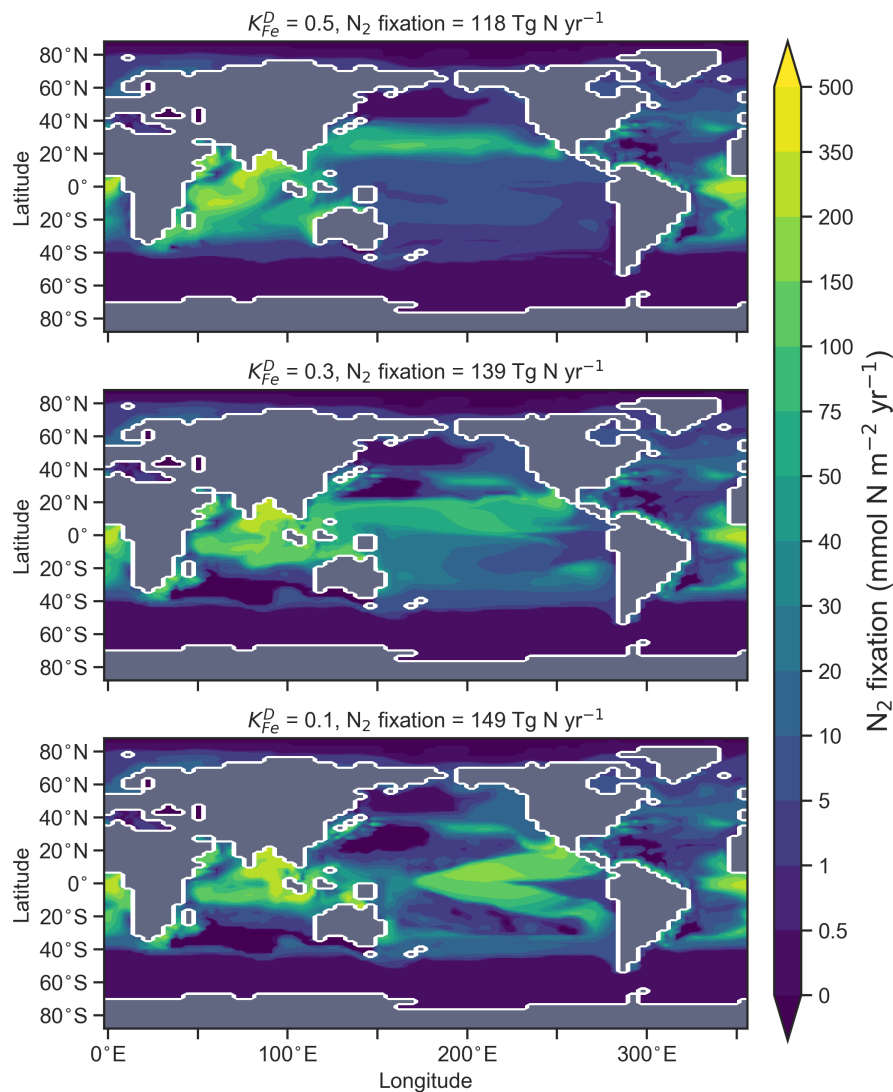
Figure 16. Change in $\delta^{15}N_{NO_3}$ caused by a stronger coupling between N_2 fixation and tropical regions of low NO_3:PO_4 concentrations (i.e. tropical upwelling zones with active water column denitrification). The top panel shows the global zonal mean change, while the bottom panel shows the average change in the euphotic zone, here defined as the top 100 metres. Areas with very low NO_3 (< 0.1 mmol m^{-3}) are masked out.

Appendix A: Ecosystem component of the OBGCM

A1   Export production

A1.1   General phytoplankton group (^{G})

The production of organic matter by the general phytoplankton group (P_{org}^G) is measured in units of mmol phosphorus (P) m^{-3} day^{-1}, and is dependent on temperature (T), nutrients (PO$_4$, NO$_3$, and Fe) and irradiance (I):

$$P_{org}^G = S_{E:P}^G \cdot \mu(T)^G \cdot \min\left(P_{lim}^G, N_{lim}^G, Fe_{lim}^G, F(I)\right) \tag{A1}$$

where,

$$S_{E:P}^G = 0.005 \, \text{mmol PO}_4 \, \text{m}^3$$

$$\mu(T)^G = 0.59 \cdot 1.0635^T \tag{A2}$$

$$F(I) = 1 - e^{G(I)} \tag{A3}$$

$$G(I) = \frac{I \cdot \alpha \cdot PAR}{\mu(T)} \tag{A4}$$

In the above, $S_{E:P}$ converts growth rates in units of day^{-1} to mmol PO$_4$ m^{-3} day^{-1}. $S_{E:P}$ conceptually represents the export to production ratio, and for simplicity we assume it does not change. $\mu(T)$ is the temperature-dependent maximum daily growth rate of phytoplankton (doublings day^{-1}), as defined by Eppley (1972). The light limitation term ($F(I)$) is the productivity versus irradiance equation used to describe phytoplankton growth defined by Clementson et al. (1998), and is dependent on I, the daily averaged shortwave incident radiation (W m^{-2}), α, the initial slope of the productivity versus radiance curve (day^{-1}/(W m^{-2})), and PAR, the fraction of shortwave radiation that is photosynthetically active.

The nutrient limitation terms (P_{lim}^G, N_{lim}^G, and Fe_{lim}^G) may be calculated in two ways.

If the option for **static nutrient limitation** is true, then Michaelis-Menten kinetics (Dugdale, 1967) is used:

$$P_{lim}^G = \frac{PO_4}{PO_4 + K_{PO_4}^G} \tag{A5}$$

$$N_{lim}^G = \frac{NO_3}{NO_3 + K_{NO_3}^G} \tag{A6}$$

$$Fe_{lim}^G = \frac{Fe}{Fe + K_{Fe}^G} \tag{A7}$$

Half-saturation coefficients ($K_{nutrient}^G$) show a large range across phytoplankton species (e.g. Timmermans et al., 2004), and so for simplicity, we set $K_{PO_4}^G = 0.1$ mmol PO$_4$ m^{-3} (Smith, 1982), $K_{NO_3}^G = 0.75$ mmol NO$_3$ m^{-3} (Eppley et al., 1969; Carpenter and Guillard, 1971) and $K_{Fe}^G = 0.1$ μmol Fe m^{-3} (Timmermans et al., 2001).

If the option for **variable nutrient limitation** is true (default), then Optimal Uptake kinetics (Smith et al., 2009) is used:

$$P^G_{lim} = PO_4 \Big/ \left(\frac{PO_4}{1-f_A} + \frac{V/A}{f_A \cdot \text{N:P}} \right) \tag{A8}$$

$$N^G_{lim} = NO_3 \Big/ \left(\frac{NO_3}{1-f_A} + \frac{V/A}{f_A} \right) \tag{A9}$$

$$Fe^G_{lim} = \frac{Fe}{Fe + K_{Fe}} \tag{A10}$$

where,

$$f_A = \max \left[\left(1+\sqrt{\frac{[NO_3]}{V/A}}\right)^{-1}, \left(1+\sqrt{\frac{[PO_4]\cdot \text{N:P}}{V/A}}\right)^{-1} \right] \tag{A11}$$

Optimal uptake kinetics varies the two terms in the denominator of the Michaelis-Menten form according to the availability of nutrients. It therefore accounts for different phytoplankton communities with different abilities for nutrient uptake, and does so using the f_A term. The V/A term represents the maximum potential nutrient uptake, V, over the cellular affinity for that nutrient, A, and is set at 0.1.

A1.2 Diazotrophs (^{D}; N$_2$ fixers)

Organic matter produced by diazotrophs (P^D_{org}) is also measured in units of mmol phosphorus (P) m^{-3} day^{-1}, and is calculated in the same form of Eq. (A1), but using the maximum growth rate $\mu(T)^D$ of Kriest and Oschlies (2015), notable changes in the limitation terms, and minimum thresholds that ensure the nitrogen fixation occurs everywhere in the ocean, except under sea ice. P^D_{org} is calculated via:

$$P^D_{org} = S^D_{E:P} \cdot \mu(T)^D \cdot \max \Big(0.01, \min \big(N^D_{lim}, P_{lim}, Fe^D_{lim}\big)\Big) \cdot \big(1 - ico\big) \tag{A12}$$

where,

$$\mu(T)^D = \max \big(0.01, -0.0042T^2 + 0.2253T - 2.7819\big) \tag{A13}$$

$$N^D_{lim} = e^{-NO_3} \tag{A14}$$

$$P^D_{lim} = \frac{PO_4}{PO_4 + K^D_{PO_4}} \tag{A15}$$

$$Fe^D_{lim} = \max \big(0.0, \tanh \big(2Fe - K^D_{Fe}\big)\big) \tag{A16}$$

The half saturation values for PO$_4$ and Fe limitation are set at 0.1 mmol m^{-1} and 0.5 μmol m^{-1}, respectively, in the default parameterisation. The motivation for making N$_2$ fixers strongly limited by Fe was the high cellular requirements of Fe for diazotrophy (see Sohm et al., 2011, and references therein). A dependency on light is omitted from the limitation term when P^D_{org} is produced. The omission of light is justified by its strong correlation with sea surface temperature (Luo et al., 2014) and its negligible effect on nitrogen fixation in the Atlantic Ocean (McGillicuddy, 2014). Finally, the fractional area coverage of sea ice (ico) is included to ensure that cold water N$_2$ fixation (Sipler et al., 2017) does not occur under ice, since a light dependency is omitted.

A1.3 Calcifiers

The calcifying group produces calcium carbonate ($CaCO_3$) in units of mmol carbon (C) m^{-3} day^{-1}. The production of $CaCO_3$ is always a proportion of the organic carbon export of the general phytoplankton group (C_{org}^G), according to:

$$CaCO_3 = C_{org}^G \cdot R_{CaCO_3} \tag{A17}$$

The ratio of $CaCO_3$ to C_{org}^G (R_{CaCO_3}) can be calculated in two ways.

5   If the option for **fixed** R_{CaCO_3} is true (default), then R_{CaCO_3} is set to 0.08 as informed by the experiments of Yamanaka and Tajika (1996). The production of $CaCO_3$ is thus 8 % of C_{org}^G everywhere.

If the option for **variable** R_{CaCO_3} is true, then R_{CaCO_3} varies as a function of the saturation state of calcite (Ω_{ca}) according to Ridgwell et al. (2007), where:

$$R_{CaCO_3} = 0.022 \cdot \left(\Omega_{ca} - 1 \right)^{\eta} \tag{A18}$$

The exponent (η) is easily modified consistent with the parameterisations of Zhang and Cao (2016) and controls the rate of
10   $CaCO_3$ production at a given value of Ω_{ca}.

A2 Remineralisation

A2.1 General phytoplankton group (^{G})

Organic matter produced by the general phytoplankton group (in units of phosphorus: P_{org}^G) at the surface is instantaneously remineralised each timestep at depth levels beneath the euphotic zone using a power law scaled to depth (Martin et al., 1987).
15   This power law defines the concentration of organic matter remaining at a given depth ($P_{org}^{G,z}$) as a function of organic matter at the surface ($P_{org}^{G,0}$) and depth itself (z). Its form is as follows:

$$P_{org}^{G,z} = P_{org}^{G,0} \cdot \left(\frac{z}{z_{rem}} \right)^{b} \tag{A19}$$

Where z_{rem} in the denominator represents the depth at which remineralisation begins and is set to be 100 metres everywhere. The OBGCM therefore does not consider sinking speeds, nor an interaction between organic matter and physical mixing. However, variations in the b exponent affect the steepness of the curve, thereby emulating sinking speeds and affecting the
20   transfer and release of nutrients from the surface to the deep ocean.

Remineralisation of P_{org}^G through the water column is therefore dependent on the exponent b value in Eq. (A19). The b exponent is calculated in two ways.

If the option for **static remineralisation** is true, then b is set to -0.858 according to Martin et al. (1987).

If the option for **variable remineralisation** is true (default), then b is dependent on the component fraction of picoplankton
25   (F_{pico}) in the ecosystem. The F_{pico} shows a strong inverse relationship to the transfer efficiency (T_{eff}) of organic matter from beneath the euphotic zone to 1,000 metres depth (Weber et al., 2016). Because F_{pico} is not explicitly simulated in OBGCM, we estimate F_{pico} from the export production field in units of carbon (C_{org}^G), calculate T_{eff} using the parameterisation of Weber

et al. (2016), and subsequently calculate the b exponent:

$$F_{pico} = 0.51 - 0.26 \cdot \frac{\text{C}_{org}^{G} \; (\text{mg C m}^{-2} \text{ hour}^{-1})}{\text{C}_{org}^{G,max} \; (\text{mg C m}^{-2} \text{ hour}^{-1})} \tag{A20}$$

$$T_{eff} = 0.47 - 0.81 \cdot F_{pico} \tag{A21}$$

$$b = \frac{\log(T_{eff})}{\log(\frac{1000}{100})} = \log(T_{eff}) \tag{A22}$$

A2.2 Diazotrophs (^{D})

Remineralisation of diazotrophs (P_{org}^{D}) is calculated in the same way as the general phytoplankton group (P_{org}^{G}), with the exception that the depth at which remineralisation occurs is raised from 100 to 25 metres in Eq. (A19). This alteration emulates the release of NO_3 from N_2 fixers well within the euphotic zone, which in some cases can exceed the physical supply from below (Capone et al., 2005). Release of their N and C-rich organic matter (see Stoichiometry section A3.2) therefore occurs higher in the water column than the general phytoplankton group.

A2.3 Suboxic environments

The remineralisation of P_{org}^{G} and P_{org}^{D} will typically require O_2 to be removed, except for in regions where oxygen concentrations are less than a particular threshold ($Den_{lim}^{O_2}$), which is set to 7.5 mmol O_2 m^{-3} and represents the onset of suboxia. In these regions, the remineralisation of organic matter begins to consume NO_3 via the process of denitrification. We calculate the fraction of organic matter that is remineralised by denitrification (F_{den}) via:

$$F_{den} = \left(1 - e^{-0.5 \cdot Den_{lim}^{O_2}} + e^{O_2 - 0.5 \cdot Den_{lim}^{O_2}}\right)^{-1} \tag{A23}$$

Such that F_{den} rises and plateaus at 100 % in a sigmoidal function as O_2 is depleted from 7.5 to 0 mmol m^{-3}.

Following this, the strength of denitrification is reduced if the ambient concentration of NO_3 is deemed to be limiting. Denitrification within the modern oxygen minimum zones only depletes NO_3 towards concentrations between 15 and 40 mmol m^{-3} (Codispoti and Richards, 1976; Voss et al., 2001). Without an additional constraint that weakens denitrification as NO_3 is drawn down, here defined as r_{den}, NO_3 concentrations quickly go to zero in simulated suboxic zones (Schmittner et al., 2008). We weaken denitrification by prescribing a lower bound at which NO_3 can no longer be consumed via denitrification, $Den_{lim}^{NO_3}$, which is set at 30 mmol NO_3 m^{-3}.

$$r_{den} = 0.5 + 0.5 \cdot \tanh\left(0.25 \cdot NO_3 - 0.25 \cdot Den_{lim}^{NO_3} - 2.5\right) \tag{A24}$$

$$\text{if} \quad F_{den} > r_{den}, \quad \text{then} \quad F_{den} = r_{den} \tag{A25}$$

F_{den} is therefore reduced if NO_3 is deemed to be limiting, and subsequently applied against both P_{org}^{G} and P_{org}^{D} to get the proportion of organic matter to be remineralised by O_2 and NO_3.

If the availability of O_2 and NO_3 is insufficient to remineralise all the organic matter at a given depth level, z, then the unremineralised organic matter will pass into the next depth level. Unremineralised organic matter will continue to pass into lower depth levels until the final depth level is reached, at which point all organic matter is remineralised by either water column or sedimentary processes. This version of CSIRO Mk3L-COAL does not consider burial of organic matter.

A2.4 Calcifiers

The dissolution of $CaCO_3$ is calculated using an e-folding depth-dependent decay, where the amount of $CaCO_3$ at a given depth z is defined by:

$$CaCO_3^z = CaCO_3^0 \cdot e^{\frac{-z}{z_{dis}}} \tag{A26}$$

Where z_{dis} represents the depth at which e^{-1} of $CaCO_3$ ($\sim$0.37) produced at the surface remains undissolved.

5   Calcifiers are not susceptible to oxygen-limited re-mineralisation nor the concentration of carbonate ion because the dissolution of $CaCO_3$ depends solely on the this depth-dependent decay. All $CaCO_3$ reaching the final depth level is remineralised without considering burial. Future work will include a full representation of carbonate compensation.

A3 Stoichiometry

The elemental constitution, or stoichiometry, of organic matter affects the biogeochemistry of the water column through uptake
10   (production) and release (remineralisation). The general phytoplankton group and diazotrophs both affect carbon chemistry, O_2, and nutrients (PO_4, NO_3 and Fe), while the calcifiers only affect carbon chemistry tracers (DIC, $DI^{13}C$ and ALK).

Alkalinity ratios for both the general and nitrogen fixing groups are the negative of the N:P ratio, such that for a loss of 1 mmol of NO_3, alkalinity will increase at 1 mmol Eq m^{-3} (Wolf-Gladrow et al., 2007).

A3.1 General phytoplankton group (^{G})

15   The stoichiometry of the general phytoplankton group is calculated in two ways.

If the option for **static stoichiometry** is true, then the C:N:Fe:P ratio is set according to the Redfield ratio of 106:16:0.00032:1 (Redfield et al., 1937).

If the option for **variable stoichiometry** is true (default), then the C:N:P ratio of P_{org}^G is made dependent on the ambient nutrient concentration according to Galbraith and Martiny (2015):

$$\text{C:P} = \left(\frac{6.9 \cdot [PO_4] + 6}{1000} \right)^{-1} \tag{A27}$$

$$\text{N:C} = 0.125 + \frac{0.03 \cdot [NO_3]}{0.32 + [NO_3]} \tag{A28}$$

$$\text{N:P} = \text{C:P} \cdot \text{N:C} \tag{A29}$$

20   Thus, the stoichiometry of P_{org}^G varies across the ocean according to the nutrient concentration, and the uptake and release of carbon, nutrients and oxygen (see section A3.4) is dependent on the concentration of surface PO_4 and NO_3. The ratio of iron to phosphorus (Fe:P) remains fixed at 0.00032, such that 0.32 μmol of Fe is consumed per mmol of PO_4. We chose to maintain a fixed Fe:P ratio because phytoplankton communities from subtropical to Antarctic waters appear to show similar iron contents (Boyd et al., 2015), despite changes in C:N:P. However, the ratio of C:N:Fe does change as a result of varying C:N:P ratios,
25   with higher C:Fe in oligotrophic environments and lower C:Fe in eutrophic regions.

A3.2 Diazotrophs (^{D})

The stoichiometry of diazotrophs is fixed at a C:N:P:Fe ratio of 331:50:1:0.00064, which represents values reported in the literature (Kustka et al., 2003; Karl and Letelier, 2008; Mills and Arrigo, 2010). Diazotrophs do not consume NO_3, rather they consume N_2, which is assumed to be of unlimited supply, and release NO_3 during remineralisation.

A3.3 Calcifiers

Calcifying organisms produce $CaCO_3$, which includes DIC, $DI^{13}C$ and ALK, and these tracers are consumed and released at a ratio of 1:0.998:2, respectively, relative to organic carbon. Thus, the ratio of C:DI^{13}C:Alk relative to each unit of phosphorus consumed by the general phytoplankton group is equal to the rain ratio of $CaCO_3$ to organic phosphorus multiplied by 106:105.8:212. This group has no effect on nutrient tracers or oxygen values.

A3.4 Stoichiometry of remineralisation

The requirements for oxygen (O_2^{rem}:P) and nitrate (NO_3^{rem}:P) during oxic and suboxic remineralisation, respectively, are calculated from the C:N:P ratios of organic matter via the equations of Paulmier et al. (2009). Additional knowledge of the hydrogen and oxygen content of the organic matter is also required to calculate O_2^{rem}:P and NO_3^{rem}:P. However, the hydrogen and oxygen content of phytoplankton depends strongly on the proportions of lipids, carbohydrates and proteins that constitute the cell. As there is no empirical model for predicting these physiological components based on environmental variables, we continue Redfield's legacy by assuming that all organic matter is a carbohydrate of the form CH_2O. Future work, however, should address this obvious bias.

To calculate O_2^{rem}:P and NO_3^{rem}:P, we therefore need to first calculate the amount of hydrogen and oxygen in organic matter via:

$$H:P = 2C:P + 3N:P + 3 \tag{A30}$$
$$O:P = C:P + 4 \tag{A31}$$

Once a C:N:P:H:O ratio for organic matter is known, we calculate O_2^{rem}:P and NO_3^{rem}:P in units of mmol m^{-3} P^{-1} using the equations of Paulmier et al. (2009):

$$O_2^{rem}:P = -(C:P + 0.25H:P - 0.5O:P - 0.75N:P + 1.25) - 2N:P \tag{A32}$$
$$NO_3^{rem}:P = -(0.8C:P + 0.25H:P - 0.5O:P - 0.75N:P + 1.25) + 0.6N:P \tag{A33}$$

The calculation of O_2^{rem}:P accounts for the oxygen that is also needed to oxidise ammonium to nitrate.

From these calculations we find the following requirements of oxic and suboxic remineralisation, assuming the static stoichiometry option for the general phytoplankton group:

$$O_2^{rem}:P_{org}^G = 138$$

$$NO_3^{rem}:P_{org}^G = 94.4$$

$$O_2 rem:P_{org}^D = 431$$

$$NO_3^{rem}:P_{org}^D = 294.8$$

These numbers change dynamically alongside C:N:P ratios when the stoichiometry of organic matter is allowed the vary.

A4 Sedimentary processes

5   The remineralisation of organic matter within the sediments is provided as an option in the OBGCM. Sedimentary denitrification, and its slight preference for the light isotopes of fixed nitrogen ($\epsilon_{sed}^{15N} = 3$ ‰), is an important component of the marine nitrogen cycle and its isotopes. It acts as an additional sink of NO_3, and reduces the $\delta^{15}N$ value of the global ocean by offsetting the strong fractionation of water column denitrification ($\epsilon_{wc}^{15N} = 20$ ‰).

    If sedimentary processes are active, the empirical model of Bohlen et al. (2012) is used to estimate the rate of sedimentary

10   denitrification, where the removal of NO_3 is dependent on the rate of particulate organic carbon ($C_{org}^G + C_{org}^D$) arriving at the sediments and the ambient concentrations of oxygen and nitrate. In the following, we assume that the concentrations of NO_3 and O_2 that are available in the sediments are $\frac{2}{3}$ of the concentration in overlying water column based on observations of transport across the diffusive boundary layer (Gundersen and Jorgensen, 1990).

$$\Delta NO_3(sed) = \left(\alpha + \beta \cdot 0.98^{\left(O_2 - NO_3\right)}\right) \cdot \left(C_{org}^G + C_{org}^D\right) \tag{A34}$$

$$\text{where,} \quad \alpha = 0.04 \quad \text{and} \quad \beta = 0.1 \tag{A35}$$

In the above, both the α and β values were halved from the values of Bohlen et al. (2012) to raise global mean NO_3 con-

15   centrations and lower the sedimentary to water column denitrification ratio to between 1 and 2. If NO_3 is not available, the remaining organic matter is remineralised using oxygen if the environment is sufficiently oxygenated. An additional limitation is set for sediments underlying hypoxic waters ($O_2 < 40$ mmol m^{-3}), where oxic remineralisation is weakened towards zero according to a hyperbolic tangent function ($0.5 + 0.5 \cdot \tanh(0.2 \cdot O_2 - 5)$). If oxygen is also limiting, the remaining organic matter is remineralised via sulfate reduction. As sulfate is not explicitly simulated, we assumed that sulfate is always available

20   to account for the remaining organic matter.

    Thus, sedimentary denitrification is heavily dependent on the rate of organic matter arriving at the sediments. However, a large amount of sedimentary remineralisation is not captured using only these parameterisations because the coarse resolution of the OGCM enables it to resolve only the largest continental shelves, such as the shallow Indonesian seas. Many small areas of raised bathymetry in pelagic environments are also unresolved by the OGCM. To address this insufficiency and increase the

25   global rate of sedimentation and sedimentary denitrification, we coupled a sub-grid scale bathymetry to the course resolution OGCM following the methodology of Somes et al. (2013) using the ETOPO5 $\frac{1}{12}^{th}$ of a degree dataset. For each latitude by

longitude grid point, we calculated the fraction of area that would be represented by shallower levels in the OGCM if this finer resolution bathymetry were used. At each depth level above the deepest level, the fractional area represented by sediments on the sub-grid scale bathymetry can be used to remineralise all forms of exported matter (C_{org}^G, C_{org}^D and $CaCO_3$) via sedimentary processes.

Also following the methodology of Somes et al. (2013), we included an option to amplify sedimentary denitrification in the upper 250 metres to account for narrow continental shelves that are not resolved by the OGCM. Narrow shelves experience strong rates of upwelling and productivity, and hence high rates of sedimentary denitrification (Gruber and Sarmiento, 1997). To amplify shallow rates of sedimentary denitrification, we included an optional acceleration factor (Γ_{sed}), set to 3.0 in the default parameterisation, dependent on the total fraction of shallower depths not covered by the sub-grid scale bathymetry:

$$\Delta NO_3(sed) = \Delta NO_3(sed) \cdot \left(\left(1 - F_{sgb}\right) \cdot \Gamma_{sed} + 1 \right) \tag{A36}$$

For those grids with a low fraction covered by the sub-grid scale bathymetry (F_{sgb}), the amplification of sedimentary denitrification is therefore greatest.

Appendix B: ~~Default parameterisation~~ Parameterisation of the OBGCM ecosystem component

Default parameters for the marine ecosystem component of CSIRO Mk3L-COAL are outlined in Tables A1, A2, and A3. The values presented in these tables are required as input when running the ocean model.

Table A1. ~~Default parameter~~ Parameter values controlling export production in the ecosystem component of the CSIRO Mk3L-COAL ocean model. ~~Default settings:~~ ~~Michaelis-Menton == False, Optimal Uptake == True, fix == True and Vary CaCO3 == False.~~

Parameter	Action	Value	Active when
General phytoplankton (^{G})			
$S_{E:P}^G$	export to production ratio	0.005 mmol P m^{-3} day^{-1}	Always
α	initial slope of production versus irradiance curve	0.025 day^{-1}/(W m^{-2})	Always
PAR	fraction of shortwave radiation that is photosynthetically active	0.5	Always
$K_{PO_4}^G$	half saturation coefficient for phosphate	0.1 mmol P m^{-3}	Michaelis-Menton == True
$K_{NO_3}^G$	half saturation coefficient for nitrate	0.75 mmol N m^{-3}	Michaelis-Menton == True
K_{Fe}^G	half saturation coefficient for iron	0.1 μmol Fe m^{-3}	Michaelis-Menton == True
V/A	Maximum potential uptake over affinity for nutrient	0.1	Optimal Uptake == True
Diazotrophs (^{D})			
$S_{E:P}^D$	export to production ratio	0.005 mmol P m^{-3} day^{-1}	fix == True
K_{Fe}^D	half saturation coefficient for iron	0.5 μmol Fe m^{-3}	fix == True
K_{Fe}^D	half saturation coefficient for phosphate	0.1 mmol PO$_4$ m^{-3}	fix == True
Calcifiers			
R_{CaCO_3}	ratio of CaCO$_3$ produced per unit carbon of P_{org}^G	0.08	Vary CaCO3 == False
R_{CaCO_3}	ratio of CaCO$_3$ produced per unit carbon of P_{org}^G	0.022	Vary CaCO3 == True
η	exponent varying R_{CaCO_3} due to calcite saturation	0.53, 0.81 or 1.09	Vary CaCO3 == True

Table A2. ~~Default parameter~~ Parameter values controlling remineralisation in the ecosystem component of the CSIRO Mk3L-COAL ocean model. Default settings: *ReminPico == True, fix == True, den == True, and sedfluxes == True.*

Parameter	Action	Value	Active when
General phytoplankton (^{G})			
b	remineralisation profile exponent	-0.858	ReminPico == False
b	remineralisation profile exponent	-0.7 to -1.2	ReminPico == True
z_{rem}	depth at which remineralisation begins	100 m	Always
Diazotrophs (^{D})			
z_{rem}	depth at which remineralisation begins	25 m	~~Always~~ fix == True
Calcifiers			
z_{dis}	depth at which e^{-1} CaCO$_3$ remains undissolved	3500 m	Always
Suboxic environments (affects ^{G} and ^{D})			
$Den^{O_2}_{lim}$	Dissolved oxygen concentration when denitrification ~~occurs~~ begins	7.5 mmol m^{-3}	~~Always~~ den == True
$Den^{O_2}_{lim}$	Nitrate concentration when denitrification is limited	30.0 mmol m^{-3}	~~Always~~ den == True
Sediments (affects ^{G} and ^{D})			
α	First constant in Bohlen Eq. (A34)	0.04	~~Always~~ sedfluxes == True
β	Second constant in Bohlen Eq. (A34)	0.1	~~Always~~ sedfluxes == True
Γ_{sed}	Sedimentary remineralisation amplification factor	3.0	~~Always~~ sedfluxes == True

Table A3. ~~Default parameter~~ Parameter values controlling stoichiometry in the ecosystem component of the CSIRO Mk3L-COAL ocean model. Default settings: *Vary Stoich == True, Vary frac13 == False* and *fix == True*.

Parameter	Action	Value	Active when
General phytoplankton (^{G})			
C:^{13}C:ALK:N:Fe:P	Nutrient stoichiometry of general phytoplankton	106:~~103.8~~:16:16:0.00032:1	Vary Stoich == False
O_2^{rem}:NO_3^{rem}:P	Remineralisation requirements of O_2 and NO_3	-138:-94.4:1	Vary Stoich == False
C:P	Carbon stoichiometry of general phytoplankton	(50 to 170):1	Vary Stoich == True
N:P	Nitrogen stoichiometry of general phytoplankton	(7 to 26):1	Vary Stoich == True
O_2^{rem}:P	Remineralisation requirements of O_2	(-220 to -60):1	Vary Stoich == True
NO_3^{rem}:P	Remineralisation requirements of NO_3	(-42 to -150):1	Vary Stoich == True
$^{13}C\varepsilon_{bio}$	Carbon isotope fractionation during biological assimilation	21 ‰	Vary frac13 == False
$^{13}C\varepsilon_{bio}$	Carbon isotope fractionation during biological assimilation	15 to 25 ‰	Vary frac13 == True
Diazotrophs (^{D})			
C:^{13}C:ALK:N:Fe:P	Nutrient stoichiometry of general phytoplankton	331:327:-50:50:0.00064:1	~~Always~~ fix == True
O_2^{rem}:NO_3^{rem}:P	Remineralisation requirements of O_2 and NO_3	-431:-294.8:1	~~Always~~ fix == True
Calcifiers			
C:^{13}C:ALK:P	Nutrient stoichiometry of calcifiers	106:105.8:212:1	Always

References

Altabet, M. A. and Francois, R.: Nitrogen isotope biogeochemistry of the Antarctic Polar Frontal Zone at 170 degrees W, Deep Sea Research Part II: Topical Studies in Oceanography, 48, 4247–4273, https://doi.org/10.1016/S0967-0645(01)00088-1, 2001.

Bohlen, L., Dale, A. W., and Wallmann, K.: Simple transfer functions for calculating benthic fixed nitrogen losses and C:N:P regeneration ratios in global biogeochemical models, Global Biogeochemical Cycles, 26, https://doi.org/10.1029/2011GB004198, 2012.

Boudreau, B. P.: Carbonate dissolution rates at the deep ocean floor, Geophysical Research Letters, 40, 744–748, https://doi.org/10.1029/2012GL054231, http://doi.wiley.com/10.1029/2012GL054231, 2013.

Boyd, P. W., Strzepek, R. F., Ellwood, M. J., Hutchins, D. A., Nodder, S. D., Twining, B. S., and Wilhelm, S. W.: Why are biotic iron pools uniform across high- and low-iron pelagic ecosystems?, Global Biogeochemical Cycles, 29, 1028–1043, https://doi.org/10.1002/2014GB005014, 2015.

Brandes, J. a. and Devol, A. H.: A global marine-fixed nitrogen isotopic budget: Implications for Holocene nitrogen cycling, Global Biogeochemical Cycles, 16, 67–1–67–14, https://doi.org/10.1029/2001GB001856, 2002.

Buchanan, P., Matear, R., Chase, Z., Phipps, S., and Bindoff, N.: Dynamic Biological Functioning Important for Simulating and Stabilizing Ocean Biogeochemistry, Global Biogeochemical Cycles, https://doi.org/10.1002/2017GB005753, 2018.

Buchanan, P. J., Matear, R. J., Lenton, A., Phipps, S. J., Chase, Z., and Etheridge, D. M.: The simulated climate of the Last Glacial Maximum and insights into the global marine carbon cycle, Climate of the Past, 12, 2271–2295, https://doi.org/10.5194/cp-12-2271-2016, 2016.

Capone, D. G., Burns, J. A., Montoya, J. P., Subramaniam, A., Mahaffey, C., Gunderson, T., Michaels, A. F., and Carpenter, E. J.: Nitrogen fixation by Trichodesmium spp.: An important source of new nitrogen to the tropical and subtropical North Atlantic Ocean, Global Biogeochemical Cycles, 19, https://doi.org/10.1029/2004GB002331, 2005.

Carpenter, E. J. and Guillard, R. R. L.: Intraspecific differences in nitrate half-saturation constants for three species of marine phytoplankton, Ecology, 52, 183–185, 1971.

Carpenter, E. J., Harvey, H. R., Brian, F., and Capone, D. G.: Biogeochemical tracers of the marine cyanobacterium Trichodesmium, Deep-Sea Research Part I: Oceanographic Research Papers, 44, 27–38, https://doi.org/10.1016/S0967-0637(96)00091-X, 1997.

Cartapanis, O., Bianchi, D., Jaccard, S. L., and Galbraith, E. D.: Global pulses of organic carbon burial in deep-sea sediments during glacial maxima, Nature Communications, 7, 1–7, https://doi.org/10.1038/ncomms10796, 2016.

Ciais, P., Tagliabue, A., Cuntz, M., Bopp, L., Scholze, M., Hoffmann, G., Lourantou, A., Harrison, S. P., Prentice, I. C., Kelley, D. I., Koven, C., and Piao, S. L.: Large inert carbon pool in the terrestrial biosphere during the Last Glacial Maximum, Nature Geoscience, 5, 74–79, https://doi.org/10.1038/ngeo1324, 2011.

Clementson, L., Parslow, J., Griffiths, F., Lyne, V., Mackey, D., Harris, G., McKenzie, D., Bonham, P., Rathbone, C., and Rintoul, S.: Controls on phytoplankton production in the Australasian sector of the subtropical convergence, Deep Sea Research Part I: Oceanographic Research Papers, 45, 1627–1661, https://doi.org/10.1016/S0967-0637(98)00035-1, 1998.

Cline, J. D. and Kaplan, I. R.: Isotopic fractionation of dissolved nitrate during denitrification in the eastern tropical north pacific ocean, Marine Chemistry, 3, 271–299, https://doi.org/10.1016/0304-4203(75)90009-2, 1975.

Codispoti, L. a. and Richards, F. a.: An analysis of the horizontal regime of denitrification in the eastern tropical North Pacific, Limnology and Oceanography, 21, 379–388, https://doi.org/10.4319/lo.1976.21.3.0379, 1976.

Craig, H.: Isotopic standards for carbon and oxygen and correction factors for mass-spectrometric analysis of carbon dioxide, Geochimica et Cosmochimica Acta, 12, 133–149, https://doi.org/10.1016/0016-7037(57)90024-8, 1957.

Dugdale, R. C.: Nutrient limitation in the Sea: Dynamics, identification, and significance, Limnology and Oceanography, 12, 685–695, 1967.

Duteil, O., Koeve, W., Oschlies, a., Bianchi, D., Galbraith, E., Kriest, I., and Matear, R.: A novel estimate of ocean oxygen utilisation points to a reduced rate of respiration in the ocean interior, Biogeosciences, 10, 7723–7738, https://doi.org/10.5194/bg-10-7723-2013, 2013.

Eide, M., Olsen, A., Ninnemann, U. S., and Johannessen, T.: A global ocean climatology of preindustrial and modern ocean $\delta 13C$, Global
5   Biogeochemical Cycles, 31, 515–534, https://doi.org/10.1002/2016GB005473, 2017.

Eppley, R. W.: Temperature and phytoplankton growth in the sea, Fishery Bulletin, 70, 1063–1085, 1972.

Eppley, R. W., Rogers, J. N., and Mccarthy, J. J.: Half-saturation constants for uptake of nitrate and ammonium by marine phytoplankton, Limnology and Oceanography, 14, 912–920, https://doi.org/10.4319/lo.1969.14.6.0912, 1969.

Freing, A., Wallace, D. W. R., and Bange, H. W.: Global oceanic production of nitrous oxide, Philosophical Transactions of the Royal Society
10   B: Biological Sciences, 367, 1245–1255, https://doi.org/10.1098/rstb.2011.0360, 2012.

Friedli, H., Lötscher, H., Oeschger, H., Siegenthaler, U., and Stauffer, B.: Ice core record of the 13C/12C ratio of atmospheric CO2 in the past two centuries, Nature, 324, 237–238, https://doi.org/10.1038/324237a0, 1986.

Galbraith, E. D. and Martiny, A. C.: A simple nutrient-dependence mechanism for predicting the stoichiometry of marine ecosystems, Proceedings of the National Academy of Sciences, 112, 201423 917, https://doi.org/10.1073/pnas.1423917112, 2015.

15 Galbraith, E. D., Kienast, M., Albuquerque, A. L., Altabet, M. A., Batista, F., Bianchi, D., Calvert, S. E., Contreras, S., Crosta, X., De Pol-Holz, R., Dubois, N., Etourneau, J., Francois, R., Hsu, T. C., Ivanochko, T., Jaccard, S. L., Kao, S. J., Kiefer, T., Kienast, S., Lehmann, M. F., Martinez, P., McCarthy, M., Meckler, A. N., Mix, A., Möbius, J., Pedersen, T. F., Pichevin, L., Quan, T. M., Robinson, R. S., Ryabenko, E., Schmittner, A., Schneider, R., Schneider-Mor, A., Shigemitsu, M., Sinclair, D., Somes, C., Studer, A. S., Tesdal, J. E., Thunell, R., and Terence Yang, J. .: The acceleration of oceanic denitrification during deglacial warming, Nature Geoscience, 6, 579–584,
20   https://doi.org/10.1038/ngeo1832, 2013.

Ganeshram, R. S., Pedersen, T. F., Calvert, S. E., and Murray, J. W.: Large changes in oceanic nutrient inventories from glacial to interglacial periods, Nature, 376, 755–758, https://doi.org/10.1038/376755a0, http://www.nature.com/articles/376755a0, 1995.

Gruber, N. and Sarmiento, J. L.: Global patterns of marine nitrogen fixation and denitrification, Global Biogeochemical Cycles, 11, 235, https://doi.org/10.1029/97GB00077, 1997.

25 Gundersen, J. K. and Jorgensen, B. B.: Microstructure of diffusive boundary layers and the oxygen uptake of the sea floor, Nature, 345, 604–607, https://doi.org/10.1038/345604a0, 1990.

Hoogakker, B. A., Lu, Z., Umling, N., Jones, L., Zhou, X., Rickaby, R. E., Thunell, R., Cartapanis, O., and Galbraith, E.: Glacial expansion of oxygen-depleted seawater in the eastern tropical Pacific, Nature, 562, 410–413, https://doi.org/10.1038/s41586-018-0589-x, http://dx.doi.org/10.1038/s41586-018-0589-x, 2018.

30 Hülse, D., Arndt, S., Wilson, J. D., Munhoven, G., and Ridgwell, A.: Earth-Science Reviews Understanding the causes and consequences of past marine carbon cycling variability through models, Earth-Science Reviews, 171, 349–382, https://doi.org/10.1016/j.earscirev.2017.06.004, http://dx.doi.org/10.1016/j.earscirev.2017.06.004, 2017.

Hunter, J. D.: Matplotlib: A 2D graphics environment, Computing In Science & Engineering, 9, 90–95, 2007.

Jahn, A., Lindsay, K., Giraud, X., Gruber, N., Otto-Bliesner, B. L., Liu, Z., and Brady, E. C.: Carbon isotopes in the ocean model of the
35   Community Earth System Model (CESM1), Geoscientific Model Development, 8, 2419–2434, https://doi.org/10.5194/gmd-8-2419-2015, 2015.

Karl, D. M. and Letelier, R. M.: Nitrogen fixation-enhanced carbon sequestration in low nitrate, low chlorophyll seascapes, Marine Ecology Progress Series, 364, 257–268, https://doi.org/10.3354/meps07547, 2008.

Kemeny, P. C., Kast, E. R., Hain, M. P., Fawcett, S. E., Fripiat, F., Studer, A. S., Martínez-García, A., Haug, G. H., and Sigman, D. M.: A seasonal model of nitrogen isotopes in the ice age Antarctic Zone: Support for weakening of the Southern Ocean upper overturning cell, Paleoceanography and Paleoclimatology, TBD, TBD, https://doi.org/10.1029/2018PA003478, http://doi.wiley.com/10.1029/2018PA003478, 2018.

5   Kriest, I. and Oschlies, A.: MOPS-1.0: modelling the regulation of the global oceanic nitrogen budget by marine biogeochemical processes, Geoscientific Model Development Discussions, 8, 1945–2010, https://doi.org/10.5194/gmdd-8-1945-2015, 2015.

Kustka, A., Sañudo-Wilhelmy, S., Carpenter, E. J., Capone, D. G., and Raven, J. A.: A revised estimate of the iron use efficiency of nitrogen fixation, with special reference to the marine cyanobacterium Trichodesmium spp. (Cyanophyta), Journal of Phycology, 39, 12–25, https://doi.org/10.1046/j.1529-8817.2003.01156.x, 2003.

10   Laws, E. A., Popp, B. N., Bidigare, R. R., Kennicutt, M. C., and Macko, S. A.: Dependence of phytoplankton carbon isotopic composition on growth rate and [CO2)aq: Theoretical considerations and experimental results, Geochimica et Cosmochimica Acta, 59, 1131–1138, https://doi.org/10.1016/0016-7037(95)00030-4, 1995.

Liu, Z., Altabet, M. A., and Herbert, T. D.: Plio-Pleistocene denitrification in the eastern tropical North Pacific: Intensification at 2.1 Ma, Geochemistry, Geophysics, Geosystems, 9, 1–14, https://doi.org/10.1029/2008GC002044, 2008.

15   Luo, Y. W., Lima, I. D., Karl, D. M., Deutsch, C. A., and Doney, S. C.: Data-based assessment of environmental controls on global marine nitrogen fixation, Biogeosciences, 11, 691–708, https://doi.org/10.5194/bg-11-691-2014, 2014.

Mao, J., Phipps, S. J., Pitman, a. J., Wang, Y. P., Abramowitz, G., and Pak, B.: The CSIRO Mk3L climate system model v1.0 coupled to the CABLE land surface scheme v1.4b: evaluation of the control climatology, Geoscientific Model Development Discussions, 4, 1611–1642, https://doi.org/10.5194/gmdd-4-1611-2011, 2011.

20   Marconi, D., Sigman, D. M., Casciotti, K. L., Campbell, E. C., Alexandra Weigand, M., Fawcett, S. E., Knapp, A. N., Rafter, P. A., Ward, B. B., and Haug, G. H.: Tropical Dominance of N_2 Fixation in the North Atlantic Ocean, Global Biogeochemical Cycles, pp. 1608–1623, https://doi.org/10.1002/2016GB005613, 2017.

Mariotti, A., Germon, J., Hubert, P., Kaiser, P., Letolle, R., Tardieux, A., and Tardieux, P.: Experimental determination of nitrogen kinetic isotope fractionation: some principles; ilustration for the denitrification and nitrification process., Plant and soil, 62, 413–430, 25   https://doi.org/10.1007/BF02374138, 1981.

Martin, J. H., Knauer, G. A., Karl, D. M., and Broenkow, W. W.: VERTEX: carbon cycling in the northeast Pacific, Deep Sea Research Part A. Oceanographic Research Papers, 34, 267–285, https://doi.org/10.1016/0198-0149(87)90086-0, 1987.

Martinez-Garcia, A., Sigman, D. M., Ren, H., Anderson, R. F., Straub, M., Hodell, D. A., Jaccard, S. L., Eglinton, T. I., and Haug, G. H.: Iron Fertilization of the Subantarctic Ocean During the Last Ice Age, Science, 343, 1347–1350, https://doi.org/10.1126/science.1246848, 30   2014.

Matear, R. J. and Holloway, G.: Modeling the inorganic phosphorus cycle of the North Pacific using an adjoint data assimilation model to assess the role of dissolved organic phosphorus, Global Biogeochemical Cycles, 9, 101–119, https://doi.org/10.1029/94GB03104, 1995.

Matear, R. J. and Lenton, A.: Quantifying the impact of ocean acidification on our future climate, Biogeosciences, 11, 3965–3983, https://doi.org/10.5194/bg-11-3965-2014, 2014.

35   Matear, R. J. and Lenton, A.: Carbon–climate feedbacks accelerate ocean acidification, Biogeosciences, 15, 1721–1732, https://doi.org/10.5194/bg-15-1721-2018, 2018.

McGillicuddy, D. J.: Do Trichodesmium spp. populations in the North Atlantic export most of the nitrogen they fix?, Global Biogeochemical Cycles, 28, 103–114, https://doi.org/10.1002/2013GB004652, 2014.

McRose, D. L., Lee, A., Kopf, S. H., Baars, O., Kraepiel, A. M., Sigman, D. M., Morel, F. M., and Zhang, X.: Effect of iron limitation on the isotopic composition of cellular and released fixed nitrogen in Azotobacter vinelandii, Geochimica et Cosmochimica Acta, 244, 12–23, https://doi.org/10.1016/j.gca.2018.09.023, https://doi.org/10.1016/j.gca.2018.09.023, 2019.

Meehl, G. A., Covey, C., Delworth, T., Latif, M., McAvaney, B., Mitchell, J. F. B., Stouffer, R. J., Taylor, K. E., Meehl, G. A., Covey, C., Delworth, T., Latif, M., McAvaney, B., Mitchell, J. F. B., Stouffer, R. J., and Taylor, K. E.: THE WCRP CMIP3 Multimodel Dataset: A New Era in Climate Change Research, Bulletin of the American Meteorological Society, 88, 1383–1394, https://doi.org/10.1175/BAMS-88-9-1383, 2007.

Menviel, L., Yu, J., Joos, F., Mouchet, A., Meissner, K. J., and England, M. H.: Poorly ventilated deep ocean at the Last Glacial Maximum inferred from carbon isotopes: A data-model comparison study, Paleoceanography, 32, 2–17, https://doi.org/10.1002/2016PA003024, 2017.

Mills, M. M. and Arrigo, K. R.: Magnitude of oceanic nitrogen fixation influenced by the nutrient uptake ratio of phytoplankton, Nature Geoscience, 3, 412–416, https://doi.org/10.1038/ngeo856, 2010.

Moore, C. M., Mills, M. M., Arrigo, K. R., Berman-Frank, I., Bopp, L., Boyd, P. W., Galbraith, E. D., Geider, R. J., Guieu, C., Jaccard, S. L., Jickells, T. D., La Roche, J., Lenton, T. M., Mahowald, N. M., Marañón, E., Marinov, I., Moore, J. K., Nakatsuka, T., Oschlies, A., Saito, M. a., Thingstad, T. F., Tsuda, A., and Ulloa, O.: Processes and patterns of oceanic nutrient limitation, Nature Geoscience, 6, 701–710, https://doi.org/10.1038/ngeo1765, 2013.

Muglia, J., Skinner, L. C., and Schmittner, A.: Weak overturning circulation and high Southern Ocean nutrient utilization maximized glacial ocean carbon, Earth and Planetary Science Letters, 496, 47–56, https://doi.org/10.1016/j.epsl.2018.05.038, 2018.

Orr, J. C., Najjar, R. G., Aumont, O., Bopp, L., Bullister, J. L., Danabasoglu, G., Doney, S. C., Dunne, J. P., Dutay, J.-C., Graven, H., Griffies, S. M., John, J. G., Joos, F., Levin, I., Lindsay, K., Matear, R. J., McKinley, G. A., Mouchet, A., Oschlies, A., Romanou, A., Schlitzer, R., Tagliabue, A., Tanhua, T., and Yool, A.: Biogeochemical protocols and diagnostics for the CMIP6 Ocean Model Intercomparison Project (OMIP), Geoscientific Model Development, 10, 2169–2199, https://doi.org/10.5194/gmd-10-2169-2017, 2017.

Ortiz, J. D., Mix, A., Rugh, W., Watkins, J., and Collier, R.: Deep-dwelling planktonic foraminifera of the northeastern Pacific Ocean reveal environmental control of oxygen and carbon isotopic disequilibria, Geochimica et Cosmochimica Acta, 60, 4509–4523, 1996.

Oschlies, A.: Equatorial nutrient trapping in biogeochemical ocean models: The role of advection numerics, Global Biogeochemical Cycles, 14, 655–667, https://doi.org/10.1029/1999GB001217, 2000.

Oschlies, A., Schulz, K. G., Riebesell, U., and Schmittner, A.: Simulated 21st century's increase in oceanic suboxia by CO_2-enhanced biotic carbon export, Global Biogeochemical Cycles, 22, 1–10, https://doi.org/10.1029/2007GB003147, 2008.

Paulmier, a., Kriest, I., and Oschlies, A.: Stoichiometries of remineralisation and denitrification in global biogeochemical ocean models, Biogeosciences, 6, 923–935, https://doi.org/10.5194/bg-6-923-2009, 2009.

Phipps, S. J., McGregor, H. V., Gergis, J., Gallant, A. J. E., Neukom, R., Stevenson, S., Ackerley, D., Brown, J. R., Fischer, M. J., and van Ommen, T. D.: Paleoclimate Data-Model Comparison and the Role of Climate Forcings over the Past 1500 Years*, Journal of Climate, 26, 6915–6936, https://doi.org/10.1175/JCLI-D-12-00108.1, 2013.

Rafter, P. A., Sigman, D. M., and Mackey, K. R.: Recycled iron fuels new production in the eastern equatorial Pacific Ocean, Nature Communications, 8, https://doi.org/10.1038/s41467-017-01219-7, 2017.

Redfield, A. C., Smith, H. P., and Ketchum, B. H.: The cycle of organic phosphorus in the Gulf of Maine, The Biological Bulletin, 73, 421–443, 1937.

Ren, H., Sigman, D. M., Meckler, A. N., Plessen, B., Robinson, R. S., Rosenthal, Y., and Haug, G. H.: Foraminiferal Isotope Evidence of Reduced Nitrogen Fixation in the Ice Age Atlantic Ocean, Science, 323, 244–248, https://doi.org/10.1126/science.1165787, 2009.

Ridgwell, a., Hargreaves, J. C., Edwards, N. R., Annan, J. D., Lenton, T. M., Marsh, R., Yool, A., and Watson, A.: Marine geochemical data assimilation in an efficient Earth System Model of global biogeochemical cycling, Biogeosciences, 4, 87–104, https://doi.org/10.5194/bg-4-87-2007, 2007.

Robinson, R. S., Kienast, M., Luiza Albuquerque, A., Altabet, M., Contreras, S., De Pol Holz, R., Dubois, N., Francois, R., Galbraith, E., Hsu, T. C., Ivanochko, T., Jaccard, S., Kao, S. J., Kiefer, T., Kienast, S., Lehmann, M., Martinez, P., McCarthy, M., Möbius, J., Pedersen, T., Quan, T. M., Ryabenko, E., Schmittner, A., Schneider, R., Schneider-Mor, A., Shigemitsu, M., Sinclair, D., Somes, C., Studer, A., Thunell, R., and Yang, J. Y.: A review of nitrogen isotopic alteration in marine sediments, Paleoceanography, 27, https://doi.org/10.1029/2012PA002321, 2012.

Schmittner, A. and Somes, C. J.: Complementary constraints from carbon (13C) and nitrogen (15N) isotopes on the glacial ocean's soft-tissue biological pump, Paleoceanography, 31, 669–693, https://doi.org/10.1002/2015PA002905, 2016.

Schmittner, A., Oschlies, A., Matthews, H. D., and Galbraith, E. D.: Future changes in climate, ocean circulation, ecosystems, and bioge-ochemical cycling simulated for a business-as-usual CO 2 emission scenario until year 4000 AD, Global Biogeochemical Cycles, 22, https://doi.org/10.1029/2007GB002953, 2008.

Schmittner, A., Gruber, N., Mix, A. C., Key, R. M., Tagliabue, A., and Westberry, T. K.: Biology and air-sea gas exchange controls on the distribution of carbon isotope ratios (δ13C) in the ocean, Biogeosciences, 10, 5793–5816, https://doi.org/10.5194/bg-10-5793-2013, 2013.

Schmittner, A., Bostock, H. C., Cartapanis, O., Curry, W. B., Filipsson, H. L., Galbraith, E. D., Gottschalk, J., Herguera, J. C., Hoogakker, B., Jaccard, S. L., Lisiecki, L. E., Lund, D. C., Martínez-Méndez, G., Lynch-Stieglitz, J., Mackensen, A., Michel, E., Mix, A. C., Oppo, D. W., Peterson, C. D., Repschläger, J., Sikes, E. L., Spero, H. J., and Waelbroeck, C.: Calibration of the carbon isotope composition (δ13C) of benthic foraminifera, Paleoceanography, 32, 512–530, https://doi.org/10.1002/2016PA003072, 2017.

Sigman, D., Karsh, K., and Casciotti, K.: Nitrogen Isotopes in the Ocean, in: Encyclopedia of Ocean Sciences, pp. 40–54, Elsevier, https://doi.org/10.1016/B978-012374473-9.00632-9, 2009.

Sigman, D. M., Hain, M. P., and Haug, G. H.: The polar ocean and glacial cycles in atmospheric CO(2) concentration., Nature, 466, 47–55, https://doi.org/10.1038/nature09149, 2010.

Sipler, R. E., Gong, D., Baer, S. E., Sanderson, M. P., Roberts, Q. N., Mulholland, M. R., and Bronk, D. A.: Preliminary estima-tes of the contribution of Arctic nitrogen fixation to the global nitrogen budget, Limnology and Oceanography Letters, pp. 159–166, https://doi.org/10.1002/lol2.10046, 2017.

Smith, I.: Global climate modelling within CSIRO: 1981 to 2006, Australian Meteorological Magazine, 56, 2007.

Smith, R. E. H.: Size-dependent phosphorus uptake kinetics and cell quota in phytoplankton, Journal of Phycology, 18, 275–284, 1982.

Smith, S., Yamanaka, Y., Pahlow, M., and Oschlies, A.: Optimal uptake kinetics: physiological acclimation explains the pattern of nitrate uptake by phytoplankton in the ocean, Marine Ecology Progress Series, 384, 1–12, https://doi.org/10.3354/meps08022, 2009.

Sohm, J. a., Webb, E. a., and Capone, D. G.: Emerging patterns of marine nitrogen fixation., Nature reviews. Microbiology, 9, 499–508, https://doi.org/10.1038/nrmicro2594, 2011.

Solomon, S., Qin, D., Manning, M., Averyt, K., and Marquis, M.: Climate change 2007-the physical science basis: Working group I contri-bution to the fourth assessment report of the IPCC, vol. 4, Cambridge university press, 2007.

Somes, C. J., Schmittner, A., Galbraith, E. D., Lehmann, M. F., Altabet, M. A., Montoya, J. P., Letelier, R. M., Mix, A. C., Bourbonnais, A., and Eby, M.: Simulating the global distribution of nitrogen isotopes in the ocean, Global Biogeochemical Cycles, 24, 1–16, https://doi.org/10.1029/2009GB003767, 2010.

Somes, C. J., Oschlies, A., and Schmittner, A.: Isotopic constraints on the pre-industrial oceanic nitrogen budget, Biogeosciences, 10, 5889–5910, https://doi.org/10.5194/bg-10-5889-2013, 2013.

Straub, M., Sigman, D. M., Ren, H., Martínez-García, A., Meckler, A. N., Hain, M. P., and Haug, G. H.: Changes in North Atlantic nitrogen fixation controlled by ocean circulation, Nature, 501, 200, 2013.

Studer, A. S., Sigman, D. M., Martínez-García, A., Thöle, L. M., Michel, E., Jaccard, S. L., Lippold, J. A., Mazaud, A., Wang, X. T., Robinson, L. F., Adkins, J. F., and Haug, G. H.: Increased nutrient supply to the Southern Ocean during the Holocene and its implications for the pre-industrial atmospheric CO2 rise, Nature Geoscience, https://doi.org/10.1038/s41561-018-0191-8, 2018.

Tagliabue, A. and Bopp, L.: Towards understanding global variability in ocean carbon-13, Global Biogeochemical Cycles, 22, 1–13, https://doi.org/10.1029/2007GB003037, 2008.

Tagliabue, A., Bopp, L., Roche, D. M., Bouttes, N., Dutay, J.-C., Alkama, R., Kageyama, M., Michel, E., and Paillard, D.: Quantifying the roles of ocean circulation and biogeochemistry in governing ocean carbon-13 and atmospheric carbon dioxide at the last glacial maximum, Climate of the Past Discussions, 5, 1463–1491, https://doi.org/10.5194/cpd-5-1463-2009, 2009.

Taylor, K. E.: Summarizing multiple aspects of model performance in a single diagram, Journal of Geophysical Research, 106, 7183, https://doi.org/10.1029/2000JD900719, 2001.

Tesdal, J. E., Galbraith, E. D., and Kienast, M.: Nitrogen isotopes in bulk marine sediment: Linking seafloor observations with subseafloor records, Biogeosciences, 10, 101–118, https://doi.org/10.5194/bg-10-101-2013, 2013.

Thyng, K. M., Greene, C. A., Hetland, R. D., Zimmerle, H. M., and DiMarco, S. F.: True Colors of Oceanography: Guidelines for Effective and Accurate Colormap Selection, Oceanography, 29, 2016.

Timmermans, K. R., Gerringa, L. J. A., Baar, H. J. W. D., Der, B. V., Veldhuis, M. J. W., Jong, J. T. M. D., Croot, P. L., Boye, M., and Boye, M.: Growth rates of large and small Southern Ocean diatoms in relation to availability of iron in natural seawater, Limnology and Oceanography, 46, 260–266, 2001.

Timmermans, K. R., van der Wagt, B., and de Baar, H. J. W.: Growth rates, half-saturation constants, and silicate, nitrate, and phosphate depletion in relation to iron availability of four large, open-ocean diatoms from the Southern Ocean, Limnology and Oceanography, 49, 2141–2151, https://doi.org/10.4319/lo.2004.49.6.2141, 2004.

Toggweiler, J. R., Dixon, K., and Bryan, K.: Simulations of radiocarbon in a coarse-resolution world ocean model: 2. Distributions of bomb-produced carbon 14, Journal of Geophysical Research, 94, 8243, https://doi.org/10.1029/JC094iC06p08243, 1989.

Voss, M., Dippner, J. W., and Montoya, J. P.: Nitrogen isotope patterns in the oxygen-deficient waters of the Eastern Tropical North Pacific Ocean, Deep Sea Research Part I: Oceanographic Research Papers, 48, 1905–1921, https://doi.org/10.1016/S0967-0637(00)00110-2, 2001.

Wada, E.: Nitrogen isotope fractionation and its significance in biogeochemical processes occurring in marine environments, Isotope marine chemistry, pp. 375–398, 1980.

Weber, T., Cram, J. A., Leung, S. W., DeVries, T., and Deutsch, C.: Deep ocean nutrients imply large latitudinal variation in particle transfer efficiency, Proceedings of the National Academy of Sciences, 113, 8606–8611, https://doi.org/10.1073/pnas.1604414113, 2016.

Wolf-Gladrow, D. A., Zeebe, R. E., Klaas, C., Körtzinger, A., and Dickson, A. G.: Total alkalinity: The explicit conservative expression and its application to biogeochemical processes, Marine Chemistry, 106, 287–300, https://doi.org/10.1016/j.marchem.2007.01.006, 2007.

Yamanaka, Y. and Tajika, E.: The role of the vertical fluxes of particulate organic matter and calcite in the oceanic carbon cycle: Studies using an ocean biogeochemical general circulation model, Global Biogeochemical Cycles, 10, 361–382, https://doi.org/10.1029/96GB00634, 1996.

Yang, S. and Gruber, N.: The anthropogenic perturbation of the marine nitrogen cycle by atmospheric deposition, Global Biogeochemical Cycles (accepted), pp. 1418–1440, https://doi.org/10.1002/2016GB005421.Received, 2016.

Zhang, H. and Cao, L.: Simulated effect of calcification feedback on atmospheric CO2 and ocean acidification, Scientific Reports, 6, 1–10, https://doi.org/10.1038/srep20284, 2016.

Zhang, J., Quay, P., and Wilbur, D.: Carbon isotope fractionation during gas-water exchange and dissolution of CO2, Geochimica et Cosmochimica Acta, 59, 107–114, 1995.

Zondervan, I., Zeebe, R. E., Rost, B., and Riebesell, U.: Decreasing marine biogenic calcification: A negative feedback on rising atmospheric pCO$_2$, Global Biogeochemical Cycles, 15, 507–516, 2001.